

NORTHWESTERN UNIVERSITY

Cation-Anion Interactions in Solid State Oxide Fluorides

A DISSERTATION

SUBMITTED TO THE GRADUATE SCHOOL
IN PARTIAL FULFILLMENT OF THE REQUIREMENTS

for the degree

DOCTOR OF PHILOSOPHY

Field of Chemistry

By

Michael Robert Marvel

EVANSTON, ILLINOIS

June 2008

© Copyright by Michael Robert Marvel 2008

All Rights Reserved

Abstract

Cation-Anion Interactions in Solid State Oxide Fluorides

Michael Robert Marvel

The early transition metal oxide fluoride molecular anions with the general formula $[MO_xF_{6-x}]^{n-}$ with $x = 1$ for $M = V^{5+}, Nb^{5+}, Ta^{5+}$ ($n = 2$) and $x = 2$ for $M = Mo^{6+}, W^{6+}$ ($n = 2$) feature distorted octahedral coordinations, that arise from electronic $d\pi-p\pi$ metal-oxide orbital interactions (similar to those observed in classic ferroelectric metal oxides). The nonlinear optical response of the oxide fluoride materials would be at a maximum when the inherent "primary" out-of-center distortions in the oxide fluoride anions are crystallographically ordered and aligned. In order to attain a greater level of predictability in designing polar materials with $[MO_xF_{6-x}]^{n-}$ anions, the relationship between the anionic group and the surrounding cationic network of bonds must be intimately understood.

Examination of the cation-anion interactions in $KNaNbOF_5$, $CsNaNbOF_5$, Rb_2NbOF_5 , Cs_2NbOF_5 , $Rb_3Na(NbOF_5)_2 \cdot H_2O$, $Rb_3Na(MoO_2F_4)_2 \cdot H_2O$, $Rb_3Na(WO_2F_4)_2 \cdot H_2O$, and $K_3Na(WO_2F_4)_2 \cdot H_2O$, largely through bond valence analyses, reveals that the cationic network of bonds surrounding the $[MO_xF_{6-x}]^{n-}$ anions arrange to accommodate both primary and secondary distortions, which arise due to inherent, electronic effects and chemical hardness, respectively. These observations suggest that specific cation combinations, i.e. Na/K, can result in polar ordering of the $[MO_xF_{6-x}]^{n-}$ anions while others do not, i.e. Na/Cs.

Polar ordering was observed in KNaNbOF_5 where there was a minimum number of contacts to the nucleophilic oxide ion, thereby preserving the primary Nb-O $d\pi$ - $p\pi$ interaction. The small, eight-coordinate potassium cations distort from the centers of their coordination polyhedra toward the negatively charged trans-fluoride ions of the $[\text{NbOF}_5]^{2-}$ anion. In contrast, an increase in the number of contacts to the oxide ion and a lengthening of the Nb-O bonds are observed in CsNaNbOF_5 . The large, ten-coordinate cesium cations reside on inversion centers.

Professor Kenneth R. Poeppelmeier
Thesis Advisor

Acknowledgements

First, I would like to extend my gratitude to my advisor, Professor Kenneth R. Poeppelmeier, for his unwavering support throughout my years as a graduate student. I have always been given the freedom to pursue interesting leads in the laboratory and for that I am grateful. I became an independent and critical thinker under your guidance Ken, and I will always have those skills to fall back on.

This work would not have been possible without the support of the National Science Foundation. Charlotte Stern also deserves a great deal of gratitude, as she collected all of the X-ray diffraction data.

I also owe a sincere thanks to my fellow graduate students and friends. Scott Barry and Jared Smit were great mentors during my first year of graduate school as well as close friends. I have had the privilege of working with many others who have made graduate school a fun experience. Jake Haag, Ian Saratovsky, Shilie Pan, Evan Stampler, Federico Rabuffetti, Erin Sorensen, Mariana Bertoni, and Tommy Albrecht have always provided comic relief and sage advice when needed most. Thanks guys!

My parents, David and Laurie, have always encouraged me to pursue my interests, academic and otherwise, and gave me a strong foundation to do just that. I love you guys for that and the countless other things you have given me over the years.

Finally, I would like to thank my beautiful fiancé and future wife, Carlie Friedman, for putting up with me for the past couple of years. Admittedly, the writing process has made me irritable at times, and you always knew just how to calm me

down. The shortcomings in this work and outside of it are mine alone, the successes are ours together. You have made my life the happiest it has ever been and I look forward to a long and bright future together. I love you Frie, now and forever!

Table of Contents

Abstract.....	3
Acknowledgments	5
List of Figures.....	11
List of Tables	17
Chapter 1 Introduction and Background	20
1.1. Background.....	21
1.2. Synthetic Techniques.....	26
1.2.1. Hydrothermal Synthesis.....	26
1.3. Chapter Summaries.....	29
Chapter 2 Cation-Anion Interactions and Polar Structures in the Solid State.....	32
2.1. Introduction.....	33
2.2. Synthesis and Characterization.....	36
2.2.1. Materials	36
2.2.2. Synthesis.....	37
2.2.3. Crystallographic Determination.....	39
2.2.4. Second-Harmonic Generation Measurement.....	40
2.3. Extended Structures	42
2.4. Anion Ordering and the Observance of Pauling's Second Crystal Rule.....	49
2.5. Noncentrosymmetry vs. Centrosymmetry	53
2.6. Intraoctahedral Distortions and the Observed SHG Response in KNaNbOF_5 ...	54
2.7. Analysis of Structural Strain.....	58
2.8. Conclusions	60
2.9. Corrections and Additions	60

Chapter 3	Chemical Hardness and the Structure-Directing Role of the cis-oxo $[\text{WO}_2\text{F}_4]^{2-}$ Anion	62
3.1.	Introduction	63
3.2.	Synthesis and Characterization	67
3.2.1.	Materials	67
3.2.2.	Synthesis	67
3.2.3.	Crystallographic Determination	69
3.2.4.	Spectroscopic Measurements	70
3.3.	Extended Structures	70
3.3.1.	$\text{Rb}_3\text{Na}(\text{NbOF}_5)_2 \cdot \text{H}_2\text{O}$	71
3.3.2.	$\text{Rb}_3\text{Na}(\text{MoO}_2\text{F}_4)_2 \cdot \text{H}_2\text{O}$	71
3.3.3.	$\text{Rb}_3\text{Na}(\text{WO}_2\text{F}_4)_2 \cdot \text{H}_2\text{O}$	72
3.3.4.	$\text{K}_3\text{Na}(\text{WO}_2\text{F}_4)_2 \cdot \text{H}_2\text{O}$	72
3.4.	Anion Distortions	79
3.5.	Pauling's Second Crystal Rule	83
3.6.	Chemical Hardness	85
3.7.	Atomic Size Effects	90
3.8.	Conclusions	92
Chapter 4	The Valence-Matching Principle and Cation-Anion Interactions in Solid State Oxide Fluorides	93
4.1.	Introduction	94
4.2.	Synthesis and Characterization	96
4.2.1.	Materials	96
4.2.2.	Synthesis	96
4.2.3.	Crystallographic Determination	97
4.3.	Results and Discussion	97
4.3.1.	The Valence-Matching Principle	97
4.3.2.	Crystal Structure of $\text{Rb}_{10}\text{Nb}_6\text{O}_7\text{F}_{26} \cdot \text{H}_2\text{O}$	101
4.4.	Conclusions	108
Chapter 5	The Crystal Structures of Rb_2NbOF_5 and Cs_2NbOF_5	109
5.1.	Introduction	110
5.2.	Synthesis and Characterization	113
5.2.1.	Materials	113
5.2.2.	Synthesis	113
5.2.3.	Crystallographic Determination	114
5.3.	Results and Discussion	115
5.4.	Conclusions	122

Chapter 6 The Elusive KNaNbOF_5	123
6.1. Introduction.....	124
6.2. Synthesis and Characterization.....	126
6.2.1. Materials	126
6.2.2. Synthesis.....	127
6.2.3. Product Identification	127
6.3. Results and Discussion	127
6.4. Conclusions.....	134
Chapter 7 Conclusions and Future Directions.....	135
7.1. Conclusions.....	136
7.1.1 Cation-Anion Interactions and Polar Structures in the Solid State.....	136
7.1.2. Chemical Hardness and the Structure-Directing Role of the cis-oxo $[\text{WO}_2\text{F}_4]^{2-}$ Anion.....	136
7.1.3. The Valence-Matching Principle and Cation-Anion Interactions in Solid State Oxide Fluorides	137
7.1.4. The Crystal Structures of Rb_2NbOF_5 and Cs_2NbOF_5	138
7.1.5. The Elusive KNaNbOF_5	138
7.2. Future Directions	139
7.2.1 Cation-Anion Interactions and Polar Structures in the Solid State.....	139
7.2.2. Chemical Hardness and the Structure-Directing Role of the cis-oxo $[\text{WO}_2\text{F}_4]^{2-}$ Anion.....	139
7.2.3. The Valence-Matching Principle and Cation-Anion Interactions in Solid State Oxide Fluorides	140
7.2.4. The Crystal Structures of Rb_2NbOF_5 and Cs_2NbOF_5	141
7.2.5. The Elusive KNaNbOF_5	141

References	142
Chapter 1.....	143
Chapter 2.....	144
Chapter 3.....	148
Chapter 4.....	150
Chapter 5.....	152
Chapter 6.....	155
Appendix	156
Electronic Appendix	160
Vita	165

List of Figures

Chapter 1 Introduction and Background

- Figure 1.1 "Primary" out-of-center distortions of the octahedrally coordinated transition metal oxide fluoride anions for (a) $[\text{MOF}_5]^{2-}$ ($M = \text{Nb}^{5+}, \text{Ta}^{5+}$), (b) $[\text{MO}_2\text{F}_4]^{2-}$ ($M = \text{Mo}^{6+}, \text{W}^{6+}$), and (c) $[\text{MO}_3\text{F}_3]^{3-}$ ($M = \text{Mo}^{6+}$) 21
- Figure 1.2 The cluster compound $[\text{pyH}]_2[\text{Cu}(\text{py})_4(\text{NbOF}_5)_2]$ with the *trans*-directing $[\text{NbOF}_5]^{2-}$ anion..... 23
- Figure 1.3 The one-dimensional linear chain structure..... 25
- Figure 1.4 Schematic of the Teflon bag hydro(solvato)thermal synthetic technique 28

Chapter 2 Cation-Anion Interactions and Polar Structures in the Solid State

- Figure 2.1 The $[\text{NbOF}_5]^{2-}$, $[\text{MoO}_2\text{F}_4]^{2-}$, and $[\text{WO}_2\text{F}_4]^{2-}$ anions. The most nucleophilic O^{2-}/F^- ions are drawn in red. Coordination to the extended bond network is through these sites 35
- Figure 2.2 Graphs of SHG responses vs. particle sizes for phase-matchable LiNbO_3 , non-phase-matchable SiO_2 , and phase-matchable KNaNbOF_5 42
- Figure 2.3 The coordination polyhedra in KNaNbOF_5 . Blue octahedra are $[\text{NbOF}_5]^{2-}$ anions, black octahedra are Na-centered and eight-coordinate orange polyhedra are K-centered. In the above schematic, all drawings are shown in the (010) plane with different polyhedra highlighted in each 47

- Figure 2.4 The Coordination polyhedra in CsNaNbOF₅. Blue octahedra are [NbOF₅]²⁻ anions, black octahedra are Na-centered, eight-coordinate orange polyhedra are Cs1-centered and eight-coordinate grey polyhedra are Cs2-centered. In the above schematic, all drawings are shown in the (010) plane with different polyhedra highlighted in each 47
- Figure 2.5 A view of the three-dimensional frameworks in KNaNbOF₅ (left) and CsNaNbOF₅ (right), formed of (001) and (100) [NaNbOF₇]_∞ layers stacked along *c* and *a*, respectively. Insets are views of the framework structural building unit..... 48
- Figure 2.6 X-ray diffraction data for RbNaNbOF₅. The diffraction data were refined in pattern-matching mode using the JADE software program in the orthorhombic space group Pbcn to lattice constants *a* = 8.157 Å, *b* = 13.137 Å, and *c* = 10.956 Å. This represents a 4.8 % volume decrease compared to the CsNaNbOF₅ phase. A small amount of a second phase (*) identified as Rb₂NbOF₅ is also present in the sample 49
- Figure 2.7 The asymmetric coordination environment surrounding the [NbOF₅]²⁻ anion in KNaNbOF₅. The ions with the most local negative charge make the most/strongest contacts to the extended bond network 52
- Figure 2.8 The asymmetric coordination environment surrounding the [NbOF₅]²⁻ anion in CsNaNbOF₅. The ions with the most local negative charge make the most/strongest contacts to the extended bond network 52
- Figure 2.9 Channels formed by the Nb/Na-O/F framework run along the length of the *b* axis in KNaNbOF₅ (left) and CsNaNbOF₅ (right). Inset are enlarged views of the channel openings with cation coordination shown..... 54
- Figure 2.10 A view of the primary Nb-O distortions in KNaNbOF₅ including all atoms (left) and only Nb and O atoms (right). The partial addition of the individual bond dipoles is enough to observe a significant SHG response (0.6 x KDP) 57

Chapter 3 Chemical Hardness and the Structure-Directing Role of the cis-oxo $[\text{WO}_2\text{F}_4]^{2-}$ Anion

- Figure 3.1 The distortion directions of the $[\text{NbOF}_5]^{2-}$ (corner), $[\text{MoO}_2\text{F}_4]^{2-}$ (edge), and $[\text{MoO}_3\text{F}_3]^{2-}$ (face) anions. Stoichiometry dictates the distortion direction of the transition metal center. The $[\text{WO}_2\text{F}_4]^{2-}$ anion, therefore, displays an edge-type distortion 65
- Figure 3.2 The general $\text{A}_3'\text{A}(\text{MO}_x\text{F}_{6-x})_2 \cdot \text{H}_2\text{O}$ ($\text{A}' = \text{K}, \text{Rb}; \text{A} = \text{Na}$) structure with $x = 1$ for $\text{M} = \text{Nb}^{5+}$ ($n = 2$) and $x = 2$ for $\text{M} = \text{Mo}^{6+}, \text{W}^{6+}$ ($n = 2$) Insets are views of corner-distorted (blue) and edge-distorted (grey) anions. The corner-distorted octahedron represents an ordered $[\text{NbOF}_5]^{2-}$ anion and partially ordered $[\text{MoO}_2\text{F}_4]^{2-}$ and $[\text{WO}_2\text{F}_4]^{2-}$ anions, where one oxide ion is disordered over the four equatorial anion sites. The edge-distorted octahedron represents ordered $[\text{MoO}_2\text{F}_4]^{2-}$ and $[\text{WO}_2\text{F}_4]^{2-}$ anions and a partially ordered $[\text{NbOF}_5]^{2-}$ anion, where the oxide ion is located on the *cis* oxide sites 73
- Figure 3.3 Thermal ellipsoid plots (50% probability) of partially ordered anions. The Nb thermal ellipsoid is a moderately-sized sphere indicating limited disorder of the oxide ion, while the Mo and W thermal ellipsoids are slightly flattened spheres reflecting the disorder of one oxide and three fluorides in the equatorial plane 82
- Figure 3.4 The $[\text{NbOF}_5]^{2-}$, $[\text{MoO}_2\text{F}_4]^{2-}$, and $[\text{WO}_2\text{F}_4]^{2-}$ anions. The most nucleophilic O^{2-}/F^- ions are drawn in red. Coordination to the extended bond network is through these sites 85

Figure 3.5	The coordination environments surrounding the $[\text{NbOF}_5]^{2-}$ (top) and $[\text{MoO}_2\text{F}_4]^{2-}$ and $[\text{WO}_2\text{F}_4]^{2-}$ anions (bottom). The more Na^+ -rich coordination environments (left) cause corner-type distortions of the metal center, while the more K^+/Rb^+ rich coordination environments cause edge-type distortions of the Nb, Mo, and W metal centers.	89
Figure 3.6	The effect of increased cationic contact on the primary Nb-O distortion in the $[\text{NbOF}_5]^{2-}$ anion. As the composition of the bond network becomes more Rb^+ -rich, the primary distortion is lengthened until it vanishes	91
Chapter 4 The Valence-Matching Principle and Cation-Anion Interactions in Solid State Oxide Fluorides		
Figure 4.1	Polyhedral representations of the $\text{Rb}_5\text{Nb}_3\text{O}_3\text{F}_{14}\cdot\text{H}_2\text{O}$ (left) and $\text{Rb}_{10}\text{Nb}_6\text{O}_7\text{F}_{26}\cdot\text{H}_2\text{O}$. The hexagonal symmetry is apparent in both structures	104
Figure 4.2	The anionic building units which compose the $\text{Rb}_{10}\text{Nb}_6\text{O}_7\text{F}_{26}\cdot\text{H}_2\text{O}$ structure. Red spheres represent oxygen atoms, yellow spheres represent fluorine atoms, and black, gray, and blue spheres represent different niobium atoms	104
Figure 4.3	The experimental (black) and calculated (blue) powder X-ray diffraction patterns of $\text{Rb}_{10}\text{Nb}_6\text{O}_7\text{F}_{26}\cdot\text{H}_2\text{O}$	105
Chapter 5 The Crystal Structures of Rb_2NbOF_5 and Cs_2NbOF_5		
Figure 5.1	The $[\text{NbOF}_5]^{2-}$, $[\text{MoO}_2\text{F}_4]^{2-}$, and $[\text{WO}_2\text{F}_4]^{2-}$ anions. The most nucleophilic O^{2-}/F^- ions are drawn in red. Coordination to the extended bond network is through these sites	111
Figure 5.2	The Rb_2NbOF_5 (left) and Cs_2NbOF_5 (right) structures.....	116

- Figure 5.3 The coordination environments surrounding the $[\text{NbOF}_5]^{2-}$ anions in CsNaNbOF_5 and KNaNbOF_5 . Increased coordination to the oxide ion in CsNaNbOF_5 causes a weakening of the primary Nb-O distortion which lengthens as a result..... 117
- Figure 5.4 The coordination environments surrounding the $[\text{WO}_2\text{F}_4]^{2-}$ anions in $\text{Na}_2\text{WO}_2\text{F}_4$ and $\text{Cs}_2\text{WO}_2\text{F}_4$. Again, increased cationic contacts to the anion causes a weakening of the primary distortion, and a disordered anion is observed 118
- Figure 5.5 The symmetrical nature of the coordination environments surrounding the $[\text{NbOF}_5]^{2-}$ anions in Rb_2NbOF_5 (left) and Cs_2NbOF_5 (right), in addition to the large number of cationic contacts to each O^{2-}/F^- ion leads to orientational disorder of the $[\text{NbOF}_5]^{2-}$ anion 119
- Figure 5.6 The effects of increased cation size on the primary Nb-O distortion of the $[\text{NbOF}_5]^{2-}$ anion. As the bond network composition surrounding the $[\text{NbOF}_5]^{2-}$ anion becomes more Rb^+ -rich, the Nb-O bond weakens until orientational disorder occurs 122

Chapter 6 The Elusive KNaNbOF_5

- Figure 6.1 A view of the primary Nb-O distortions in KNaNbOF_5 including all atoms (left) and only Nb and O atoms (right). The partial addition of the individual bond dipoles is enough to observe a significant SHG response ($0.6 \times \text{KDP}$) 124
- Figure 6.2 Graph of particle sizes vs. SHG responses for KNaNbOF_5 . The compound is phase-matchable with an SHG response $0.6 \times \text{KDP}$ 125

- Figure 6.3 A view of the three-dimensional frameworks in KNaNbOF_5 (left) and CsNaNbOF_5 (right), formed of (001) and (100) $[\text{NaNbOF}_7]_\infty$ layers stacked along c and a , respectively. Insets are views of the framework structural building unit..... 128
- Figure 6.4 Coordination polyhedra in KNaNbOF_5 . Blue octahedra are $[\text{NbOF}_5]^{2-}$ anions, black octahedra are Na-centered and eight-coordinate orange polyhedra are K-centered. In this schematic, all drawings are shown in the (010) plane with different polyhedra highlighted in each 129
- Figure 6.5 The structure of $\text{K}_2\text{NaNbO}_2\text{F}_4$. Blue octahedra are $[\text{NbOF}_5]^{2-}$ anions, orange spheres are Na^+ cations, and black spheres are K^+ cations..... 129
- Figure 6.6 Powder X-ray diffraction patterns of KNaNbOF_5 ground single crystals (red) and polycrystalline powder (black) 133

List of Tables

Chapter 1 Introduction and Background

Table 1.1 Selected Bond Distances, Bond Angles, and Bond Valence Calculations of Ordered Oxide Fluoride Anions	24
--	----

Chapter 2 Cation-Anion Interactions and Polar Structures in the Solid State

Table 2.1 Crystallographic data for CsNaNbOF ₅ and KNaNbOF ₅	40
Table 2.2 Selected Bond Lengths, Experimental Bond Valences, Theoretical Bond Valences, Bond Valence Sums, BSI and GII indices for KNaNbOF ₅	44
Table 2.3 Selected Bond lengths, Experimental Bond Valences, Theoretical Bond Valences, Bond Valence Sums, BSI and GII indices for CsNaNbOF ₅	45
Table 2.4 Estimations of the negative potentials of the ions of the (NbOF ₅) ²⁻ anions and the surrounding positive potentials in CsNaNbOF ₅ and KNaNbOF ₅ , through bond strength and bond valence calculations	46

Chapter 3 Chemical Hardness and the Structure-Directing Role of the cis-oxo [WO₂F₄]²⁻ Anion

Table 3.1 Bond Valence Sums for the [WO ₂ F ₄] ²⁻ Anion in [HNC ₆ H ₆ OH] ₂ [Cu(NC ₅ H ₅) ₄ (WO ₂ F ₄) ₂] and Na ₂ WO ₂ F ₄	65
Table 3.2 Crystallographic data for Rb ₃ Na(NbOF ₅) ₂ •H ₂ O, Rb ₃ Na(MoO ₂ F ₄) ₂ •H ₂ O, Rb ₃ Na(WO ₂ F ₄) ₂ •H ₂ O, and K ₃ Na(WO ₂ F ₄) ₂ •H ₂ O	69

Table 3.3	Estimated negative potentials of the oxide and fluoride ions and the surrounding positive potentials in $\text{Rb}_3\text{Na}(\text{NbOF}_5)_2 \cdot \text{H}_2\text{O}$, $\text{Rb}_3\text{Na}(\text{MoO}_2\text{F}_4)_2 \cdot \text{H}_2\text{O}$, $\text{Rb}_3\text{Na}(\text{WO}_2\text{F}_4)_2 \cdot \text{H}_2\text{O}$, and $\text{K}_3\text{Na}(\text{WO}_2\text{F}_4)_2 \cdot \text{H}_2\text{O}$ through bond strength and bond valence calculations	74
Table 3.4	Bond lengths and bond valences for cation-anion interactions in $\text{Rb}_3\text{Na}(\text{NbOF}_5)_2 \cdot \text{H}_2\text{O}$	75
Table 3.5	Bond lengths and bond valences for cation-anion interactions in $\text{Rb}_3\text{Na}(\text{MoO}_2\text{F}_4)_2 \cdot \text{H}_2\text{O}$	76
Table 3.6	Bond lengths and bond valences for cation-anion interactions in $\text{Rb}_3\text{Na}(\text{WO}_2\text{F}_4)_2 \cdot \text{H}_2\text{O}$	77
Table 3.7	Bond lengths and bond valences for cation-anion interactions in $\text{K}_3\text{Na}(\text{WO}_2\text{F}_4)_2 \cdot \text{H}_2\text{O}$	78
Chapter 4	The Valence-Matching Principle and Cation-Anion Interactions in Solid State Oxide Fluorides	
Table 4.1	Alkali cation Lewis Acidities , determined from all available alkali metal oxide fluoride salts.....	99
Table 4.2	Crystallographic data for $\text{Rb}_{10}\text{Nb}_6\text{O}_7\text{F}_{26} \cdot \text{H}_2\text{O}$	102
Table 4.3	Comparison of the $\text{Rb}_{10}\text{Nb}_6\text{O}_6\text{F}_{28} \cdot \text{H}_2\text{O}$ and $\text{Rb}_{10}\text{Nb}_6\text{O}_7\text{F}_{26} \cdot \text{H}_2\text{O}$ lattice constants.....	105
Table 4.4	Bond lengths and bond valence values for $\text{Rb}_{10}\text{Nb}_6\text{O}_7\text{F}_{26} \cdot \text{H}_2\text{O}$	107
Chapter 5	The Crystal Structures of Rb_2NbOF_5 and Cs_2NbOF_5	
Table 5.1	Crystallographic data for Rb_2NbOF_5 and Cs_2NbOF_5	115
Table 5.2	Nb-X (X = O/F) bond lengths for Rb_2NbOF_5 and Cs_2NbOF_5	119

Table 5.3	Compounds composed of the alkali metals and early d^0 transition metal oxide fluoride anions.....	120
-----------	---	-----

Chapter 6 The Elusive KNaNbOF_5

Table 6.1	Reaction labels, reactants, reaction conditions, and observed products for synthetic attempts at KNaNbOF_5 . Those reactions for which the isolated phase could not be identified by X-ray powder diffraction are labelled 'UID' and those for which insufficient product was obtained are labelled 'N/A'.....	130
Table 6.2	Alkali cation Lewis Acidities, determined from all available alkali metal oxide fluoride salts.....	131

CHAPTER ONE

Introduction and Background

1.1 Background

The early d^0 transition metal oxide fluoride anions $[MO_xF_{6-x}]^{n-}$ with $x = 1$ for $M = V^{5+}, Ta^{5+}$ ($n = 2$) and $x = 2$ for $M = Mo^{6+}, W^{6+}$ ($n = 2$) are useful building blocks in the construction of noncentrosymmetric materials. They possess out-of-center distortions caused by metal $d\pi$ – oxygen $p\pi$ orbital interactions. See figure 1.1. When aligned in an additive manner, these distortions lead to the observation of desirable materials properties such as piezoelectricity, ferroelectricity, and second harmonic generation. Unfortunately, controlling the distortion to align in any solid-state material is, at a minimum, difficult.

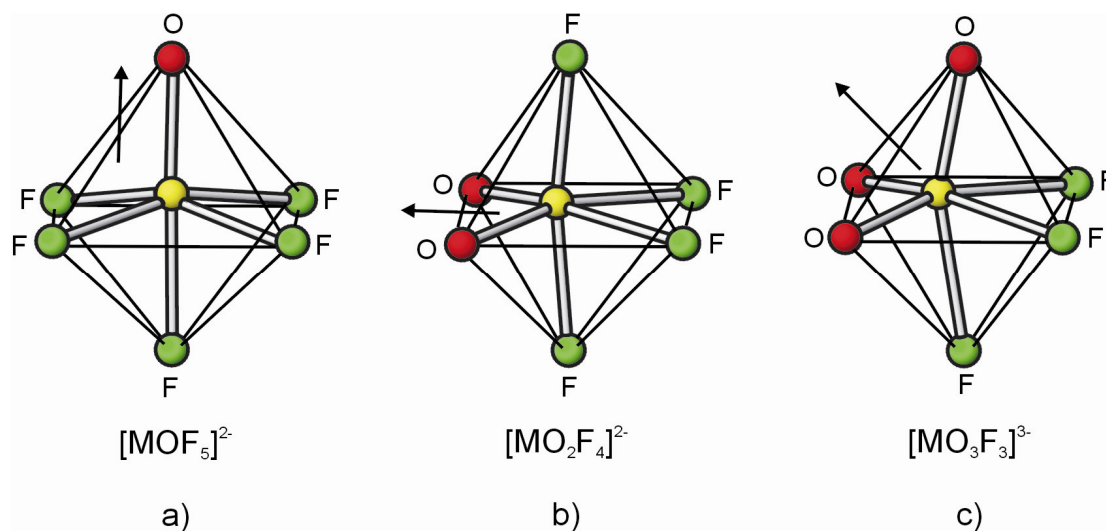


Figure 1.1. "Primary" out-of-center distortions of the octahedrally coordinated transition metal oxide fluoride anions for a) $[MOF_5]^{2-}$ ($M = Nb^{5+}, Ta^{5+}$), b) $[MO_2F_4]^{2-}$ ($M = Mo^{6+}, W^{6+}$), and c) $[MO_3F_3]^{3-}$ ($M = Mo^{6+}$).

Early work towards this goal was undertaken by Chen when he proposed the anionic group theory¹, which attributes the SHG response in a material to the anionic group. Borate groups were first employed with this theory in mind and have since been incorporated into hundreds of structures, with approximately forty percent of them being noncentrosymmetric owing to the inherently acentric nature of the borate groups. In order to attain higher levels of predictability in designing noncentrosymmetric materials, the relationship between the anionic group and the surrounding cationic bond network must also be understood. Towards this end, a large catalog of compounds containing the $[MO_xF_{6-x}]^{n-}$ anions has been created.

The first challenge encountered in the synthesis of noncentrosymmetric materials from the early d^0 transition metal oxide fluoride anions is oxide/fluoride disorder. Crystallographic disorder of the oxide and fluoride ions obscures exact bond lengths and angles and leads to a vanishing of the primary, M-O distortion. The second is to prevent these anions from crystallizing in a centrosymmetric arrangement with respect to each other. The first challenge has been overcome for all five anions and led to an analysis of their intraoctahedral distortions.

Strongly coordinating organic cations were first used to circumvent the problem of orientational disorder. "Cluster" compounds, with the general formula $[LH]_2[Cu(L)_4(MO_xF_{6-x})_2]$, in which L = pyridine, 3-aminopyridine, or 4-aminopyridine and the Cu^{2+} cation can be replaced by Cd^{2+} or Zn^{2+} , were formed.² See figure 1.2. As a result, exact M-O/F bond lengths were obtained and bond valence calculations were

used to determine the structure-directing properties of the anions. Bond valence calculations³, which employ parameterized equations to calculate residual negative charge, can provide a quantitative measure of the reactivity of different ligands of an ordered anion where true bond lengths are known. Example bond valence values are listed in Table 1.1. Ligands with the most anionic character will preferentially coordinate and thereby "direct" coordination within the structure. The oxide and *trans* fluoride retain the most residual negative charge in the monoxo $[\text{MOF}_5]^{2-}$ ($\text{M} = \text{Nb}^{5+}$, Ta^{5+}) anions; thus, they are classified as *trans*-directors. Conversely, the dioxo $[\text{MoO}_2\text{F}_4]^{2-}$ species directs coordination through two *cis* ligands and is designated a *cis*-director.⁴

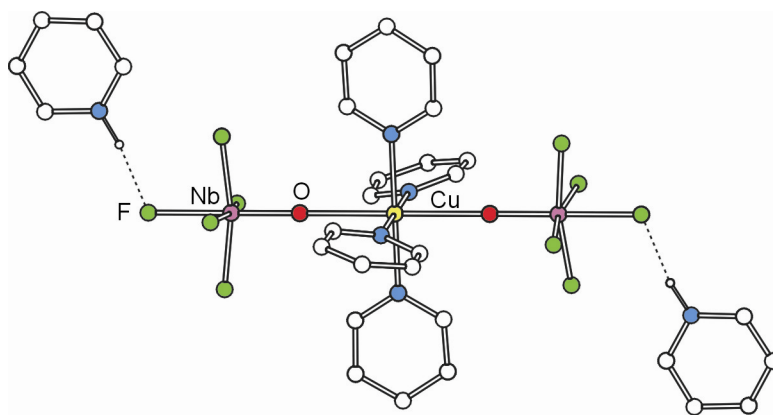


Figure 1.2. The cluster compound $[\text{pyH}]_2[\text{Cu}(\text{py})_4(\text{NbOF}_5)_2]$ with the *trans*-directing $[\text{NbOF}_5]^{2-}$ anion.

Table 1.1. Selected Bond Distances, Bond Angles, and Bond Valence Calculations of Ordered Oxide Fluoride Anions.

[NbOF₅]²⁻				[MoO₂F₄]²⁻			
	R_i , Å	S_i	$V_i - S_i$		R_i , Å	S_i	$V_i - S_i$
Nb=O1	1.760(1)	1.54	0.46	Mo=O1	1.709(2)	1.71	0.29
Nb-F1	1.953(1)	0.70	0.30	Mo=O2	1.697(2)	1.76	0.24
Nb-F2	1.923(1)	0.76	0.24	Mo-F1*	2.059(1)	0.51	0.49
Nb-F3	1.928(1)	0.75	0.25	Mo-F2*	2.114(1)	0.44	0.56
Nb-F4	1.928(1)	0.75	0.25	Mo-F3	1.939(1)	0.70	0.30
Nb-F5*	2.072(1)	0.51	0.49	Mo-F4	1.918(2)	0.74	0.26
	Σ_{Nb}	5.01			Σ_{Mo}	5.86	
O1-Nb-F5	178.87(6)			O1-Mo-F1	165.70(7)		
F1-Nb-F3	166.66(6)			O2-Mo-F2	169.72(7)		
F2-Nb-F4	167.98(6)			F3-Mo-F4	161.07(6)		
O1-Nb-F1	96.54(6)			O1-Mo-O2	102.16(9)		
O1-Nb-F2	96.46(6)			F1-Mo-F2	77.84(6)		
F5-Nb-F1	82.46(5)			O1-Mo-F3	94.35(8)		
F5-Nb-F2	84.05(6)			O1-Mo-F4	96.63(8)		
[WO₂F₄]²⁻				[MoO₃F₃]³⁻			
	R_i , Å	S_i	$V_i - S_i$		R_i , Å	S_i	$V_i - S_i$
W=O1	1.772(2)	1.50	0.50	Mo=O × 3	1.755(6)	1.51	0.49
W=O2	1.714(2)	1.75	0.25	Mo-F × 3	2.083(5)	0.48	0.52
W-F1*	2.059(2)	0.54	0.46		Σ_{Mo}	5.97	
W-F2*	2.029(2)	0.58	0.42				
W-F3	1.903(2)	0.82	0.18	O-Mo-O'	103.1(3)		
W-F4	1.908(2)	0.81	0.19	F-Mo-F'	77.3(2)		
	Σ_{W}	6.00		O-Mo-F	88.3(2)		
				O-Mo-F	161.3(3)		
O1-W-F1	167.84(9)						
O2-W-F2	170.3(1)						
F3-W-F4	162.98(9)						
O1-W-O2	100.7(1)						
F1-W-F2	78.91(8)						
O1-W-F3	94.13(9)						
O1-W-F4	93.68(9)						

* *trans* fluoride. Valence sums calculated with the formula: $S_i = \exp[(R_o - R_i)/B]$, where S_i = bond valence of bond "i", R_o = constant dependent on the bonded elements, R_i = bond length of bond "i", and $B = 0.370$. ΣS_M = bond valence sum for the metal. V_i = oxidation state for each ligand. $V_i - S_i$ = calculated charge of the ligand. $R_o(\text{W-O}) = 1.921$ Å, $R_o(\text{W-F}) = 1.836$ Å, $R_o(\text{Mo-O}) = 1.907$ Å, $R_o(\text{Mo-F}) = 1.808$ Å, $R_o(\text{Nb-O}) = 1.911$ Å, $R_o(\text{Nb-F}) = 1.822$ Å.

The structure directing properties of the anions were confirmed by crystallization in linear chain compounds of the formula $M(\text{py})_4\text{M}'\text{O}_x\text{F}_{6-x}$ where $M = \text{Cu}^{2+}, \text{Zn}^{2+}, \text{Cd}^{2+}$; $M' = \text{Nb}^{5+}, \text{W}^{6+}$; and $\text{py} = \text{pyridine}$.⁵ See figure 1.3. Additional pyridine derivatives, such as 3-aminopyridine and 4-aminopyridine, have also been incorporated into this structure.⁶ The one-dimensional linear chain structures are comprised of alternating $[\text{M}'\text{O}_x\text{F}_{6-x}]^{n-}$ anions and $\text{M}(\text{L})_4$ cations, where $\text{L} = \text{a pyridine derivative}$.

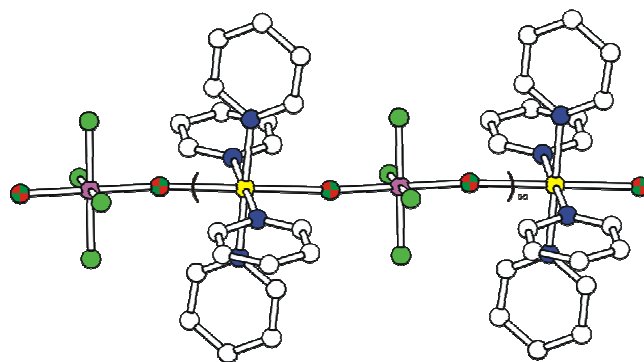


Figure 1.3. The one-dimensional linear chain structure.

The second condition, oxide fluoride ordering in a noncentrosymmetric space group, was accomplished in $\text{Cd}(3\text{-apy})_4\text{NbOF}_5$.⁶ However, the multiple hydrogen bond contacts to the $[\text{NbOF}_5]^{2-}$ anion led to a severe decrease in the strength of the primary Nb-O distortion owing to a weakening of the Nb-O π bonding. This is an unfavorable

condition as any weakening of this bond would ultimately mitigate the effects of polar ordering.

The results presented here describe the use of alkali metal cations to control the intraoctahedral distortions of the d^0 transition metal oxide fluoride anions. In contrast to large, organic cations, crystallizing the $[MO_xF_{6-x}]^{n-}$ anions with multiple, different alkali metal cations offers a unique way to order the anions and preserve the primary M-O distortions critical to the materials properties associated with their alignment.⁷

1.2 Synthetic Techniques

1.2.1 Hydrothermal Synthesis

Mild hydro(solvato)thermal techniques are an effective, low temperature approach to the synthesis of transition metal oxide fluoride materials. The combination of low temperatures (typically under 200 °C) and autogenous pressures facilitates single crystal growth that is suitable for single crystal X-ray diffraction. All of the reactants for the synthesis, which consist of metal oxides, alkali fluorides, and aqueous hydrofluoric acid (HF) are added to a Teflon [fluoro(ethylene-propylene)] (FEP) bag.⁸ Aqueous HF acts as both a mineralizer and as a fluoride source.

The bags are made by folding a 3.5 by 3.0 inch piece of FEP film in half along its shorter axis and sealing it on two sides with a thermal impulse sealer. After the

reactants are added, the third side of the pouch is sealed and placed in either a 250 ml polytetrafluoroethylene Teflon-lined or a 2 L Parr autoclave. The 2 L autoclave is unlined and therefore the individual reaction bags must be placed in an additional FEP pouch, with dimensions of 3.5 inches wide and 6.0 inches long, before being placed in the autoclave. The pressure vessels are filled 33% with deionized water, are heated for 24 h at 150 °C, and are then cooled to room temperature over an additional 24 h. The bags are opened in air and the products are recovered by vacuum filtration. The "Teflon bag" approach offers a number of synthetic advantages, which include a pseudo-combinatorial approach for a number of different reactions to be run under identical reaction conditions, as well as providing an inexpensive reaction vessel that can withstand the harsh chemical environment under which the oxide fluoride products are synthesized. A schematic of the synthetic process is shown in Figure 1.4.

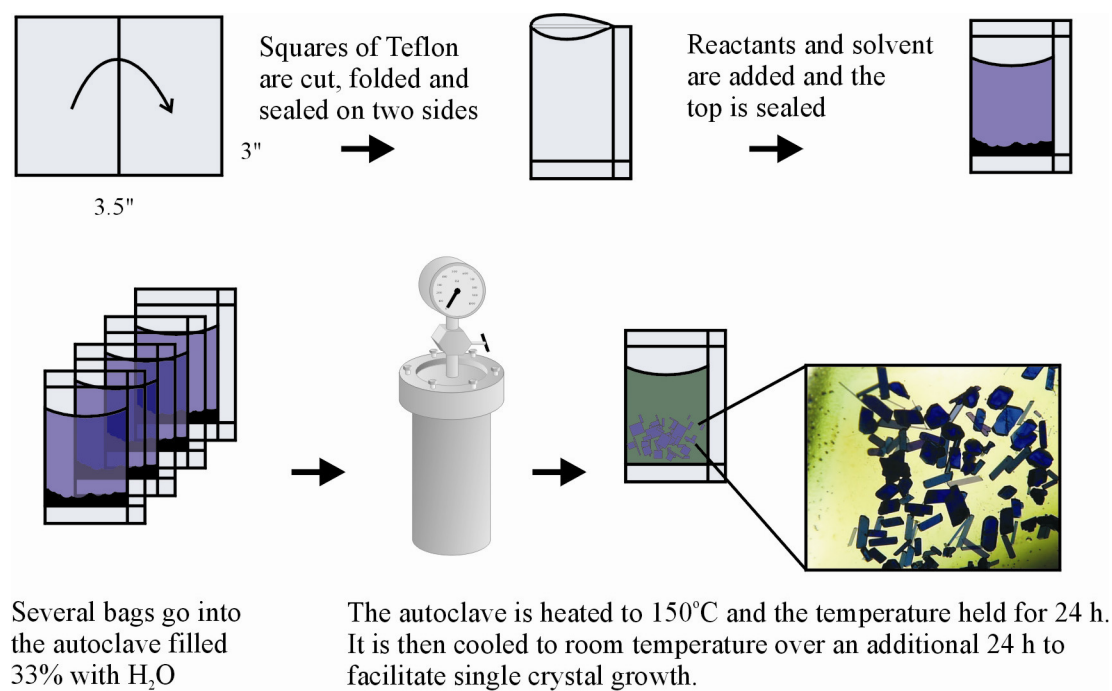


Figure 1.4. Schematic of the Teflon bag hydro(solvato)thermal synthetic technique.

1.3 Chapter Summaries

The crystal structure analyses presented in **Chapter 2** examine the underlying causes of oxide-fluoride ordering in compounds containing the early d^0 transition metal oxide fluoride anions, the effects of the extended bond network on the observed primary and secondary distortions, and how changes to the bond network lead to different crystal symmetries. Specifically, this chapter details how the interactions of the $[\text{NbOF}_5]^{2-}$ anion with the combination of Na/K or Na/Cs differ significantly. For instance, the lattice-derived secondary distortions, in addition to the primary electronic distortions they act upon, lead to a shorter Nb–O bond and oxygen being two-coordinate in the case of Na/K versus a longer Nb–O bond with oxygen three-coordinate for the combination Na/Cs. Thus, the noncentrosymmetric structure (KNaNbOF_5) maintains the larger primary electronic distortion of the $[\text{NbOF}_5]^{2-}$ anion along with a low coordination number of the electropositive K-ion consistent with the largest bond strain index (BSI). In contrast, the Cs-ions of the centrosymmetric structure (CsNaNbOF_5) can exhibit significantly higher coordination numbers and the $[\text{NbOF}_5]^{2-}$ anion a greatly reduced primary distortion.

Chapter 3 examines the structure-directing role of the cis-oxo $[\text{WO}_2\text{F}_4]^{2-}$ anion. Coordination to the most charged sites on the cis-oxo $[\text{WO}_2\text{F}_4]^{2-}$ anion in $\text{K}_3\text{Na}(\text{WO}_2\text{F}_4)_2 \cdot \text{H}_2\text{O}$ and $\text{Rb}_3\text{Na}(\text{WO}_2\text{F}_4)_2 \cdot \text{H}_2\text{O}$ shows unambiguously that the network

of bonds surrounding the $[\text{WO}_2\text{F}_4]^{2-}$ anion arranges so that its strongest/shortest contacts are made to the two F sites that are opposite the *cis*-O atoms. The $[\text{WO}_2\text{F}_4]^{2-}$ anion may therefore be labeled a *cis*-director unreservedly for the first time. Similarly, the network of bonds surrounding the *trans*-directing $[\text{NbOF}_5]^{2-}$ and *cis*-directing $[\text{MoO}_2\text{F}_4]^{2-}$ anions in $\text{Rb}_3\text{Na}(\text{NbOF}_5)_2 \cdot \text{H}_2\text{O}$ and $\text{Rb}_3\text{Na}(\text{MoO}_2\text{F}_4)_2 \cdot \text{H}_2\text{O}$ display a cation-anion affinity which results in preferential interaction of the small Na^+ cations with the non-polarizable fluoride ions and the larger K^+ and Rb^+ cations with the more polarizable oxide ions. These directional effects are quantified with bond valence and Pauling's second crystal rule (PSCR) sums.

Chapter 4 highlights the use of the valence-matching principle as a simple, *a priori* method of evaluating the possibility of cation-anion interactions in solid state oxide fluorides. When the Lewis acid strength, i.e. the characteristic valence/mean coordination number, of a cation approaches the Lewis base strength of an anion, the two constituents form a stable structure. Previously applied to silicates and borates, this principle is brought to bear on the crystal chemistry of compounds containing the noncentrosymmetric $[\text{MO}_x\text{F}_{6-x}]^{n-}$ anions ($x = 1$ for $M = \text{Nb}^{5+}$ ($n = 2$) and $x = 2$ for $M = \text{Mo}^{6+}$, W^{6+} ($n = 2$)) and reveals why the small Na^+ cation consistently crystallizes in stable structures with the $[\text{MO}_x\text{F}_{6-x}]^{n-}$ anions and the larger alkali metal cations (K^+ , Rb^+ , Cs^+) form stable structures with oligomeric oxide fluoride anions such as $[\text{Nb}_6\text{O}_7\text{F}_{26}]^{10-}$. Additionally, the $\text{A}_{10}\text{Nb}_6\text{O}_7\text{F}_{26}$ ($\text{A} = \text{K}, \text{Rb}, \text{Cs}$) phase is reported for the first time and its crystal structure is described.

The crystal structures of Rb_2NbOF_5 and Cs_2NbOF_5 are discussed in **Chapter 5**. In both structures, orientational disorder of the $[\text{NbOF}_5]^{2-}$ anion prohibits a bond valence analysis of the structure, however, valuable information can still be gleaned. For example, the sizes of the alkali cation(s) which compose the surrounding bond network clearly effect the intraoctahedral distortion of the anion.

Chapter 6 describes the numerous attempts aimed at the synthesis of high quality single crystals of KNaNbOF_5 , an SHG active and piezoelectric material. Crystals of this phase were grown on two separate occasions, but a consistent, reproducible synthetic route has not been determined. Most of the synthetic attempts led to the formation of the cubic, elpasolite $\text{K}_2\text{NaNbO}_2\text{F}_4$. This chapter details the many synthetic attempts made and addresses possible reasons for their collective failure.

Chapter 7 highlights future directions that may be pursued as a result of the work described in this thesis.

CHAPTER TWO

Cation-Anion Interactions and Polar Structures in the Solid State

2.1 Introduction

Noncentrosymmetric materials are a fertile topic of research owing to the important physical properties that may be observed in such materials: pyroelectricity, ferroelectricity, piezoelectricity or second harmonic generation (SHG). Optimization of the latter property has been based largely on Chen's anionic group theory¹, which attributes the SHG response in a material to the anionic group. This theory has proven useful by the continuous discovery of new NLO borates, for example, $\text{KBe}_2\text{BO}_3\text{F}_2$ ² and $\text{Sr}_2\text{Be}_2\text{B}_2\text{O}_7$ ³. While the design of SHG materials by selection of anionic groups that are able to produce high nonlinearities is a mostly successful method, it does not guarantee that one of the requirements for SHG materials, i.e., noncentrosymmetry, will be fulfilled.⁴ In order to attain higher levels of predictability in designing noncentrosymmetric materials, the relationship between the anionic group and the surrounding bond network must also be understood. In this context, two compounds containing the acentric $[\text{NbOF}_5]^{2-}$ anion have been synthesized: noncentrosymmetric KNaNbOF_5 and centrosymmetric CsNaNbOF_5 . This suggests that the noncentrosymmetric packing of the $[\text{NbOF}_5]^{2-}$ anion is related to the substitution of Cs^+ by the smaller K^+ cation in the $[\text{NaNbOF}_5]_\infty$ framework.

The $[\text{NbOF}_5]^{2-}$ anion is part of a large group of early d⁰ transition metal oxide fluoride octahedra: $[\text{MO}_x\text{F}_{6-x}]^{n-}$ with $x = 1$ for $M = \text{V}^{5+}, \text{Ta}^{5+}$ ($n = 2$) and $x = 2$ for $M = \text{Mo}^{6+}, \text{W}^{6+}$ ($n = 2$). Inherent to these anions are out-of-center "primary" electronic

distortions that arise from metal $d\pi$ -oxygen $p\pi$ orbital interactions.⁵ For example, the Nb atom moves from the center of the $[\text{NbOF}_5]^{2-}$ octahedron toward the oxide, forming a short Nb–O bond and a long *trans* Nb–F bond. This distortion is similar to that present in the technologically useful LiNbO_3 and KTiOPO_4 (KTP) materials. Other, secondary distortions are largely dependent on anion interactions with the extended bond network.

The first challenge one encounters in synthesizing a noncentrosymmetric material based on the $M^V\text{OF}_5^{2-}$ ($M = \text{V}, \text{Nb}, \text{Ta}$) or $M^{VI}\text{O}_2\text{F}_4^{2-}$ ($M = \text{Mo}, \text{W}$) anions is to prevent oxide-fluoride ligand disorder around the transition metal. The second is to prevent these anions from crystallizing in a centrosymmetric arrangement with respect to each other. The former, the challenge of O/F ordering, was overcome for all five anions, and led to an analysis of their intra-octahedral distortions.⁶ The latter, ordering in a noncentrosymmetric space group, was accomplished with the $[\text{NbOF}_5]^{2-}$ anion in inorganic-organic hybrid compounds, but, surprisingly, never in an inorganic solid-state environment.

In inorganic-organic hybrid structures with cluster⁷ and chain⁸ motifs, the residual charge distribution on the oxide and fluoride ions bound to the M metal center dictates which specific cationic contacts are made to the oxide and fluoride ions. In general, the oxide and *trans*-fluoride ions of the $[\text{NbOF}_5]^{2-}$ anion are the most reactive and preferentially coordinate to the extended bond network. Consequently, the $[\text{NbOF}_5]^{2-}$ anion is a *trans*-director. Similarly, one oxide ion and the fluoride ion *trans* to that oxide in $[\text{WO}_2\text{F}_4]^{2-}$ are the most nucleophilic⁹. In contrast, $[\text{MoO}_2\text{F}_4]^{2-}$ forms

primary contacts through the two fluoride ions *trans* to the two oxide ions and the anion is a *cis*-director. See Figure 2.1. Understanding these directional effects in early d^0 transition metal oxide fluoride anions is essential in the design of new noncentrosymmetric materials.

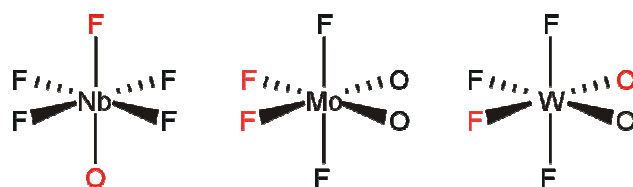


Figure 2.1. The $[\text{NbOF}_5]^{2-}$, $[\text{MoO}_2\text{F}_4]^{2-}$, and $[\text{WO}_2\text{F}_4]^{2-}$ anions. The most nucleophilic O^{2-}/F^- ions are drawn in red. Coordination with the extended bond network takes place through these sites.

The structure-directing role of octahedral oxide fluoride anions in inorganic solids has not been elucidated because the anions typically crystallize with the oxide and fluoride ions disordered. As a step toward the construction of new solids with ordered oxide and fluoride ions, it has proven effective to create multiple solid state contacts with different metal cations to the individual oxide and fluoride ions.^{10, 11} Pauling's second crystal rule (PSCR) states that in a crystal structure, anions with the largest negative charges will occupy positions of the largest positive potential (bond strength¹²). This rule has been further quantified with the bond valence model where the bond strengths are correlated to interatomic distances.¹³ As a result, this principle is

only applicable to compounds containing ordered oxide fluoride anions of the early d^0 transition metals where accurate bond lengths are obtained.

KNaNbOF_5 and CsNaNbOF_5 were targeted because the different alkali cations (K vs. Na and Cs vs. Na) should provide sufficiently different coordination environments to observe oxide and fluoride ordering^{14, 15}. Indeed, the six ions each reside on symmetry-unique positions and each is coordinated to the extended bond network in a unique manner. Because the individual $[\text{NbOF}_5]^{2-}$ anions adopt a single orientation within the structure, accurate Nb–O and Nb–F bond lengths are obtained. Moreover, the $[\text{NbOF}_5]^{2-}$ anions in KNaNbOF_5 crystallize in a noncentrosymmetric arrangement with respect to each other. The crystal structure analyses presented here examine the underlying causes of oxide-fluoride ordering in these two compounds, the effects of the extended bond network on the observed primary and secondary distortions, and how changes to the bond network lead to different crystal symmetries.

2.2 Synthesis and Characterization

2.2.1 Materials

Caution. Hydrofluoric acid is toxic and corrosive, and must be handled with extreme caution and the appropriate protective gear! If contact with the liquid or vapor occurs, proper treatment procedures should be followed immediately.¹⁶⁻¹⁸

Materials. Nb₂O₅ (99.9%, Aldrich), NaF (99.9%, Aldrich), KF (99.9%, Aldrich), RbF (99.9%, Aldrich), CsF (99.9%, Aldrich), and aqueous hydrofluoric acid (HF) (48% HF by weight, Aldrich) were used as received. Owing to their hygroscopic nature, the alkali fluorides were manipulated under nitrogen in a dry box.

2.2.2 Synthesis

All reactants were sealed in Teflon [fluoro(ethylenepropylene)] "pouches".¹⁹ The pouches were placed in a 125 mL Teflon (PTFE) lined Parr pressure vessel filled 33% with deionized H₂O as backfill. The pressure vessel was heated for 24 hours at 150°C and cooled to room temperature over an additional 24 hours. The pouches were opened in air, and the products were recovered by vacuum filtration.

KNaNbOF₅. KNaNbOF₅ was synthesized by reacting 0.0233 g (4.010×10^{-4} mol) of KF, 0.1000 g (4.010×10^{-4} mol) of Na₂NbOF₅ (see synthesis below), and 1.0 g (0.0555 mol) of deionized H₂O. Colorless plates were recovered in low yield. Increasing the amount of KF in the reaction vessel while holding all other starting materials constant led to the formation of K₂NaNbO₂F₄.²⁰ Decreasing the amount of KF in the reaction vessel led to the reprecipitation of Na₂NbOF₅. For further tests, polycrystalline KNaNbOF₅ was synthesized in 100% yields by solid-state methods by reacting stoichiometric amounts of KF and NaNbOF₄ at 385°C for 18 hours under flowing argon.

RbNaNbOF₅. Polycrystalline RbNaNbOF₅ was synthesized in high yields by solid-state methods by reacting stoichiometric amounts of RbF and NaNbOF₄ (see synthesis below) at 385°C for 18 hours under flowing argon.

CsNaNbOF₅. CsNaNbOF₅ was synthesized by reacting 0.0608 g (4.002×10^{-4} mol) of CsF, 0.1344 g (0.0032 mol) of NaF, 0.4253 g (0.0016 mol) of Nb₂O₅, and 1.200 g (0.0600 mol) of 48% aqueous HF. Colorless needles were recovered in 80% yield based on Nb. Increasing the CsF:NaF ratio while holding all other starting materials constant led to the formation of cesium niobium oxide fluoride salts. Decreasing the CsF:NaF ratio while holding all other starting materials constant led to the formation of Na₂NbOF₅. Synthesis of large amounts of polycrystalline CsNaNbOF₅ by solid-state methods for further tests was not pursued because its centrosymmetric crystal structure precludes SHG, ferroelectric, and piezoelectric activity.

NaNbOF₄ and Na₂NbOF₅. NaNbOF₄ was synthesized by reacting 0.1344 g (0.0032 mol) of NaF, 0.4253 g (0.0016 mol) of Nb₂O₅, and 1.200 g (0.0600 mol) of 48% aqueous HF for approximately 2 hours. A white polycrystalline powder was recovered in 88% yield based on Nb. Longer reaction times led to the destruction of the infinite chains of oxide-linked (NbO₂F₄)_n octahedra, and the formation of discrete [NbOF₅]²⁻ units to give Na₂NbOF₅²¹.

2.2.3 Crystallographic Determination

Single-crystal X-ray diffraction data were collected with Mo K α radiation ($\lambda = 0.71073 \text{ \AA}$) on a Bruker SMART-1000 CCD diffractometer and integrated with the SAINT-Plus program²². The structures were solved by direct methods and refined against F^2 by full-matrix least-squares techniques²³. A face-indexed absorption correction was performed numerically using the program XPREP. The value of the Flack parameter²⁴ in KNaNbOF₅, estimated at 0.27(0.10), was then refined and converged at 0.28(0.11), but with no improvement of R(F) (0.0420). The opposite configuration converged for a slightly higher R(F) value of 0.0433. Although no definitive assignment of the absolute structure can be made, these results indicate that the absolute configuration reported is likely correct. All structures were checked for missing symmetry elements with PLATON²⁵. The final refinement includes anisotropic displacement parameters. Crystallographic data for CsNaNbOF₅ and KNaNbOF₅ are given in Table 2.1.

Table 2.1. Crystallographic data for CsNaNbOF₅ and KNaNbOF₅.

Formula	CsNaNbOF ₅	KNaNbOF ₅
fw	359.81	266.01
Space group	Pbcn (No. 60)	Pna2 ₁ (No. 33)
a (Å)	8.3155(7)	11.8653(11)
b (Å)	13.3176(11)	5.8826(6)
c (Å)	11.1314(9)	8.1258(8)
V(Å ³)	1232.7(7)	567.2(5)
Z	8	4
T(°C)	-120(1)	-120(1)
λ(Å)	0.71069	0.71069
ρ _{calc} (g/cm ³)	3.88	3.12
μ (mm ⁻¹)	7.86	2.95
R(F) ^a	0.0266	0.0419
wR ₂ (F ²) ^b	0.0680	0.1132
Flack parameter	n/a	0.27(0.10)

$$^a R = \frac{\sum ||F_o| - |F_c||}{\sum |F_o|}$$

$$^b wR_2 = [\sum w(F_o^2 - F_c^2)^2 / \sum w(F_o^2)^2]^{1/2}$$

2.2.4 Second-Harmonic Generation Measurement

A powder second-harmonic test was carried out on the KNaNbOF₅ sample by means of the Kurtz-Perry method.¹⁷ About 100 mg of powder was hand-pressed into a pellet which was irradiated with a pulsed infrared beam (100 ns, 15 mJ, 10 Hz) produced by a Q-switched Nd:YAG laser of wavelength 1064 nm. A 532 nm filter was used to absorb the fundamental and pass the visible light onto a photomultiplier. A combination of a half-wave achromatic retarder and a polarizer was used to control the intensity of the incident power, which was measured with an identical photomultiplier connected to the same high voltage source. This procedure was then repeated using a

standard nonlinear optical material, in this case microcrystalline KH_2PO_4 (KDP), and the ratio of the second-harmonic intensity outputs was calculated. Since the SHG efficiency of powders has been shown to depend strongly on particle size,^{26, 27} polycrystalline KNaNbOF_5 was ground and sieved (Newark Wire Cloth Company) into distinct particle size ranges (20–120 μm). To make relevant comparisons with known SHG materials, crystalline SiO_2 and LiNbO_3 were ground and sieved into the same particle size ranges. KNaNbOF_5 , like LiNbO_3 , was phase-matchable. The SHG response of KNaNbOF_5 was determined to be $0.6 \times \text{KDP}$. Graphs of SHG responses vs. particle sizes for LiNbO_3 , $\alpha\text{-SiO}_2$, and KNaNbOF_5 are available in Figure 2.2.

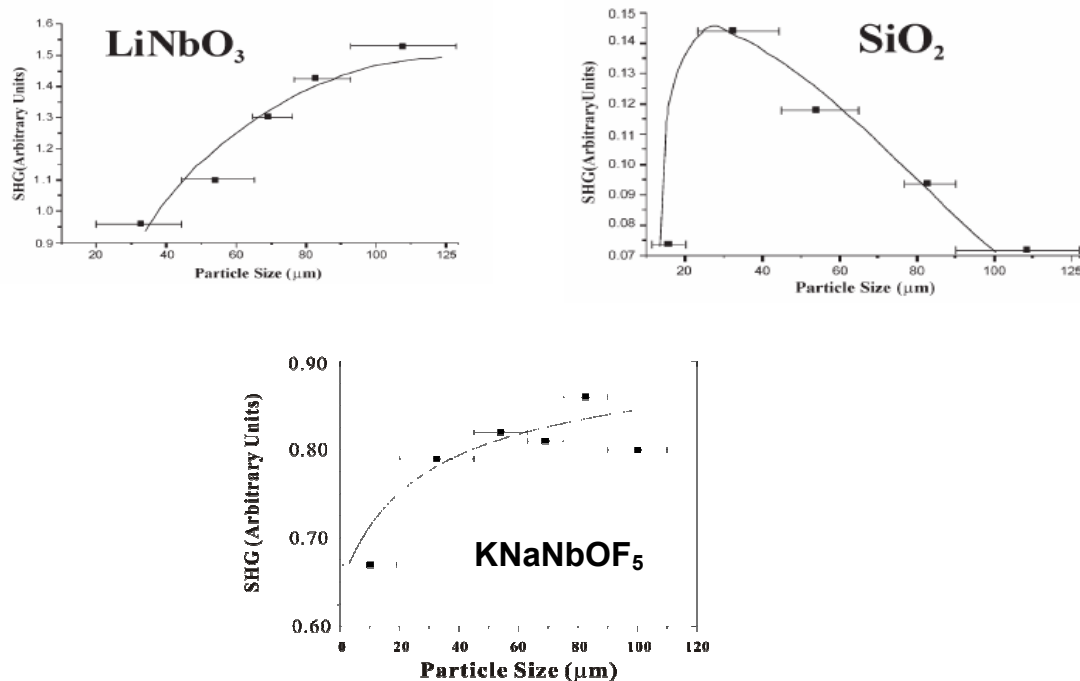


Figure 2.2. Graphs of SHG responses vs. particle sizes for phase-matchable LiNbO_3 , non-phase-matchable SiO_2 , and phase-matchable KNaNbOF_5 .

2.3 Extended Structures

Polyhedral representations of KNaNbOF_5 and CsNaNbOF_5 are shown in Figures 2.3 and 2.4. Individual six-coordinate Na, eight-coordinate K, and eight-coordinate Cs polyhedra are also shown. For the sake of comparison between the two structures, a maximum Cs–F bond distance of 3.40 Å has been chosen. However, the Cs1 and Cs2 coordination numbers can be increased to ten and twelve, respectively, if

this value is fixed at 3.56 Å. Both the KNaNbOF_5 and CsNaNbOF_5 structures can be described as three-dimensional frameworks formed of (001) and (100) $[\text{NaNbOF}_7]_\infty$ layers stacked along c and a , respectively. The layers are composed of smaller $[\text{NaNbO}_2\text{F}_8]^{6-}$ building units that delineate four-sided windows, which stack to form channels. The K^+ and Cs^+ cations are located in these channels. See Figure 2.5.

In KNaNbOF_5 , the Nb–O(1) bond length is 1.745(5) Å, while the *trans* fluoride Nb–F(1) bond length is 2.114(4) Å. As expected, the Nb atom is located out of the plane formed by the equatorial fluorides, whose Nb–F distances range from 1.940(5) to 1.968(4) Å. In CsNaNbOF_5 , the Nb–O(1) bond length is 1.800(3) Å and the *trans* fluoride Nb–F(1) bond length is 2.056(2) Å, i.e. longer and shorter, respectively, than the corresponding bond lengths in KNaNbOF_5 . The Nb atom, located out of the plane formed by the equatorial fluorides, forms four equatorial Nb–F bonds with distances that range from 1.930(2) to 1.955(2) Å. Selected bond distances are reported in Tables 1.2 and 1.3, with their associated experimental and theoretical bond valences and bond valence sums.

Based on powder diffraction data, RbNaNbOF_5 is isostructural with CsNaNbOF_5 (See Figure 2.6)

Table 2.2. Selected Bond Lengths, Experimental Bond Valences, Theoretical Bond Valences, Bond Valence Sums, BSI and GII indices for KNaNbOF₅.

KNaNbOF ₅	K	Na	Nb	$V_i = \sum_j S_{ij}$ $z_i = \sum_j s_{ij}$
R_{ij} (Å)	2.834(5)	2.343(6)	1.745(5)	
S_{ij} (vu) O	0.15	0.23	1.57	1.95
s_{ij} (vu)	0.43	0.45	1.12	2.00
R_{ij} (Å)	2.638(4)	2.726(4)	2.250(4)	2.114(4)
S_{ij} (vu) F1	0.17	0.14	0.21	0.52
s_{ij} (vu)	0.07	0.07	0.10	0.76
R_{ij} (Å)	2.732(2)		2.257(6)	1.946(4)
S_{ij} (vu) F2	0.14		0.21	0.81
s_{ij} (vu)	0.10		0.12	0.79
R_{ij} (Å)	2.700(4)	2.826(4)	2.446(5)	1.968(4)
S_{ij} (vu) F3	0.15	0.10	0.12	0.77
s_{ij} (vu)	0.07	0.07	0.10	0.76
R_{ij} (Å)	2.822(5)		2.297(8)	1.940(5)
S_{ij} (vu) F4	0.11		0.19	0.83
s_{ij} (vu)	0.10		0.12	0.79
R_{ij} (Å)	2.853(4)		2.205(5)	1.941(4)
S_{ij} (vu) F5	0.10		0.24	0.83
s_{ij} (vu)	0.10		0.12	0.79
$V_j = \sum_i S_{ij}$	1.05	1.21	5.32	BSI = 0.15
$z_j = \sum_i s_{ij}$	1.00	1.00	5.00	GII = 0.16

R_{ij} = bond length of the bond "ij".

S_{ij} = $\exp[(R_0 - R_{ij})/B]$ experimental bond valence of bond "ij", where R_0 = constant dependent on i and j bonded elements, and $B = 0.37$.

$R_0(\text{Nb-O}) = 1.911$, $R_0(\text{Nb-F}) = 1.87$; $R_0(\text{Na-O}) = 1.803$, $R_0(\text{Na-F}) = 1.677$;

$R_0(\text{Cs-O}) = 2.417$, $R_0(\text{Cs-F}) = 2.33$; $R_0(\text{K-O}) = 2.132$, $R_0(\text{K-F}) = 1.992$.

s_{ij} = theoretical bond valence of bond "ij", calculated by solving the network equations based

on the methods described by Brown.^{28, 29}

V_i , V_j = experimental valences of anions "i" and cations "j".

z_i , z_j = charge or formal valence of anions "i" and cations "j".

BSI = $[\langle (S_{ij} - s_{ij})^2 \rangle]^{1/2}$ Bond Strain Index.

GII = $[\langle (V_{ij} - z_{ij})^2 \rangle]^{1/2}$ Global Instability Index.

Table 2.3. Selected Bond Lengths, Experimental Bond Valences, Theoretical Bond Valences, Bond Valence Sums, BSI and GII indices for CsNaNbOF₅.

CsNaNbOF ₅ ^a	Cs1	Cs2	Na	Nb	$V_i = \sum_j S_{ij}$ $z_i = \sum_j s_{ij}$
R _{ij} (Å)	2 × 3.247(3)	2 × 3.231(3)	2.300(3)	1.800(3)	
S_{ij} (vu)	2 × 0.11	2 × 0.11	0.26	1.35	1.83
<i>s_{ij} (vu)</i>	2 × 0.31	2 × 0.31	0.36	1.03	2.00
R _{ij} (Å)	2 × 3.037(2)	2 × 2.964(2)	2.259(3)	2.056(2)	
S_{ij} (vu)	2 × 0.15	2 × 0.18	0.21	0.60	1.14
<i>s_{ij} (vu)</i>	2 × 0.06	2 × 0.06	0.11	0.78	1.00
R _{ij} (Å)	2 × 3.202(2)		2.293(2)	1.941(2)	
S_{ij} (vu)	2 × 0.10		0.19	0.82	1.11
<i>s_{ij} (vu)</i>	2 × 0.08		0.13	0.79	1.00
R _{ij} (Å)	2 × 3.110(2)	2 × 3.045(2)	2.401(3)	1.955(2)	
S_{ij} (vu)	2 × 0.12	2 × 0.14	0.14	0.79	1.20
<i>s_{ij} (vu)</i>	2 × 0.06	2 × 0.06	0.11	0.78	1.00
R _{ij} (Å)			2.318(2)	1.946(2)	
S_{ij} (vu)			0.18	0.81	0.99
<i>s_{ij} (vu)</i>			0.17	0.83	1.00
R _{ij} (Å)		2 × 3.335(2)	2.238(3)	1.930(2)	
S_{ij} (vu)		2 × 0.07	0.22	0.85	1.14
<i>s_{ij} (vu)</i>		2 × 0.08	0.13	0.79	1.00
$V_j = \sum_i S_{ij}$	0.94	1.00	1.20	5.24	BSI = 0.12
$z_j = \sum_i s_{ij}$	1.00	1.00	1.00	5.00	GII = 0.15

Table 2.4. Estimations of the negative potentials of the ions of the $(\text{NbOF}_5)^{2-}$ anions and the surrounding positive potentials in CsNaNbOF_5 and KNaNbOF_5 , through bond strength and bond valence calculations.

CsNaNbOF₅			
Bond	Anionic BV (vu) ^a	Cationic PSCR sum (vu) ^b	Cationic BV sum (vu) ^c
Nb–O	0.65	0.42	0.48
Nb–F1	0.40	0.42	0.54
Nb–F2	0.17	0.29	0.28
Nb–F3	0.21	0.42	0.40
Nb–F4	0.19	0.17	0.18
Nb–F5	0.15	0.29	0.29
KNaNbOF₅			
Bond	Anionic BV (vu) ^a	Cationic PSCR sum (vu) ^b	Cationic BV sum (vu) ^c
Nb–O	0.43	0.29	0.38
Nb–F1	0.48	0.42	0.52
Nb–F2	0.19	0.29	0.33
Nb–F3	0.23	0.42	0.38
Nb–F4	0.17	0.29	0.30
Nb–F5	0.17	0.29	0.34

^a Anionic BV (Bond Valence) = $z_i - S_{\text{Nb-O/F}}$, where z_i is the electric charge of each ligand and $S_{\text{Nb-O/F}}$ is taken from the Table 2 or 3 for each Nb–O/F bond.

^b Cationic PSCR sum = $\sum_j \mathbf{s}'_{j,\text{cat}} = \sum_j \frac{z_{j,\text{cat}}}{v_{j,\text{cat}}}$, where $z_{j,\text{cat}}$ is the electric charge of each A_i alkali cation bonded to a given ligand and $v_{j,\text{cat}}$ is its coordination number.

^c Cationic BV (bond valence) sum = $\sum_i S_{i,\text{cat}}$, where $S_{i,\text{cat}}$ is taken from Table 2 or 3 for each A_i –O/F bond.

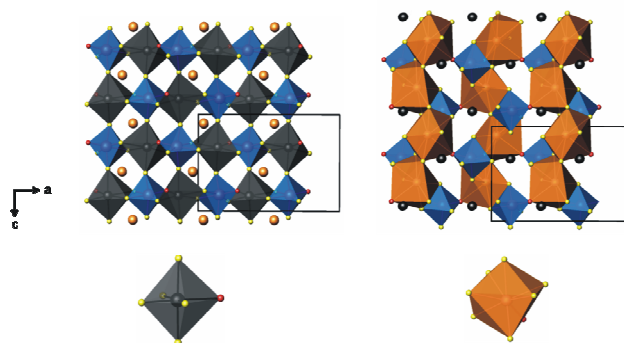


Figure 2.3. The coordination polyhedra in KNaNbOF_5 . Blue octahedra are $[\text{NbOF}_5]^{2-}$ anions, black octahedra are Na-centered and eight-coordinate orange polyhedra are K-centered. In the above schematic, all drawings are shown in the (010) plane with different polyhedra highlighted in each.

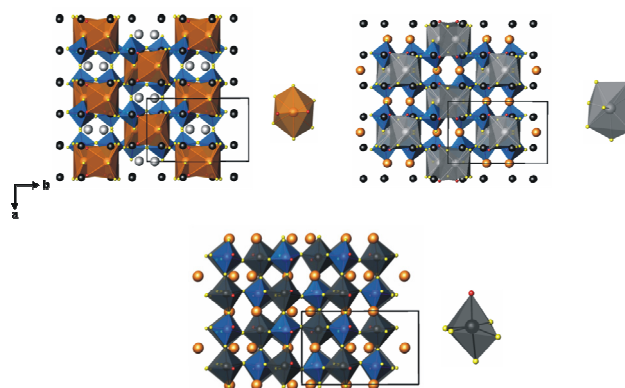


Figure 2.4. The coordination polyhedra in CsNaNbOF_5 . Blue octahedra are $[\text{NbOF}_5]^{2-}$ anions, black octahedra are Na-centered, eight-coordinate orange polyhedra are Cs1-centered and eight-coordinate grey polyhedra are Cs2-centered. In the above schematic, all drawings are shown in the (001) plane with different polyhedra highlighted in each.

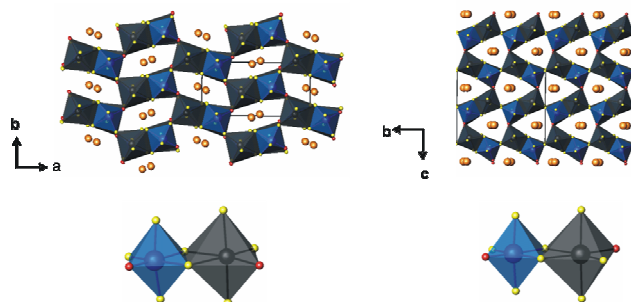


Figure 2.5. A view of the three-dimensional frameworks in KNaNbOF_5 (left) and CsNaNbOF_5 (right), formed of (001) and (100) $[\text{NaNbOF}_7]_\infty$ layers stacked along c and a , respectively. Insets are views of the framework structural building unit.

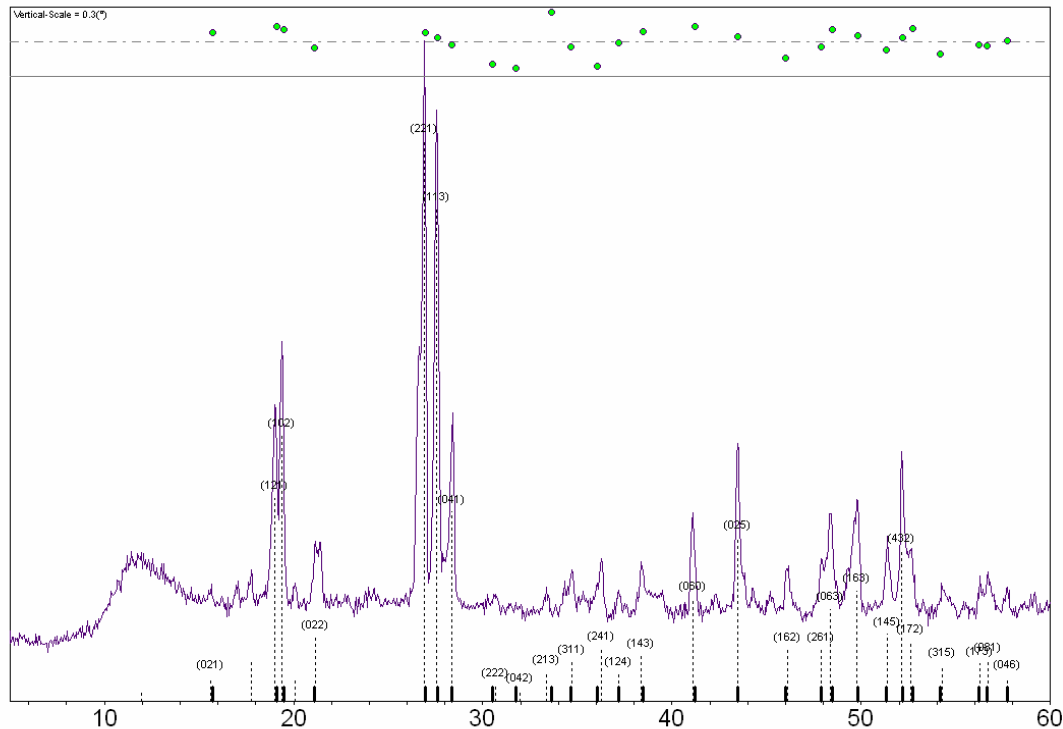


Figure 2.6. X-ray diffraction data for RbNaNbOF_5 . The diffraction data were refined in pattern-matching mode using the JADE software program in the orthorhombic space group Pbcn to lattice constants $a = 8.157 \text{ \AA}$, $b = 13.137 \text{ \AA}$, and $c = 10.956 \text{ \AA}$. This represents a 4.8 % volume decrease compared to the CsNaNbOF_5 phase. A small amount of a second phase (*) identified as Rb_2NbOF_5 ^{42,43} is also present in the sample.

2.4 Anion Ordering and the Observance of Pauling's Second Crystal Rule

The construction of noncentrosymmetric materials from early d^0 transition metal oxide fluoride anions first requires that the oxide and fluoride ions crystallize without

disorder. This is the case in both KNaNbOF_5 and CsNaNbOF_5 . Oxide/fluoride order can be understood in the context of Pauling's second crystal rule, which states that anions with the largest negative potentials will occupy sites having the largest positive potentials. The assessment of the positive potential in the crystal frameworks, carried out by calculating the PSCR (bond strength) sum³⁰ and bond valence sum^{13, 31} around each anionic position, should match as closely as possible the assessment of the negative potentials of each oxide and fluoride ion (Tables 2.2, 2.3 and 2.4). The central Nb atom has been excluded from the PCSR calculations since we are only interested in the oxide/fluoride interactions with the extended network.

In inorganic-organic hybrid compounds that contain the $[\text{NbOF}_5]^{2-}$ anion, the anions connect to the extended network through the most charged oxide and fluoride ions. Similarly, in KNaNbOF_5 , the F1 and F3 fluoride ions, which occupy positions in contact with two eight-coordinate K^+ cations and one six-coordinate Na^+ cation ($2 \times 1/8 + 1/6 = 0.42$ PSCR sum and bond valence sums of 0.52 and 0.38 vu, respectively), retain the most negative potential (0.48 and 0.23 vu, respectively). The three remaining fluorides have less negative potential: 0.19, 0.17 and 0.17 vu for F2, F4 and F5, respectively. They are each two-coordinate, with lower bond valence sums of 0.33, 0.30, and 0.34 vu, respectively, and PSCR sums of 0.29 (Table 2.4 and Figure 2.7). The same behavior is observed in CsNaNbOF_5 where the three-coordinate anionic sites are occupied by the three most nucleophilic ions (O1, F1 and F3) while F2, F4, and F5 are less reactive and are one- or two-coordinate (Table 2.4 and Figure 2.8).

The observation that the O1 site in KNaNbOF_5 makes only two cationic contacts, in contrast to a high negative potential (0.43 vu), is understandable when other crystal chemical factors are considered. The polarizability of the oxide and fluoride ions also influences their interactions with the extended bond network. For instance, the “harder” (relative to oxide) F1 *trans*-fluoride interacts with three small, relatively non-polarizable Na^+ (2.250(4) Å) and K^+ (2.638(4) Å and 2.726(4) Å) cations. At the same time, the central Nb atom displaces away from the *trans*-fluoride toward the “softer” oxide ion, which only attracts two cations, one Na^+ at 2.343(6) Å and one K^+ at 2.834(5) Å. In contrast, the oxide ion in CsNaNbOF_5 is three-coordinate, owing to the larger size of Cs^+ .

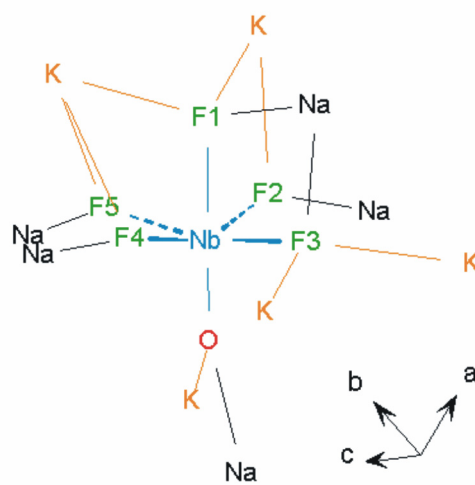


Figure 2.7. The asymmetric coordination environment surrounding the $[\text{NbOF}_5]^{2-}$ anion in KNaNbOF_5 . The ions with the most local negative charge make the most/strongest contacts to the extended bond network.

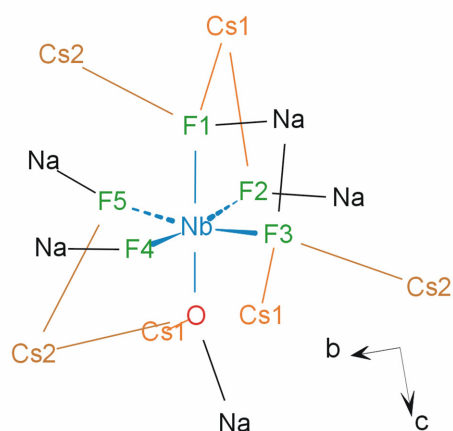


Figure 2.8. The asymmetric coordination environment surrounding the $[\text{NbOF}_5]^{2-}$ anion in CsNaNbOF_5 . The ions with the most local negative charge make the most/strongest contacts to the extended bond network.

2.5 Noncentrosymmetry vs. Centrosymmetry

Oxide/fluoride ordering is only the first condition that must be met to engineer noncentrosymmetric materials with (V, Nb, or Ta)OF₅²⁻ or (Mo, or W)O₂F₄²⁻ anions. The anions must also crystallize in an acentric arrangement with respect to one another. Predictability in this second step can be achieved through an understanding of bond network-anion interactions.

Both KNaNbOF₅ and CsNaNbOF₅ contain channels that run along the length of the *b* axes. The K⁺ cations move from the centers of the channels towards the trans-fluoride ligands (Table 2.2), the sites on the [NbOF₅]²⁻ anions with the most negative electrostatic potential (Figure 2.9), resulting in a 2₁ screw axis along *c*. In contrast, the larger Cs⁺ cations occupy inversion centers in the channel centers.

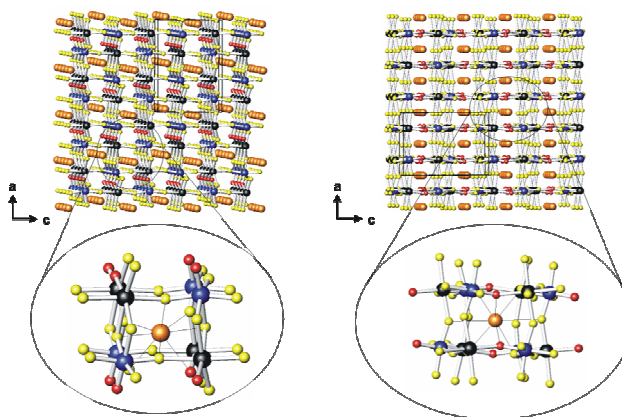


Figure 2.9. Channels formed by the Nb/Na–O/F framework run along the length of the *b* axis in KNaNbOF₅ (left) and CsNaNbOF₅ (right). Inset are enlarged views of the channel openings with cation coordination shown.

2.6 Intraoctahedral Distortions and the Observed SHG response in KNaNbOF₅

The complete alignment of dipole moments along the polar axis of a structure has been cited as the basis for highly efficient nonlinear optical materials, quantified by a structural parameter (C)¹. The polar distortion present in the $[\text{NbOF}_5]^{2-}$ anion is similar in magnitude to that of the NbO_6 octahedron in LiNbO_3 .³² However, the influence of bond networks are reported to play a role in altering the metal oxide fluoride polyhedra from their idealized geometries.⁶

Both compounds exhibit primary, Nb–O distortions owing to crystallographic order of the octahedral anion. Centrosymmetry precludes the dipoles in CsNaNbOF₅ from summing in an additive manner. KNaNbOF₅ crystallizes in point group class

mm², and thus, though the individual bond dipoles do not align in an additive manner, they do not completely cancel each other. See Figure 2.10. The net polarity of KNaNbOF₅ leads to a fairly high SHG response ($0.6 \times \text{KDP}$). This value seems reasonable when it is considered that the NbO₆ octahedron is capable of producing SHG responses on the order of $13 \times \text{KDP}$, as in LiNbO₃.³³ Similarly, in borates, a common group of SHG materials, partial cancellation of the second-order susceptibilities does not preclude the observation of a significant SHG response. For example, the BO₃ groups in the recently discovered Li₆CuB₄O₁₀ are oriented in opposite directions in alternating planes, yet an SHG response similar to that in KDP is observed.³⁴ In β -BaB₂O₄, the second-order susceptibility tensors cancel to a lesser extent, and an SHG response of $4 \times \text{KDP}$ is observed.³⁵

Because the coordination sites of the bond network are asymmetrically arranged about the anion in both KNaNbOF₅ and CsNaNbOF₅, secondary distortions can be observed.³⁶ Unlike the primary, second-order Jahn-Teller distortions which are inherent to the $[\text{MO}_x\text{F}_{6-x}]^{2-}$ anions, these distortions arise from interactions between the extended three-dimensional bond network and the oxide and fluoride ions. When a ligand in a $[\text{MO}_x\text{F}_{6-x}]^{2-}$ anion interacts with its cationic environment, the *M*-O or *M*-F bond is weakened somewhat while its length increases to maintain its atomic valence, following the distortion theorem of the bond valence model. As a result, the central transition metal forms shorter, stronger bonds with the other oxide and fluoride ligands.^{6, 36}

The $[\text{NbOF}_5]^{2-}$ anion in KNaNbOF_5 exhibits a secondary distortion caused by electrostatic interactions with its cationic environment. Three cationic contacts are made to F3, while the remaining equatorial fluorides accept only two cationic contacts each (Table 2.2 and Figure 2.7). Consequently, the niobium-equatorial fluoride bond length, Nb–F3 (1.968(4) Å), is significantly larger than the remaining three at 1.940(5), 1.941(4), and 1.946(4) Å. The difference in Nb-equatorial fluoride bond lengths shows that as the coordination number of an oxide or fluoride ion on the $[\text{NbOF}_5]^{2-}$ group increases, the strength of its interaction with the central Nb atom decreases. It is interesting to note in this context that $M\text{--O/F}$ bond weakening also occurs in $\text{Cs}_2\text{WO}_2\text{F}_4$ ³⁷, where each oxide or fluoride anion is surrounded by four equidistant cesium cations so that each ligand is in an identical coordination environment and the anion is disordered. In contrast, in $\text{Na}_2\text{WO}_2\text{F}_4$ ³⁸, each oxide or fluoride ligand is coordinated by only two sodium cations and the anion retains $\text{W}\text{--O/F}$ ordering.

The secondary distortion in CsNaNbOF_5 shares the same bond axis as the primary, Nb–O distortion. It is detectable, however, through comparison to the primary distortion in KNaNbOF_5 . Tables 2.2 and 2.3 list the O^{2-}/F^- ions and their cationic interactions for KNaNbOF_5 and CsNaNbOF_5 , respectively. Clearly, the $[\text{NbOF}_5]^{2-}$ anion is connected to the extended bond network in similar fashions: the fluoride *trans* to the oxide ligand and one equatorial fluoride accept three cationic contacts, while the remaining fluoride ions accept two or one. See Figures 2.7 and 2.8. The striking difference occurs at the oxide ions. The KNaNbOF_5 oxide ligand makes two cationic

contacts whereas the CsNaNbOF_5 oxide ligand makes three. As a result the Nb–O bond in CsNaNbOF_5 (1.800(3) Å) is lengthened relative to the Nb–O bond in KNaNbOF_5 (1.744(5) Å). The difference in these two bond lengths can be taken as the lower limit of the magnitude of the secondary distortion in CsNaNbOF_5 . The exact magnitude cannot be determined because a secondary distortion, though weaker, must also be present along the O–Nb–F axis in KNaNbOF_5 owing to an inequality in the strength of the interactions between the oxide and *trans*-fluoride ions. The observation that increasing the number of ionic contacts to the oxide ligand in a $[\text{MO}_x\text{F}_{6-x}]^{2-}$ anion leads to a decrease in the primary distortion of the anion agrees with previous computational work where it was shown that as the number of bond network contacts made to the $[\text{NbOF}_5]^{2-}$ group increases, the steady weakening of the Nb–O interaction is due almost solely to a loss of π bonding³⁹.

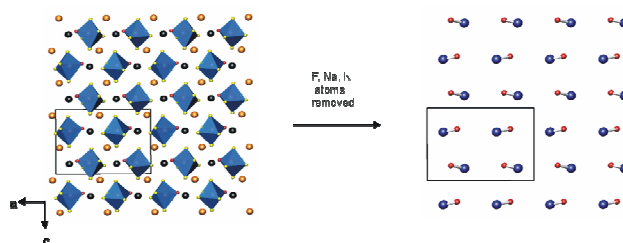


Figure 2.10. A view of the primary Nb–O distortions in KNaNbOF_5 including all atoms (left) and only Nb and O atoms (right). The partial addition of the individual bond dipoles is enough to observe a significant SHG response ($0.6 \times \text{KDP}$).

2.7 Analysis of Structural Strain

The primary electronic and secondary bond network-induced intraoctahedral distortions present in these compounds clearly cause deviations from PSCR which can be measured by determining the extent to which each structure violates the valence sum and equal valence rules. The valence sum rule²⁸ states the sum of experimental bond valences around each atom is equal to the atomic valence, while the equal valence rule²⁸ states the sum of bond valences around any loop in the bond network, with regard to the direction of the bond, is zero. These rules are collectively known as the network equations.²⁸ Their solutions, reported in tables 2.2 and 2.3, are referred to as theoretical bond valences (s_{ij}). For example (see Table 2.2), the K^+ bonds to F1 and F3, and F2, F4 and F5 have s_{ij} values of 0.07 vu and 0.10 vu, respectively, reflecting the fact that F1 and F3 are four-coordinate and F2, F4 and F5 are three-coordinate. Similarly, s_{ij} values for oxide bonds (K-O, Na-O, Nb-O) are greater than those for fluoride bonds owing to the oxide ion's higher negative charge. The ionic nature of the K-O and Na-O bonds accounts for the larger percentage the s_{K-O} (.43 of 1.00) and s_{Na-O} (.45 of 1.00) values contribute to the cation valence relative to the s_{Nb-O} value (1.12 of 5.00). The Nb^{5+} cation distributes its valence more equally among the ions in its coordination sphere.

Two indices have been proposed to measure the extent to which a structure violates the network equations. The global instability index (GII⁴⁰) and bond strain index (BSI⁴¹) measure deviation from the valence sum rule and equal valence rule, respectively. A GII or BSI value greater than 0.05 vu indicates a structure is strained while a GII value greater than 0.20 vu indicates a structure is unstable. The high values for both indices of KNaNbOF₅ and CsNaNbOF₅ indicate the structures are distorted. The BSI value for KNaNbOF₅ (BSI = 0.15) is significantly larger than that for CsNaNbOF₅ (BSI = 0.12), while the GII have similar values (0.16 and 0.15, respectively). The larger BSI and GII values for KNaNbOF₅ reflect the presence of primary and secondary distortions that are collectively greater in magnitude than those observed in CsNaNbOF₅. The stronger primary distortion observed in KNaNbOF₅ is also empirically apparent in the higher theoretical bond valence of the Nb-O bond (1.12 vu) compared to that of the CsNaNbOF₅ Nb-O bond (1.03 vu). Increased cationic contact to the oxide ion clearly weakens the primary Nb-O distortion. Thus, it is expected that in a series of compounds composed of the same basic building units, i.e. [NbOF₅]²⁻ and alkali cations, the one that is noncentrosymmetric and polar will have the greatest value of both the BSI and GII.

2.8 Conclusions

The interactions of the $[\text{NbOF}_5]^{2-}$ anion with the combination of Na/K or Na/Cs differ significantly. These lattice-derived secondary distortions, in addition to the primary electronic distortions they act upon, lead to a shorter Nb–O bond and oxygen being two-coordinate in the case of Na/K versus a longer Nb–O bond with oxygen three-coordinate for the combination Na/Cs. Thus, the noncentrosymmetric structure (KNaNbOF_5) maintains the larger primary electronic distortion of the $[\text{NbOF}_5]^{2-}$ anion along with a low coordination number of the electropositive K-ion consistent with the largest bond strain index (BSI). In contrast, the Cs-ions of the centrosymmetric structure (CsNaNbOF_5) can exhibit significantly higher coordination numbers and the $[\text{NbOF}_5]^{2-}$ anion a greatly reduced primary distortion. Thus, structures that increase the number of cationic contacts to the oxide ion, which weaken the metal $d\pi$ -oxygen $p\pi$ interaction, are unlikely to result in noncentrosymmetric, polar structures.

2.9 Corrections and Additions

The $R_0(\text{Nb-F})$ value of 1.87 Å used to calculate the bond valences reported in tables 2.2 and 2.3 led to an overestimation of the amounts of strain, reflected in the high BSI and GII values, in both KNaNbOF_5 and CsNaNbOF_5 . The crystal chemistry which distinguishes the two structures, however, remains the same. That is, the small K^+ cation

makes fewer contacts to the $[\text{NbOF}_5]^{2-}$ anion than the Cs^+ cation and so KNaNbOF_5 retains a stronger, primary Nb-O distortion than CsNaNbOF_5 and is noncentrosymmetric and polar. If the value 1.822 \AA is used for $R_0(\text{Nb-F})$, the BSI and GII values in both KNaNbOF_5 and CsNaNbOF_5 are significantly lowered and the valences of the Nb atoms more closely approach 5^+ . Revised tables in which the value $R_0(\text{Nb-F}) = 1.822 \text{ \AA}$ is used to calculate the bond valences for KNaNbOF_5 and CsNaNbOF_5 are given in the appendix .

CHAPTER THREE

Chemical Hardness and the Structure-Directing Role of

the cis-oxo $[\text{WO}_2\text{F}_4]^{2-}$ Anion

3.1 Introduction

Noncentrosymmetric materials are a fertile topic of research owing to the important physical properties that may be observed in such materials: pyroelectricity, ferroelectricity, piezoelectricity or second harmonic generation (SHG). Optimization of the latter property has been based largely on Chen's anionic group theory,¹ which attributes the SHG response in a material to the anionic group and has led to the discovery of new NLO borates, for example, $\text{KBe}_2\text{BO}_3\text{F}^2$ and $\text{Sr}_2\text{Be}_2\text{B}_2\text{O}_7$.³ While the selection of anionic groups that result in high nonlinearities is a successful method, it does not guarantee that noncentrosymmetry, one of the requirements for SHG materials, will be fulfilled.⁴ The synthesis of noncentrosymmetric materials requires an intimate understanding of the relationship between the anionic group and the surrounding network of bonds in a crystal. The isostructural $\text{Rb}_3\text{Na}(\text{NbOF}_5)_2 \cdot \text{H}_2\text{O}$, $\text{Rb}_3\text{Na}(\text{MoO}_2\text{F}_4)_2 \cdot \text{H}_2\text{O}$, $\text{Rb}_3\text{Na}(\text{WO}_2\text{F}_4)_2 \cdot \text{H}_2\text{O}$, and $\text{K}_3\text{Na}(\text{WO}_2\text{F}_4)_2 \cdot \text{H}_2\text{O}$ phases have been synthesized to probe this relationship. One $[\text{MO}_x\text{F}_{6-x}]^{n-}$ ($x = 1$ for $M = \text{Nb}^{5+}$, ($n = 2$) and $x = 2$ for $M = \text{Mo}^{6+}$, W^{6+} ($n = 2$)) anion is ordered and the other is partially ordered, and although these phases crystallize in a centrosymmetric space group, the observed effects of the bond networks on the geometries of the $[\text{NbOF}_5]^{2-}$, $[\text{MoO}_2\text{F}_4]^{2-}$, and $[\text{WO}_2\text{F}_4]^{2-}$ anions provide insight for their use as acentric building blocks.

Inherent to the $[\text{MO}_x\text{F}_{6-x}]^{n-}$ anions are out-of-center "primary" electronic distortions that arise from metal $d\pi$ -oxygen $p\pi$ orbital interactions.⁵ For example, the Nb atom moves from the center of the $[\text{NbOF}_5]^{2-}$ octahedron toward the oxide, forming

a short Nb–O bond and a long *trans* Nb–F bond. Similarly, in keeping with its oxide stoichiometry, the Mo center in the dioxo $[\text{MoO}_2\text{F}_4]^{2-}$ anion distorts toward the *cis* oxides (edge), forming two short M–O bonds and two long *trans* M–F bonds (Figure 3.1).⁶ Bond valence calculations⁷ can be used to explain the intraoctahedral geometries of the $[\text{MO}_x\text{F}_{6-x}]^{n-}$ anions when accurate bond lengths are available owing to crystallographic order of the anions.⁶ Historically, the $[\text{NbOF}_5]^{2-}$ and $[\text{MoO}_2\text{F}_4]^{2-}$ anions are much easier to order than the $[\text{WO}_2\text{F}_4]^{2-}$ anion owing to a significant difference between the nucleophilicities of the two most reactive oxide or fluoride ions and the remaining four O^{2-}/F^- ions bound to Nb or Mo.^{6, 8} As a result, two cationic contacts made to the O^{2-}/F^- ions with the most residual negative charge are sufficient to order the $[\text{NbOF}_5]^{2-}$ and $[\text{MoO}_2\text{F}_4]^{2-}$ anions. These contacts are always made to two *trans* positions and two *cis* positions, respectively. Thus, the $[\text{NbOF}_5]^{2-}$ anion is labeled a *trans*-director and the $[\text{MoO}_2\text{F}_4]^{2-}$ anion a *cis*-director.⁶ In contrast, the twice ordered $[\text{WO}_2\text{F}_4]^{2-9, 10}$ anion has three or four nucleophilic O^{2-}/F^- ions and requires an increased number of cationic contacts which may be made in either a *trans* or a *cis* fashion. See table 3.1.

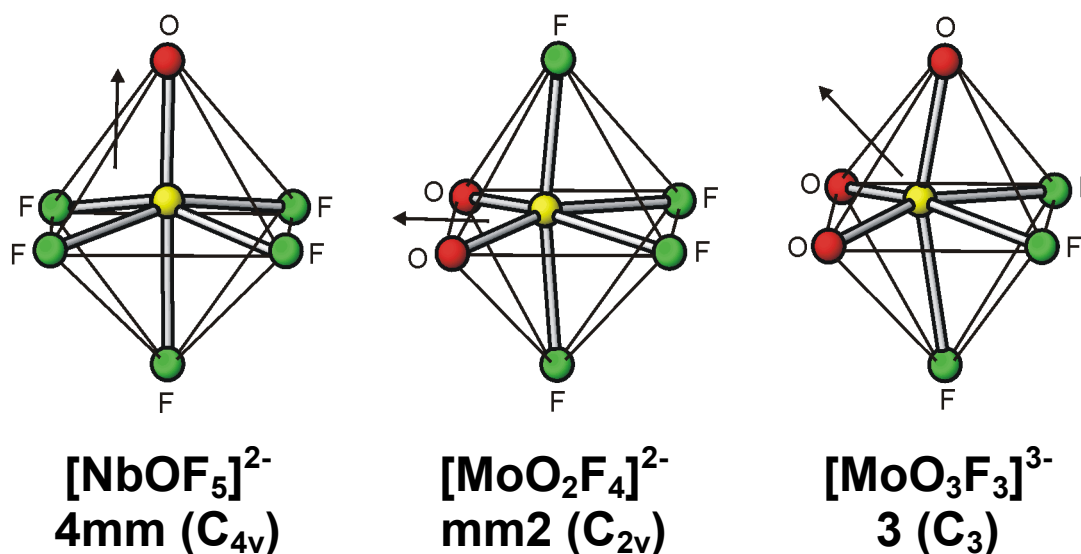


Figure 3.1. The distortion directions of the $[\text{NbOF}_5]^{2-}$ (corner), $[\text{MoO}_2\text{F}_4]^{2-}$ (edge), and $[\text{MoO}_3\text{F}_3]^{2-}$ (face) anions. Stoichiometry dictates the distortion direction of the transition metal center. The $[\text{WO}_2\text{F}_4]^{2-}$ anion, therefore, displays an edge-type distortion.

Table 3.1. Bond Valence Sums for the $[\text{WO}_2\text{F}_4]^{2-}$ Anion in $[\text{HNC}_6\text{H}_6\text{OH}]_2[\text{Cu}(\text{NC}_5\text{H}_5)_4(\text{WO}_2\text{F}_4)_2]$ and $\text{Na}_2\text{WO}_2\text{F}_4$

	R_i (Å)	S_i	$V - S_i$	Cationic BV Sum
$[\text{HNC}_6\text{H}_6\text{OH}]_2[\text{Cu}(\text{NC}_5\text{H}_5)_4(\text{WO}_2\text{F}_4)_2]$				
W-O(1)	1.772(2)	1.50	0.50	
W-O(2)	1.714(2)	1.75	0.25	
W-F(1)	2.059(2)	0.54	0.46	
W-F(2)	2.029(2)	0.58	0.42	
W-F(3)	1.903(2)	0.82	0.18	
W-F(4)	1.908(2)	0.81	0.19	
$\text{Na}_2\text{WO}_2\text{F}_4$				
W-O x 2	1.750(9)	1.57	0.43	0.36
W-F(1) x 2	1.932(8)	0.77	0.23	0.33
W-F(2) x 2	2.039(9)	0.58	0.42	0.43

Owing to the difficulty associated with ordering the $[\text{WO}_2\text{F}_4]^{2-}$ anion, only two compounds containing ordered $[\text{WO}_2\text{F}_4]^{2-}$ anions were reported prior to this work: $\text{Na}_2\text{WO}_2\text{F}_4$ ¹⁰ and $[\text{HNC}_6\text{H}_6\text{OH}]_2[\text{Cu}(\text{NC}_5\text{H}_5)_4(\text{WO}_2\text{F}_4)_2]$ ⁹. The $[\text{WO}_2\text{F}_4]^{2-}$ anion in $[\text{HNC}_6\text{H}_6\text{OH}]_2[\text{Cu}(\text{NC}_5\text{H}_5)_4(\text{WO}_2\text{F}_4)_2]$ directs coordination in a *trans* fashion because one oxide ion and its *trans* fluoride are most reactive because they retain more residual negative charge than the remaining oxide and fluoride ions (Table 3.1). The $[\text{WO}_2\text{F}_4]^{2-}$ anion in $\text{Na}_2\text{WO}_2\text{F}_4$ possesses equivalent, symmetry-related oxide ions (0.43 vu) that are more reactive than the remaining ions bound to the tungsten metal center. See table 3.1. However, the slightly less reactive fluoride ions (0.42 vu) *trans* to the two oxides form the strongest/shortest interactions with the surrounding bond network, as evidenced by their large cationic bond valence sums (0.43 vu). See table 3.1. Consequently, the $[\text{WO}_2\text{F}_4]^{2-}$ anion is labeled a *cis*-director. Secondary distortive effects, imposed by the bond network, mitigate the primary distortive effects, which place the most residual negative charge on the *cis* oxides.

The crystal structure analyses presented here examine the underlying causes of oxide/fluoride ordering in $\text{Rb}_3\text{Na}(\text{NbOF}_5)_2\cdot\text{H}_2\text{O}$, $\text{Rb}_3\text{Na}(\text{MoO}_2\text{F}_4)_2\cdot\text{H}_2\text{O}$, $\text{Rb}_3\text{Na}(\text{WO}_2\text{F}_4)_2\cdot\text{H}_2\text{O}$, and $\text{K}_3\text{Na}(\text{WO}_2\text{F}_4)_2\cdot\text{H}_2\text{O}$ and how the network of bonds surrounding the $[\text{MO}_x\text{F}_{6-x}]^{n-}$ anions arrange with regard not only to the residual negative charge left on the oxide and fluoride ions owing to primary distortions, but also with regard to secondary distortive effects.

3.2 Synthesis and Characterization

3.2.1 Materials

Caution. Hydrofluoric acid is toxic and corrosive, and must be handled with extreme caution and the appropriate protective gear! If contact with the liquid or vapor occurs, proper treatment procedures should immediately be followed.¹¹⁻¹³

Materials. Nb₂O₅ (99.9%, Aldrich), Na₂WO₄•2H₂O, Na₂MoO₄•2H₂O, NaF (99.9%, Aldrich), KF (99.9%, Aldrich), RbF(99.9%, Aldrich), and aqueous hydrofluoric acid (HF) (48% HF by weight, Aldrich) were used as received. Owing to their hygroscopic nature, the alkali fluorides were manipulated under nitrogen in a dry box.

3.2.2 Synthesis.

All reactants were sealed in Teflon [fluoro(ethylenepropylene)] "pouches." The pouches were placed in a Parr pressure vessel filled 33% with deionized H₂O as backfill.¹⁴ The pressure vessel was heated for 24 h at 150 °C and cooled to room temperature over an additional 24 h. Upon heating, 0.5 – 1.0 g of backfill H₂O flowed into each reaction pouch. The pouches were opened in air, and the products were recovered by vacuum filtration. In all of the reactions described, the A:Na:M (A = K, Rb; M = Nb, Mo, W) ratio of starting materials was kept at 1:2:1 and solvent water or 48% HF_(aq) was added in excess. Reactions that deviated from this ratio by more than a

factor of two led to the precipitation of undesired phases, i.e. homocationic transition metal oxide fluoride salts of varying composition.

Rb₃Na(NbOF₅)₂•H₂O. Rb₃Na(NbOF₅)₂•H₂O was synthesized by reacting 0.0418 g (0.0004 mol) of RbF, 0.1000 g (0.0004 mol) of Na₂NbOF₅ (see below), and 1.000 g of H₂O. Colorless needles were recovered in 40% yield based on Nb. Attempts to synthesize Rb₃Na(NbOF₅)₂•H₂O from Nb₂O₅, NaF, RbF, and 48% aqueous HF led to the isolation of a mixed phase product of Na₂NbOF₅ and Rb₅Nb₃O₃F₁₄•H₂O.¹⁵

Rb₃Na(MoO₂F₄)₂•H₂O. Rb₃Na(MoO₂F₄)₂•H₂O was synthesized by reacting 0.4319 g (0.0041 mol) of RbF, 1.000 g (0.0041 mol) of Na₂MoO₄•2H₂O, and 1.000 g (0.0500 mol) of 48% aqueous HF. Colorless needles were recovered in 60% yield based on Mo.

Rb₃Na(WO₂F₄)₂•H₂O. Rb₃Na(WO₂F₄)₂•H₂O was synthesized by reacting 0.3166 g (0.0030 mol) of RbF, 1.000 g (0.0030 mol) of Na₂WO₄•2H₂O, and 1.000 g (0.0500 mol) of 48% aqueous. Colorless needles were recovered in 55% yield based on W.

K₃Na(WO₂F₄)₂•H₂O. K₃Na(WO₂F₄)₂•H₂O was synthesized by reacting 0.1755 g (0.0030 mol) of KF, 1.000 g (0.0030 mol) of Na₂WO₄•2H₂O, and 1.000 g (0.0500 mol) of 48% aqueous HF. Colorless needles were recovered in 57% yield based on W.

Na₂NbOF₅. Na₂NbOF₅ was synthesized by reacting 0.1344 g (0.0032 mol) of NaF, 0.4253 g (0.0016 mol) of Nb₂O₅, and 1.200 g (0.0600 mol) of 48% aqueous HF for 24 hours.

3.2.3 Crystallographic Determination.

Single-crystal X-ray diffraction data were collected with Mo K α radiation ($\lambda = 0.71073 \text{ \AA}$) on a Bruker SMART-1000 CCD diffractometer and integrated with the SAINT-Plus program.¹⁶ The structures were solved by direct methods and refined against F^2 by full-matrix least-squares techniques.¹⁷ A face-indexed absorption correction was performed numerically using the program XPREP. All structures were checked for missing symmetry elements with PLATON.¹⁸ The final refinement includes anisotropic displacement parameters. Crystallographic data for $\text{Rb}_3\text{Na}(\text{NbOF}_5)_2 \cdot \text{H}_2\text{O}$, $\text{Rb}_3\text{Na}(\text{MoO}_2\text{F}_4)_2 \cdot \text{H}_2\text{O}$, $\text{Rb}_3\text{Na}(\text{WO}_2\text{F}_4)_2 \cdot \text{H}_2\text{O}$, and $\text{K}_3\text{Na}(\text{WO}_2\text{F}_4)_2 \cdot \text{H}_2\text{O}$ are given in Table 3.2.

Table 3.2. Crystallographic data for $\text{Rb}_3\text{Na}(\text{NbOF}_5)_2 \cdot \text{H}_2\text{O}$, $\text{Rb}_3\text{Na}(\text{MoO}_2\text{F}_4)_2 \cdot \text{H}_2\text{O}$, $\text{Rb}_3\text{Na}(\text{WO}_2\text{F}_4)_2 \cdot \text{H}_2\text{O}$, and $\text{K}_3\text{Na}(\text{WO}_2\text{F}_4)_2 \cdot \text{H}_2\text{O}$.

Formula	$\text{Rb}_3\text{Na}(\text{NbOF}_5)_2 \cdot \text{H}_2\text{O}$	$\text{Rb}_3\text{Na}(\text{MoO}_2\text{F}_4)_2 \cdot \text{H}_2\text{O}$	$\text{Rb}_3\text{Na}(\text{WO}_2\text{F}_4)_2 \cdot \text{H}_2\text{O}$	$\text{K}_3\text{Na}(\text{WO}_2\text{F}_4)_2 \cdot \text{H}_2\text{O}$
fw	619.76	619.82	881.11	742.00
space group	C2/m (No. 15)	C2/m (No.15)	C2/m (No. 15)	C2/m (No. 15)
a (Å)	20.613	20.803	20.452	20.154
b (Å)	6.060	6.004	6.002	5.934
c (Å)	12.097	11.974	11.994	11.812
V (Å ³)	1263.90	1237.27	1231.24	1176.51
Z	8	8	8	6
T (°C)	-120(1)	-120(1)	-120(1)	-120(1)
λ (Å)	0.71069	0.71069	0.71069	0.71069
ρ_{calc} (g/cm ³)	3.28	3.35	4.58	3.00
μ (mm ⁻¹)	9.64	10.01	30.05	15.32
$R(F)^a$	0.0455	0.0343	0.0549	0.0292
$wR2(F^2)^b$	0.1372	0.1024	0.1552	0.0729

^a $R = \sum ||F_o| - |F_c|| / \sum |F_o|$ ^b $wR_2 = [\sum w(F_o^2 - F_c^2)^2 / \sum w(F_o^2)^2]^{1/2}$

3.2.4 Spectroscopic Measurements

Mid-infrared (400-4000 cm^{-1}) spectra of Na_2NbOF_5 and $\text{Rb}_3\text{Na}(\text{NbOF}_5)_2 \cdot \text{H}_2\text{O}$ were collected using a Bio-Rad FTS-60 FTIR spectrometer operating at 2 cm^{-1} resolution.

3.3 Extended Structures

The generic crystal framework for $\text{A}_3'\text{A}(\text{MO}_x\text{F}_{6-x})_2 \cdot \text{H}_2\text{O}$ ($\text{A}' = \text{K}, \text{Rb}; \text{A} = \text{Na}$) with $x = 1$ for $M = \text{Nb}^{5+}$ ($n = 2$) and $x = 2$ for $M = \text{Mo}^{6+}, \text{W}^{6+}$ ($n = 2$) is shown in Figure 3.2. The K and Rb cations are twelve-coordinate and the smaller Na cations are six-coordinate. Two crystallographically distinct M atoms are present, giving rise to two different, discrete $[\text{MO}_x\text{F}_{6-x}]^{n-}$ anions. All of the individual M-O and M-F bonds are ordered in one of the anions. In the other, one oxide ion is disordered over two and four anion positions in $\text{Rb}_3\text{Na}(\text{NbOF}_5)_2 \cdot \text{H}_2\text{O}$ and $\text{Rb}_3\text{Na}(\text{MoO}_2\text{F}_4)_2 \cdot \text{H}_2\text{O}$, $\text{Rb}_3\text{Na}(\text{WO}_2\text{F}_4)_2 \cdot \text{H}_2\text{O}$, and $\text{K}_3\text{Na}(\text{WO}_2\text{F}_4)_2 \cdot \text{H}_2\text{O}$, respectively. It should be noted that, throughout the following discussion, M1-centered anions and therefore all the individual M1-O and M1-F bonds are ordered, and M2-centered anions are partially ordered. Selected bond lengths are given in tables 3.4-3.7 with their associated bond valences and bond valence sums where appropriate.

3.3.1 $\text{Rb}_3\text{Na}(\text{NbOF}_5)_2 \cdot \text{H}_2\text{O}$.

The structure of $\text{Rb}_3\text{Na}(\text{NbOF}_5)_2 \cdot \text{H}_2\text{O}$ is built from Na^+ and Rb^+ cations and water molecules bonded to $[\text{NbOF}_5]^{2-}$ anions. The atomic X-ray scattering factors of oxygen and fluorine are similar, so bond valence relationships were used to determine the position of each around the Nb atoms. The short bond (1.726 Å) between Nb1 and one anion position (O1) indicates that it is occupied by an oxide ion. The long bond (2.149 Å) *trans* to the oxide ion is assigned to a fluoride ion (F1). The equatorial Nb1–F distances are of intermediate values ranging from 1.942 to 1.958 Å. The Nb2-centered anion has two short Nb2–X1 distances (1.830 Å) which indicate the oxide ion and a fluoride ion are disordered $\frac{1}{2}$ each over *cis* anion sites. The two long Nb2–F4 bonds (2.040 Å) are *trans* to the Nb2–X1 bonds. The remaining fluorides, F5 and F6, are located at distances of 1.932 and 1.924 Å from Nb2.

3.3.2 $\text{Rb}_3\text{Na}(\text{MoO}_2\text{F}_4)_2 \cdot \text{H}_2\text{O}$.

The structure of $\text{Rb}_3\text{Na}(\text{MoO}_2\text{F}_4)_2 \cdot \text{H}_2\text{O}$ is built from Na^+ and Rb^+ cations and water molecules bonded to $[\text{MoO}_2\text{F}_4]^{2-}$ anions. All of the Mo1–O/F bonds are ordered and one Mo2–O bond is ordered. As a result, two short Mo1–O1 bonds at 1.723 Å x 2 are observed *trans* to two long Mo1–F1 bonds at 2.072 Å each. The Mo1–F2 and Mo1–F3 bond distances are shorter at 1.963 and 1.891 Å, respectively. One short Mo2–O2 bond (1.690 Å) is observed *trans* to a long Mo2–F4 bond (2.118 Å). The remaining Mo2–X1/X2 distances are neither short (indicative of oxide) nor long (indicative of

fluoride) at 1.849 Å x 2 and 1.965 Å x 2. The other oxide ion and the three remaining fluorides are each disordered $\frac{1}{4}$ and $\frac{3}{4}$ over the X sites.

3.3.3 Rb₃Na(WO₂F₄)₂•H₂O.

The structure of Rb₃Na(MoO₂F₄)₂•H₂O is built from Na⁺ and Rb⁺ cations and water molecules bonded to [WO₂F₄]²⁻ anions. Based on bond valence calculations, all of the anion sites surrounding the W1 atom could be identified as oxide or fluoride ions. Short W1-O1 bonds (1.726 Å x 2) and long W1-F1 bonds (2.057 Å x 2) are observed along with intermediate W1-F2 (1.948 Å) and W1-F3 (1.915 Å) bonds. The W2-centered anion is only partially ordered and has one short W2-O2 bond at 1.715 Å and one long W2-F4 bond at 2.118 Å. The remaining W2-X1/X2 bond distances of 1.897 and 1.890 Å indicate disorder of the remaining oxide and three fluoride ions $\frac{1}{4}$ and $\frac{3}{4}$ each over the equatorial X1 and X2 sites.

3.3.4 K₃Na(WO₂F₄)₂•H₂O.

The structure of K₃Na(WO₂F₄)₂•H₂O is built from Na⁺ and K⁺ cations and water molecules bonded to [WO₂F₄]²⁻ anions. The same ordering phenomena observed in Rb₃Na(WO₂F₄)₂•H₂O is present and bond lengths are given in table 3.7.

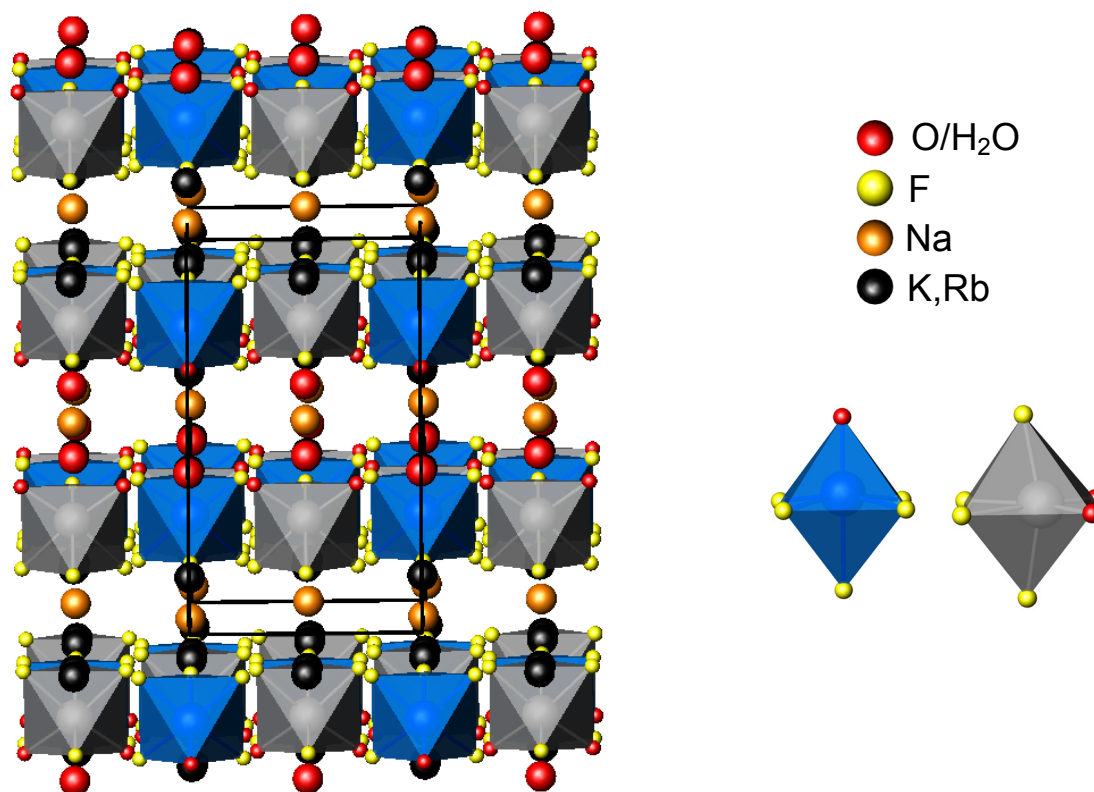


Figure 3.2. The general $A_3'A(MO_xF_{6-x})_2 \cdot H_2O$ ($A' = K, Rb$; $A = Na$) structure with $x = 1$ for $M = Nb^{5+}$ ($n = 2$) and $x = 2$ for $M = Mo^{6+}, W^{6+}$ ($n = 2$). Insets are views of corner-distorted (blue) and edge-distorted (grey) anions. The corner-distorted octahedron represents an ordered $[NbOF_5]^{2-}$ anion and partially ordered $[MoO_2F_4]^{2-}$ and $[WO_2F_4]^{2-}$ anions, where one oxide ion is disordered over the four equatorial anion sites. The edge-distorted octahedron represents ordered $[MoO_2F_4]^{2-}$ and $[WO_2F_4]^{2-}$ anions and a partially ordered $[NbOF_5]^{2-}$ anion, where the oxide ion is located on the *cis* oxide sites.

Table 3.3. Estimated negative potentials of the oxide and fluoride ions and the surrounding positive potentials in $\text{Rb}_3\text{Na}(\text{NbOF}_5)_2 \cdot \text{H}_2\text{O}$, $\text{Rb}_3\text{Na}(\text{MoO}_2\text{F}_4)_2 \cdot \text{H}_2\text{O}$, $\text{Rb}_3\text{Na}(\text{WO}_2\text{F}_4)_2 \cdot \text{H}_2\text{O}$, and $\text{K}_3\text{Na}(\text{WO}_2\text{F}_4)_2 \cdot \text{H}_2\text{O}$ through bond strength and bond valence calculations.

Bond	Anionic BV (vu) ^a	Cationic PSCR sum (vu) ^b	Cationic BV sum (vu) ^c
Nb2–O1	0.35	0.08	0.16
Nb2–F1	0.53	0.50	0.48
Nb2–F2 x2	0.21	0.33	0.40
Nb2–F3 x 2	0.18	0.25	0.43
Nb1–F4 x 2	0.37	0.50	0.44
Mo1–O1 x 2	0.36	0.25	0.29
Mo1–F1 x 2	0.51	0.50	0.48
Mo1–F2	0.34	0.25	0.31
Mo1–F3	0.20	0.25	0.31
Mo2–O2	0.20	0.08	0.13
Mo2–F4	0.57	0.5	0.52
W1–O1 x 2	0.31	0.25	0.31
W1–F1 x 2	0.46	0.50	0.46
W1–F2	0.27	0.25	0.33
W1–F3	0.21	0.25	0.31
W2–O2	0.26	0.08	0.16
W2–F4	0.54	0.5	0.50
W1–O1 x 2	0.32	0.25	0.25
W1–F1 x 2	0.45	0.5	0.41
W1–F2	0.20	0.25	0.23
W1–F3	0.19	0.25	0.23
W2–O2	0.27	0.08	0.15
W2–F4	0.50	0.50	0.44

^a Anionic BV (Bond Valence) = $z_i - S_{\text{M-O/F}}$, where z_i is the electric charge of each ligand and $S_{\text{Nb-O/F}}$ is taken from the Table 2 or 3 for each M–O/F bond.

^b Cationic PSCR sum = $\sum_j s'_{j,\text{cat}} = \sum_j \frac{z_{j,\text{cat}}}{v_{j,\text{cat}}}$, where $z_{j,\text{cat}}$ is the electric charge of each A_i alkali cation bonded to a given ligand and $v_{j,\text{cat}}$ is its coordination number.

^c Cationic BV (bond valence) sum = $\sum_i S_{i,\text{cat}}$, where $S_{i,\text{cat}}$ is taken from Table 3.5, 3.6 or 3.7 for each A_i –O/F bond.

Table 3.4. Bond lengths and bond valences for cation-anion interactions in $\text{Rb}_3\text{Na}(\text{NbOF}_5)_2 \cdot \text{H}_2\text{O}$.

		Rb1	Rb2	Rb3	Na1	Na2	O3(H ₂ O)	Nb1	Nb2
R _{ij} (Å)	O1			2.947			3.065 x 2		1.726
S _{ij} (vu)				0.156					1.650
R _{ij} (Å)	F1	3.034 x 2	3.267	3.189	2.320				2.149
S _{ij} (vu)		0.094 x 2	0.050	0.062	0.176				0.471
R _{ij} (Å)	F2 x 2	2.952		2.958		2.330			1.958
S _{ij} (vu)		0.118		0.116		0.171			0.788
R _{ij} (Å)	F3 x 2	2.921	2.887, 2.842						1.942
S _{ij} (vu)		0.128	0.140, 0.158						0.822
R _{ij} (Å)	X1 x 2		3.203	3.039, 3.126			2.945	1.830	
S _{ij} (vu)								1.175	
R _{ij} (Å)	F4 x 2	3.036, 3.043	3.360	3.307	2.339			2.040	
S _{ij} (vu)		0.094, 0.092	0.039	0.045	0.167			0.631	
R _{ij} (Å)	F5	2.928		3.078 x 2				1.932	
S _{ij} (vu)		0.126		0.084 x 2				0.846	
R _{ij} (Å)	F6	2.939	3.089 x 2					1.924	
S _{ij} (vu)		0.122	0.081 x 2					0.863	

R_{ij} = bond length of the bond "ij".

$S_{ij} = \exp[(R_0 - R_{ij})/B]$ experimental bond valence of bond "ij", where R_0 = constant dependent on i and j bonded elements, and $B = 0.37$.

$R_0(\text{Nb-O}) = 1.911$, $R_0(\text{Nb-F}) = 1.87$; $R_0(\text{Mo-O}) = 1.907$, $R_0(\text{Mo-F}) = 1.81$; $R_0(\text{W-O}) = 1.921$,

$R_0(\text{W-F}) = 1.83$; $R_0(\text{Na-O}) = 1.803$, $R_0(\text{Na-F}) = 1.677$; $R_0(\text{K-O}) = 2.132$,

$R_0(\text{K-F}) = 1.992$; $R_0(\text{Rb-O}) = 2.26$, $R_0(\text{Rb-F}) = 2.16$.

3.4 Anion Distortions

Monoxo complexes of d^0 metals, i.e. $[\text{NbOF}_5]^{2-}$, are expected to adopt a *trans* configuration in order that the strongly π donating oxide ligands can make maximum use of the available empty d orbitals on the metal center.¹⁹ Similarly, the $[\text{MoO}_2\text{F}_4]^{2-}$ dioxo complex adopts a *cis* configuration when ordered. In contrast, the $[\text{WO}_2\text{F}_4]^{2-}$ anion has been observed in both *trans* and *cis* configurations owing to distortive effects caused by the surrounding bond network.⁵ Bond networks, which surround d^0 transition metal centered oxide fluoride octahedra, have previously been shown to act upon the inherent primary distortions from which the anions derive most of their distortion character, i.e. magnitude and direction. For example, increased cationic contact to the oxide ion in CsNaNbOF_5 weakens the primary Nb-O distortion, which lengthens as a result.²⁰ Similarly, the formation of bonds between an $\text{M}(\text{L})_4^{2+}$ ($\text{M} = \text{Cd}^{2+}, \text{Cu}^{2+}$; $\text{L} = 3\text{-aminopyridine}, 4\text{-aminopyridine}$) cation and the oxide and/or *trans*-fluoride ions of the $[\text{NbOF}_5]^{2-}$ anion weakens the π component of the Nb=O bond. At the same time, hydrogen bond interactions between the equatorial fluorides and the aminopyridine groups both lengthen the equatorial Nb-F bonds and can further reduce the symmetry of the $[\text{NbOF}_5]^{2-}$ anion.⁷ These effects are referred to as secondary distortions²¹ and rarely do they so conspicuously influence anion geometry as in $\text{Rb}_3\text{Na}(\text{NbOF}_5)_2 \cdot \text{H}_2\text{O}$, $\text{Rb}_3\text{Na}(\text{MoO}_2\text{F}_4)_2 \cdot \text{H}_2\text{O}$, $\text{Rb}_3\text{Na}(\text{WO}_2\text{F}_4)_2 \cdot \text{H}_2\text{O}$, and $\text{K}_3\text{Na}(\text{WO}_2\text{F}_4)_2 \cdot \text{H}_2\text{O}$.

The intraoctahedral geometries and structure-directing properties of the ordered Nb1 and Mo1-centered anions are in keeping with previous observations. The Nb1 atom forms a short bond with one oxide ion (O1). A long Nb(1)-F1 bond is observed *trans* to the Nb(1)-O(1) bond. The O(1) and F(1) ions retain much more residual negative charge than the remaining oxide and fluoride ions and consequently, the strongest/shortest interactions between the $[\text{Nb}(1)\text{OF}_5]^{2-}$ anion and the surrounding bond network occur at these sites and the anion is a *trans*-director. The Mo(1) atom forms short bonds with equivalent, symmetry-related oxide ions at 1.723 Å each. The distortion of the Mo(1) atom towards the *cis* oxides leaves 0.51 vu of residual negative charge on each of the *trans* fluoride ions, which interact strongly with the surrounding bond network to make the $[\text{Mo}(1)\text{O}_2\text{F}_4]^{2-}$ anion a *cis*-director.

The $[\text{W}(1)\text{O}_2\text{F}_4]^{2-}$ anions that compose $\text{K}_3\text{Na}(\text{WO}_2\text{F}_4)_2 \cdot \text{H}_2\text{O}$ and $\text{Rb}_3\text{Na}(\text{WO}_2\text{F}_4)_2 \cdot \text{H}_2\text{O}$ exhibit atypical structure-directing behavior. The fluoride ions *trans* to the oxide ions retain the most residual negative charge and coordination to the bond network is strongest at these sites. Consequently, the $[\text{W}(1)\text{O}_2\text{F}_4]^{2-}$ anions are *cis*-directors. A *cis*-directing $[\text{WO}_2\text{F}_4]^{2-}$ anion has been observed on one previous occasion, in the solid state structure of $\text{Na}_2\text{WO}_2\text{F}_4$, where the symmetry-equivalent oxide ions retain slightly more residual negative charge (0.1 vu) than their *trans*-fluoride counterparts. The difficulty encountered in attempts to order the $[\text{WO}_2\text{F}_4]^{2-}$ anion results from the lack of disparity between the residual negative charges of the two most reactive O^{2-}/F^- ions and the remaining nucleophilic ions. One configuration of the anion

is not greatly favored over another, and thus the $[\text{WO}_2\text{F}_4]^{2-}$ can adopt either a *trans* or *cis* configuration. In contrast, the $\text{K}_3\text{Na}(\text{WO}_2\text{F}_4)_2 \cdot \text{H}_2\text{O}$ and $\text{Rb}_3\text{Na}(\text{WO}_2\text{F}_4)_2 \cdot \text{H}_2\text{O}$ $[\text{W}(1)\text{O}_2\text{F}_4]^{2-}$ anions possess *trans*-fluoride ions with significantly more residual negative charge (0.15 vu) than their less reactive oxide counterparts. The $[\text{W}(1)\text{O}_2\text{F}_4]^{2-}$ anions can therefore be designated *cis*-directors unreservedly for the first time.

The Nb(2) atom at the center of the partially ordered $[\text{Nb}(2)\text{OF}_5]^{2-}$ anion forms bonds of mixed Nb-O and Nb-F character to *cis* X1 positions at 1.830 Å. In keeping with the anion's stoichiometry, the two X1 positions that form this edge are each assigned ½ oxide and ½ fluoride ions. Refining relative O/F populations is fruitless because of the similarity of the atomic X-ray scattering factors and neutron cross sections of O^{2-} and F^- . However, on the basis of close inspection of bond lengths and anisotropic thermal ellipsoids, this assignment is correct. The Nb(2)-X1 bond length of 1.830 Å is a suitable intermediate between the typically short Nb-O (1.720-1.750 Å) and long *trans* Nb-F bond (2.000-2.150 Å). Additionally, the moderately-sized spherical thermal ellipsoid of the niobium indicates limited disorder of the oxide ion. See figure 3.3. The long bonds *trans* to the two Nb(2)-X1 bonds at 2.040 Å can unambiguously be designated Nb(2)-F(4) bonds. Five cationic contacts are made to each F4 ion, in keeping with the large amount of residual negative charge left on the F4 ions following the out-of-center distortion of the Nb(2) atom.

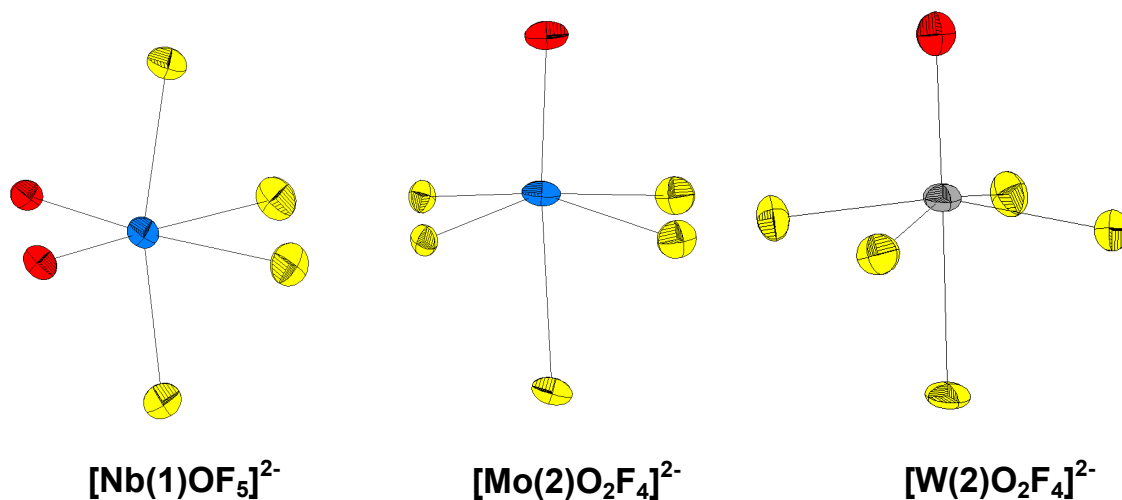


Figure 3.3. Thermal ellipsoid plots (50% probability) of partially ordered anions. The Nb thermal ellipsoid is a moderately-sized sphere indicating limited disorder of the oxide ion, while the Mo and W thermal ellipsoids are slightly flattened spheres reflecting the disorder of one oxide ion and three fluorides in the equatorial plane.

The IR spectrum of $\text{Rb}_3\text{Na}(\text{NbOF}_5)_2 \cdot \text{H}_2\text{O}$ shows peaks at $\nu_s(\text{Nb-O}) \approx 920 \text{ cm}^{-1}$ and 950 cm^{-1} , which suggests the presence of two $[\text{NbOF}_5]^{2-}$ anions in structurally nonequivalent positions. See figure S1. The Nb-O stretching region starts at approximately 910 cm^{-1} and goes to 960 cm^{-1} . In contrast, the Nb-O₂ stretching region occurs at a significantly lower frequency range ($820\text{-}895 \text{ cm}^{-1}$).²² The observed peaks, therefore, confirm that the distortion of the Nb2 atom towards the X1-X1 edge of its octahedron represents an average of two $[\text{NbOF}_5]^{2-}$ orientations in which the oxide ion is disordered over *cis* ligand sites and not a primary edge-type distortion as observed for the $[\text{NbO}_2\text{F}_4]^{3-}$ anion.

The $\text{Rb}_3\text{Na}(\text{WO}_2\text{F}_4)_2 \cdot \text{H}_2\text{O}$ and $\text{K}_3\text{Na}(\text{WO}_2\text{F}_4)_2 \cdot \text{H}_2\text{O}$ $[\text{W}(2)\text{O}_2\text{F}_4]^{2-}$ anions adopt *trans* configurations, in which the W2 atoms distort toward the oxide corners of their $[\text{W}(2)\text{O}_2\text{F}_4]^{2-}$ octahedra. A corner-type distortion of a W atom has been observed before in $[\text{pyH}]_2[\text{Cu}(\text{py})_4(\text{WO}_2\text{F}_4)_2]^{8-}$, where one W=O bond is ordered and the other oxide ion and three fluoride ions are disordered $\frac{1}{4}$ and $\frac{3}{4}$ over the equatorial ligand sites to reflect the anion stoichiometry. Similarly, the $\text{Rb}_3\text{Na}(\text{MoO}_2\text{F}_4)_2 \cdot \text{H}_2\text{O}$ Mo(2) metal center forms one short bond at 1.690 Å and one long bond at 2.118 Å to an oxide and *trans* fluoride ion, respectively, leaving the second oxide ion and its *trans* fluoride counterpart disordered along with the other two remaining fluorides. The W(2) and Mo(2) thermal ellipsoids are flattened spheres, reflecting the observed disorder in the equatorial planes. See figure 3.3.

3.5 Pauling's Second Crystal Rule

The interactions of oxide and fluoride ions with their bond networks can be understood in the context of Pauling's second crystal rule²³, which states that anions with the largest negative potentials will occupy sites having the largest positive potentials. The assessment of the positive potential in the crystal frameworks, carried out by calculating the PSCR (bond strength) sum and bond valence sum around each anionic position, should match as closely as possible the assessment of the negative

potentials of each oxide and fluoride ion (Table 3.3). The central M atom has been excluded from the PSCR calculations since we are only interested in the oxide/fluoride interactions with the bond network.

In inorganic-organic hybrid compounds^{14, 24} that contain the $[MO_xF_{6-x}]^{n-}$ anions, the anions connect to the bond network through the most charged oxide and fluoride ions (Figure 4). Similarly, in $Rb_3Na(NbOF_5)_2 \cdot H_2O$, the fluoride trans to the oxide ion (F1) retains the most residual negative charge (0.53 vu) and makes contact with four twelve-coordinate Rb^+ cations and one six-coordinate Na^+ cation ($1/12 + 1/12 + 1/12 + 1/12 + 1/6 = 0.5$ PSCR Sum, 0.48 bond valence sum). The remaining fluoride ions, F2 and F3, retain less residual negative charge (0.21 vu and 0.18 vu, respectively) and are three-coordinate, with PSCR Sums of 0.33 and 0.25. The nucleophilic oxide ion makes only one cationic contact, however, it accepts two hydrogen bonds from equidistant water molecules to satisfy its valence. This is not unexpected, as the oxide ions with the highest nucleophilicities are preferential hydrogen bond acceptors in organically-templated uranium sulfates²⁵. Similar behavior is observed in $Rb_3Na(MoO_2F_4)_2 \cdot H_2O$, $Rb_3Na(WO_2F_4)_2 \cdot H_2O$, and $K_3Na(WO_2F_4)_2 \cdot H_2O$, where the five-coordinate anion sites are occupied by the highly reactive *trans*-fluoride ions (F1). In contrast, F2 and F3 are less reactive and are three-coordinate. The *cis*-oxide ions are also three-coordinate with respect to the alkali cations and additionally, act as hydrogen bond acceptors.

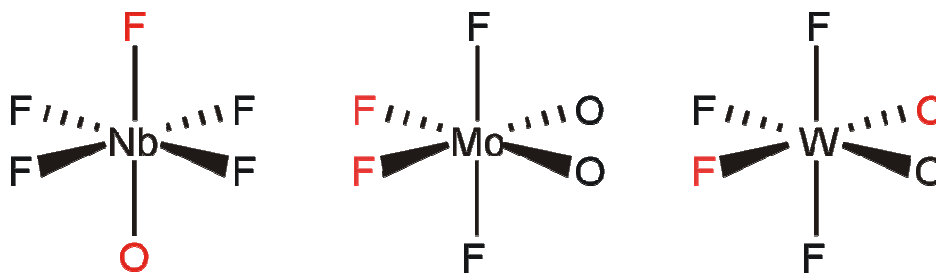


Figure 3.4. The $[\text{NbOF}_5]^{2-}$, $[\text{MoO}_2\text{F}_4]^{2-}$, and $[\text{WO}_2\text{F}_4]^{2-}$ anions. The most nucleophilic O^{2-}/F^- ions are drawn in red. Coordination with the extended bond network takes place through these sites.

The same behavior is also observed around the Nb₂, Mo₂, and W₂-centered octahedra. These anionic octahedra are only partially ordered. The oxide ion is localized on *cis* anion sites bound to Nb₂, and one oxide is ordered and the other disordered over the four equatorial anion sites bound to Mo₂ and W₂. As a result, two long Nb-F bonds are observed around Nb₂ (2 × 2.040 Å) and long Mo-F and W-F bonds are observed around Mo₂ (2.118 Å) and W₂ (2.084 Å). These fluoride ions are most reactive with respect to their less nucleophilic counterparts and are five-coordinate. The remaining anion sites are at most, three-coordinate.

3.6 Chemical Hardness.

The difference in the polarizabilities of the fluoride ($0.81 \times 10^{-24} \text{ cm}^3$) and oxide ($3 \times 10^{-24} \text{ cm}^3$) anions²⁶ contributes to their segregation in heterocationic crystal lattices. The combination of a small alkali metal cation (Na^+) and a large alkali metal cation

(K⁺, Rb⁺, Cs⁺) creates hard/soft²⁷ mismatch. The fluoride ions preferentially bond to the smaller Na⁺ cations and the oxide ions are drawn primarily to the larger alkali cations (K⁺, Rb⁺, Cs⁺). For instance, in the recently reported mixed cation niobium oxide fluorides, KNaNbOF₅ and CsNaNbOF₅, the high fluoride:oxide ratio in the compounds leads to a crystal framework in which the Na⁺ cations are drawn into shorter, stronger electrostatic interactions than their larger counterparts (K⁺, Cs⁺).²⁰ Bond valence sums showed that the Na⁺ cations are significantly overbonded (1.20 vu) and the K⁺ and Cs⁺ cations are ideally bound (1.0 vu). Similarly, the fluoride ions in Na₂WO₂F₄²⁸ have approximately equal or greater cationic bond valence sums than the more nucleophilic oxide ions. See table 3.1.

Bond valence sums were used to quantify both the relative strength and residual negative charge of each bond and respective ligand in Rb₃Na(NbOF₅)₂•H₂O, Rb₃Na(MoO₂F₄)•H₂O, Rb₃Na(WO₂F₄)₂•H₂O, and K₃Na(WO₂F₄)₂•H₂O. All calculations were performed using parameters compiled by Brese and O'Keefe²⁹. The valence of each ordered A⁺-F/O²⁻ (A⁺ = alkali cation) bond was calculated; see Tables 4-7. Large bond valence values indicate short, strong bonding interactions. Bond valence sums based on disordered anions are not reliable owing to obscured bond lengths. Therefore, the discussion of bond valence sums will be limited to those Mⁿ⁺/A⁺-O²⁻/F⁻ interactions in which the O²⁻/F⁻ ions are crystallographically ordered. Calculation of the valences for O--H and F--H interactions was not possible since the hydrogen atoms could not be located on the Fourier difference map.

The oxide ions make contact solely with K^+ or Rb^+ cations and water molecules. Tables 3.4-3.7 show that the K^+/Rb^+-O^{2-} bond valences are higher than the K^+/Rb^+-F^- bond valences. For example, the strongest Rb^+-O^{2-} interaction (0.131 vu) in $Rb_3Na(MoO_2F_4)\cdot H_2O$ is stronger than all individual Rb^+-F^- interactions. In contrast, the fluoride ions with the most residual negative charge (F1, F4) form strong interactions with Na^+ cations. For example, according to tables 3.4-3.7, the contribution of the Na^+ cations to the valences of the fluoride ions is significantly greater than that of the K^+ and Rb^+ cations. Moreover, the coordination spheres of the two sodium cations do not contain oxide ions. Taken together, these facts indicate a cation-anion affinity based on chemical hardness where the small fluoride ions preferentially interact with Na^+ cations and the larger, more polarizable oxide ions interact with K^+ and Rb^+ cations.

The compositions of the bond networks surrounding the *cis*-directing and *trans*-directing anions are different and reflect the cation-anion affinity realized through bond valence analyses. For example, the partially ordered $[Nb(2)OF_5]^{2-}$ anion and *cis*-configured $[Mo(1)O_2F_4]^{2-}$ and $[W(1)O_2F_4]^{2-}$ anions make twenty distinct contacts to K^+ or Rb^+ cations and two contacts to Na^+ cations. See Figure 3.5. These K^+/Rb^+ -rich bond networks, owing to their oxide affinity, order both oxide ions bound to Mo(1) and W(1) and confine the oxide ion bound to Nb(2) to *cis* anion sites. In contrast, the *trans*-configured $[Nb(1)OF_5]^{2-}$, $[Mo(2)O_2F_4]^{2-}$, and $[W(2)O_2F_4]^{2-}$ anions make fifteen K^+/Rb^+ contacts and three Na^+ contacts. The bond network composition of 15 K^+/Rb^+ : 3 Na^+ cations is not capable of ordering the dioxo anions. This observation has significant

implications as it shows that careful choice of the bond network constituents influences anion geometry.

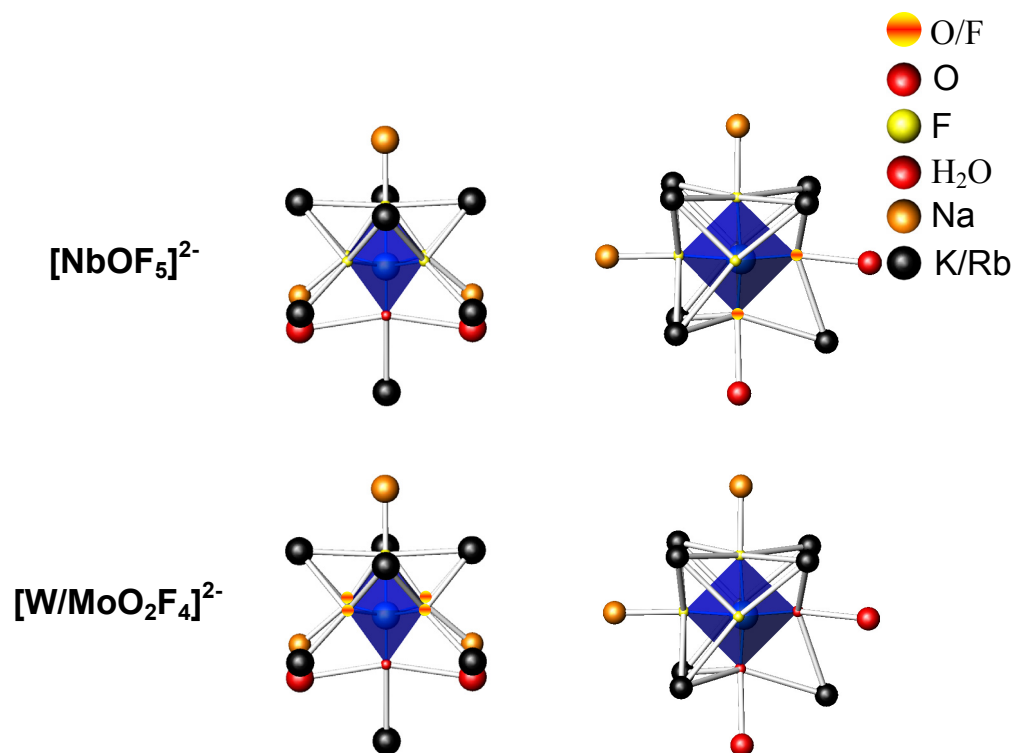


Figure 3.5. The coordination environments surrounding the $[\text{NbOF}_5]^{2-}$ (top) and $[\text{MoO}_2\text{F}_4]^{2-}$ and $[\text{WO}_2\text{F}_4]^{2-}$ anions (bottom). The more Na^+ -rich coordination environments (left) cause corner-type distortions of the metal center, while the more K^+/Rb^+ rich coordination environments cause edge-type distortions of the Nb, Mo, and W metal centers.

3.7 Atomic Size Effects

An examination of all compounds containing octahedral transition metal oxide fluoride anions and alkali cations reveals that all of the compounds containing Na^+ cations have crystallographically ordered anions. The small Na^+ cation can satisfy its atomic valence by making fewer contacts to the anions than the larger alkali metal cations, and as a result, they retain strong M-O primary distortions owing to strong metal $d\pi$ – oxygen $p\pi$ orbital overlap.

Comparison of four compounds containing the $[\text{NbOF}_5]^{2-}$ anion with bond network compositions having different Na:Rb ratios illustrates the unique bond network effects of the Na^+ cation. In Na_2NbOF_5 ,³⁰ each oxide and fluoride ion contacts two Na^+ cations and a short, Nb-O bond (1.765 Å) is observed. The RbNaNbOF_5 ²⁰ bond network increases the number of contacts to the oxide ion to satisfy the coordination sphere of Rb and a longer, weaker Nb-O bond (1.800 Å) is observed. The addition of more Rb^+ cations to the bond network in $\text{Rb}_3\text{Na}(\text{NbOF}_5)_2 \cdot \text{H}_2\text{O}$ results in cocrystallization of disordered and ordered $[\text{NbOF}_5]^{2-}$ anions with Nb-O and Nb-X x 2 bond lengths of 1.726 Å and 1.830 Å, respectively. Finally, each anion site bound to the Nb atom in Rb_2NbOF_5 ³¹ contacts four equidistant Rb^+ cations and the $[\text{NbOF}_5]^{2-}$ anion is disordered and Nb-X bond lengths range from 1.920 to 1.940 Å, see Figure 3.6.

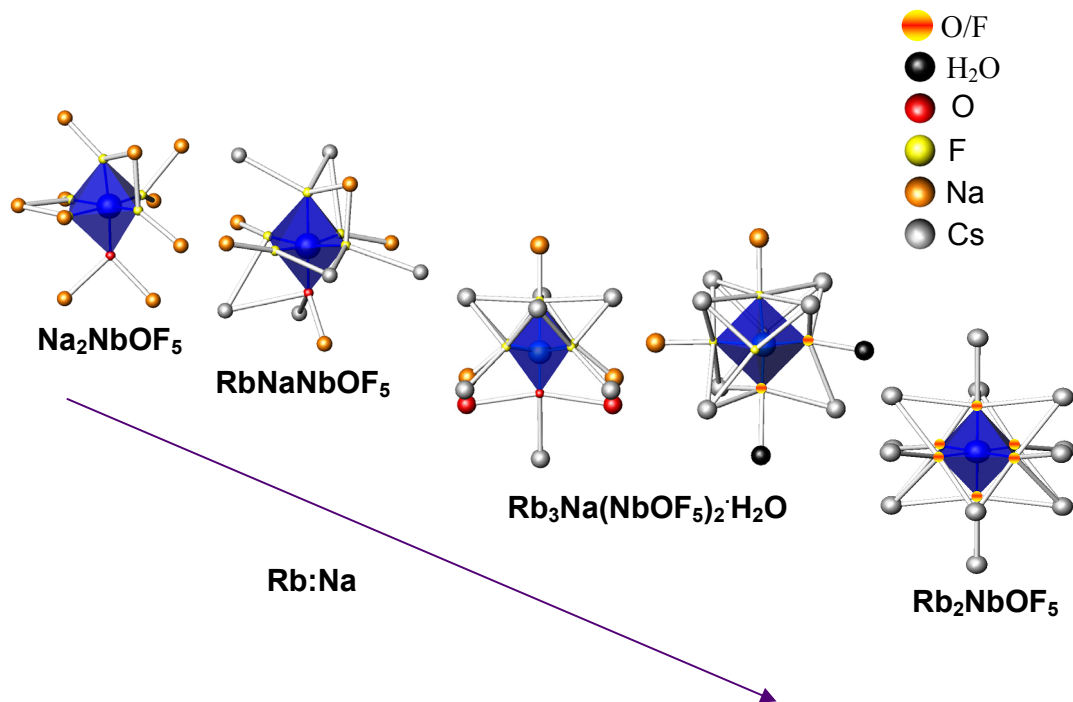


Figure 3.6. The effect of increased cation size on the primary Nb-O distortion in the $[\text{NbOF}_5]^{2-}$ anion. As the composition of the bond network becomes more Rb^+ -rich, the primary distortion is lengthened until it vanishes.

3.8 Conclusions

In structures where both oxygen and fluorine are found together in one structure with heterocationic bond networks, the small, hard cations (Na^+) preferentially interact with the fluoride ions. The larger, softer cations (K^+ and Rb^+) preferentially interact with the more polarizable oxide ions, which also act as hydrogen bond acceptors. The primary, out-of-center distortions experienced by $[\text{MO}_x\text{F}_{6-x}]^{n-}$ anions, which leave the individual oxide and fluoride ions differently charged, are therefore not the only factors which determine the structure-directing properties of the anions. The network of bonds surrounding the anions in a crystal also arranges in response to secondary distortive effects caused by chemical hardness.

CHAPTER FOUR

The Valence-Matching Principle and Cation-Anion Interactions in

Solid State Oxide Fluorides

4.1 Introduction

The search for new nonlinear optical materials is one that has been ongoing for many years.¹ The majority of synthetic approaches employ acentric, anionic building units (i.e. $[\text{MO}_x\text{F}_{6-x}]^{n-}$ anions with $x = 1$ for $M = \text{Nb}^{5+}$ ($n = 2$) and $x = 2$ for $M = \text{Mo}^{6+}$, W^{6+} ($n = 2$)) with the expectation that they pack in a noncentrosymmetric arrangement with respect to each other. Often, this requires clever manipulation of the surrounding network of bonds.² The valence-matching principle offers an *a priori* method of evaluating the possibility of cation-anion interactions that may lead to noncentrosymmetric crystal packing of the $[\text{MO}_x\text{F}_{6-x}]^{n-}$ anions, as observed in KNaNbOF_5 . The isolation of the $[\text{NbOF}_5]^{2-}$ anion from hydrofluoric acid solutions of Nb(V) is cation-dependent and can also be understood in the context of the valence-matching principle.

The complexation of Nb(V) in hydrofluoric acid solutions has been studied extensively with vibrational spectroscopy, which indicates that the $[\text{NbF}_6]^-$ and $[\text{NbOF}_5]^{2-}$ ions are in equilibrium.³ Shifting this equilibrium in one direction or another by addition of alkali metal fluorides or dilution of the acid solution creates the conditions necessary for the precipitation of complex fluoroniobates or oxofluoroniobates. Compounds of the type ANbF_6 or A_2NbF_7 ($A = \text{Na}^+$, K^+ , Rb^+ , Cs^+) are obtained by introducing alkali metal fluorides into solutions in which the $[\text{NbF}_6]^-$ ion predominates, and precipitation of oxyfluorides of the type Na_2NbOF_5 ⁴ and

$A_{10}Nb_6O_7F_{26} \cdot H_2O$ ($A = K^+, Rb^+, Cs^+$) is characteristic for less acidic solutions in which the $[NbOF_5]^{2-}$ anion predominates. Attempts to precipitate niobium oxide fluoride compounds from solutions of intermediate composition with approximately equal concentration of the $[NbF_6]^-$ and $[NbOF_5]^{2-}$ ions leads to the precipitation of $A_5Nb_3OF_{18}$ -type ($A = K^+, Rb^+, Cs^+$) compounds.⁵

Although the K^+ , Rb^+ , and Cs^+ cations do not precipitate from aqueous hydrofluoric acid solutions of Nb(V) with the desired $[NbOF_5]^{2-}$ anion, they can bring forward the $[NbOF_5]^{2-}$ anion when combined with the Na^+ cation. Recently, two-cation salts of the $[NbOF_5]^{2-}$ anion have been isolated. These include $KNaNbOF_5$, $Rb_3Na(NbOF_5)_2 \cdot H_2O$, and $CsNaNbOF_5$. These results can be understood in the context of the valence-matching principle, which states that the most stable structures will form when the Lewis acid strength of the cation closely matches the Lewis base strength of the anion.

4.2 Synthesis and Characterization

4.2.1 Materials

Caution. Hydrofluoric acid is toxic and corrosive, and must be handled with extreme caution and the appropriate protective gear! If contact with the liquid or vapor occurs, proper treatment procedures should be followed immediately.^{6,7}

Materials. Nb₂O₅ (99.9%, Aldrich), NaF (99.9%, Aldrich), KF (99.9%, Aldrich), RbF (99.9%, Aldrich), CsF (99.9%, Aldrich) and aqueous hydrofluoric acid (HF) (48% HF by weight, Aldrich) were used as received. Owing to their hygroscopic nature, the alkali fluorides were manipulated under nitrogen in a dry box.

4.2.2 Synthesis

All reactants were sealed in Teflon [fluoro(ethylenepropylene)] "pouches."⁸ The pouches were placed in a Parr pressure vessel filled 33% with deionized H₂O as backfill. The pressure vessel was heated for 24 h at 150 °C and cooled to room temperature at a rate of 0.1°C/min. The pouches were opened in air, and the products were recovered by vacuum filtration.

Rb₁₀Nb₆O₇F₂₆•H₂O. Rb₁₀Nb₆O₇F₂₆•H₂O was synthesized by reacting 0.3343 g (0.0032 mol) of RbF, 0.4253 g (0.0016 mol) of Nb₂O₅, and 1.200 g (0.0600 mol) of 48% aqueous HF. Clear, colorless needles were recovered in high yield.

4.2.3 Crystallographic Determination

Single-crystal X-ray diffraction data were collected with Mo K α radiation ($\lambda = 0.71073$ Å) on a Bruker SMART-1000 CCD diffractometer and integrated with the SAINT-Plus program.⁹ The structures were solved by direct methods and refined against F^2 by full-matrix least-squares techniques.¹⁰ A face-indexed absorption correction was performed numerically using the program XPREP. All structures were checked for missing symmetry elements with PLATON.¹¹ The final refinement includes anisotropic displacement parameters.

4.3 Results and Discussion

4.3.1 The Valence-Matching Principle

The valence matching principle was first used as a predictive tool to show why many stoichiometrically allowed silicate structures do not exist.¹² Later, the principle was applied to the crystal chemistry of numerous other oxides and oxysalts,¹³ and more specifically, to borates.¹⁴ Such examples clearly illustrate the power of the valence matching principle as an *a priori* analytical tool that may be used to consider the possibility of any cation-anion interaction.

The valence matching principle¹⁵ states that the most stable structures will form when the Lewis acid strength of the cation closely matches the Lewis base strength of the anion. The Lewis acid strength of a cation is defined as the characteristic valence/mean coordination number. Similarly, the Lewis base strength of an anion is the characteristic valence of the bonds formed by the anion.¹³

Na_2SO_4 provides an illustrative example of the valence-matching principle at work. The Lewis basicity of the $(\text{SO}_4)^{2-}$ anion is 0.17 v.u., which agrees very well with the Lewis acidity of 0.16 v.u. for Na. Thus, the Na- (SO_4) bond is in accordance with the valence-matching principle and Na_2SO_4 is a stable structure. Similarly, Ca_2SiO_4 is stable as the mineral larnite because the Lewis basicity of the $(\text{SiO}_4)^{2-}$ anion (0.33 v.u.) closely matches the Lewis acidity of Ca (0.29 v.u.). In contrast, Na_4SiO_4 is not a very stable material because the Lewis acidity of Na (0.17 v.u.) does not approach closely enough the Lewis basicity of $(\text{SiO}_4)^{2-}$.¹³

In the same way that the possibility of Na/Ca- SO_4/SiO_4 interactions were considered, the probability of observing interactions between alkali metal cations and $[\text{MO}_x\text{F}_{6-x}]^{n-}$ anions ($x = 1$ for $M = \text{Nb}^{5+}$ ($n = 2$) and $x = 2$ for $M = \text{Mo}^{6+}$, W^{6+} ($n = 2$)) may be evaluated. Table 4.1 lists Lewis acid strengths for the alkali cations. These values were determined by examining all relevant structures, that is, those in which the alkali cations are found together with an oxide fluoride anion in a shared structure. Based on the average cation coordination numbers determined from these structures, the Lewis acidities of the alkali cations are 0.167 v.u. for Na^+ , 0.104 v.u. for K^+ , 0.083

v.u. for Rb^+ , and 0.125 v.u. for Cs^+ . The Lewis base strengths for the niobium oxide fluoride anions were similarly obtained from relevant, available structures. In all pertinent structures, the oxide and fluoride ions of the $[\text{NbOF}_5]^{2-}$ anion are all one, two, or three-coordinate, leading to a Lewis basicity of 0.16 v.u. for the $[\text{NbOF}_5]^{2-}$ anion. The Lewis basicity of the $[\text{Nb}_6\text{O}_7\text{F}_{26}]^{10-}$ anion, 0.11 v.u., decreases with respect to the $[\text{NbOF}_5]^{2-}$ anion, since all but one of the oxide and fluoride ions are three-coordinate.

Table 4.1. Alkali cation Lewis Acidities, determined from all available alkali metal oxide fluoride salts .

Cation	Lewis Acidity (v.u.)
Li^+	n/a
Na^+	0.167
K^+	0.104
Rb^+	0.083
Cs^+	0.125

The closeness of the Lewis acidity and Lewis basicity of the Na^+ cation (0.167 v.u.) and $[\text{NbOF}_5]^{2-}$ anion (0.16 v.u.) make them ideal candidates to form a stable, shared structure. The remaining alkali cations have significantly lower Lewis acidities, and thus, cannot bring forward the $[\text{NbOF}_5]^{2-}$ anion from solution. Instead, they crystallize with larger, less Lewis basic, oligomeric niobium oxide fluoride anions . KNaNbOF_5 and CsNaNbOF_5 exist as stable structures since the average of their cation

Lewis acidities (0.136 v.u. and 0.146 v.u., respectively) approaches closely the Lewis basicity of the $[\text{NbOF}_5]^{2-}$ anion (0.16 v.u.). The Rb^+ cation, with a Lewis acidity of 0.083 v.u., is unable to precipitate with the $[\text{NbOF}_5]^{2-}$ anion from solution, even with the Na^+ cation present to mitigate the large valence difference of 0.08 v.u..

$\text{Rb}_3\text{Na}(\text{NbOF}_5)_2 \cdot \text{H}_2\text{O}$ forms as the stable compound from hydrofluoric acid solutions of Na^+ , Nb^{5+} , and Rb^+ . The water molecule acts as a bond valence mediator which narrows the gap between the Lewis acidity and basicity of the Rb^+ cation and $[\text{NbOF}_5]^{2-}$ anion, respectively. This phenomenon has been observed before in alkali metal oxalates, where the small alkali cations (Li^+ , Na^+) crystallize in anhydrous structures along with the $[\text{C}_2\text{O}_4]^{2-}$ anion: $\text{A}_2\text{C}_2\text{O}_4$. In contrast, the monohydrated phase $[\text{A}_2(\text{C}_2\text{O}_4) \cdot \text{H}_2\text{O}]$ is observed when the oxalate anion is paired with the larger, less acidic K^+ , Rb^+ , and Cs^+ cations.¹⁶

Clever synthetic methods are required to circumvent the problem of isolating compounds not accessible from solution. For example, the synthesis of RbNaNbOF_5 can be accomplished from the solid state reaction of stoichiometric amounts of RbF and NaNbOF_4 .² NaNbOF_4 must first be formed from a hydrofluoric acid solution of NaF and Nb_2O_5 . In this way, solution chemistry and solid state chemistry are inextricably linked. Single crystals of Rb_2NbOF_5 and Cs_2NbOF_5 can be obtained through dissolution of Na_2NbOF_5 in hydrothermal solutions along with a large excess of either Rb^+ or Cs^+ , respectively. Slow cooling of the solution yields high quality single crystals of the metathesis products: Rb_2NbOF_5 and Cs_2NbOF_5 .

4.3.2 Crystal Structure of $\text{Rb}_{10}\text{Nb}_6\text{O}_7\text{F}_{26}\cdot\text{H}_2\text{O}$

Crystallographic data for $\text{Rb}_{10}\text{Nb}_6\text{O}_7\text{F}_{26}\cdot\text{H}_2\text{O}$ is given in table 4.2. $\text{Rb}_{10}\text{Nb}_6\text{O}_7\text{F}_{26}\cdot\text{H}_2\text{O}$ is built up of Rb^+ cations and water molecules hydrogen bonded to $[\text{Nb}_2\text{O}_2\text{F}_9]^{3-}$ and $[\text{Nb}_2\text{O}_3\text{F}_8]^{4-}$ anions. See figures 4.1 and 4.2. Crystal structures containing similar species are notoriously difficult to refine owing to their high reactivities. The high fluoride content leads to rapid hydrolysis in air. For instance, crystals of $\text{H}_3\text{O}^+\text{W}_2\text{O}_2\text{F}_9^-$ ¹⁷ quickly deteriorate to 60% of their original scattering power during data collection and high R values are obtained (0.098). Crystals of $(\text{NH}_4)_3[\text{Mo}_2\text{O}_2\text{F}_9]$ ¹⁸ undergo similar decomposition and their data are also poorly refined, with representative values $R = 0.167$ and $R_w = 0.18$.

Table 4.2. Crystallographic data for $\text{Rb}_{10}\text{Nb}_6\text{O}_7\text{F}_{26}\cdot\text{H}_2\text{O}$

Formula	$\text{Rb}_{10}\text{Nb}_6\text{O}_7\text{F}_{26}\cdot\text{H}_2\text{O}$
fw	2036.16
space group	P3 (no. 143)
a (Å)	20.353
b (Å)	20.353
c (Å)	8.098
V (Å ³)	2905.18
Z	6
T (°C)	-120(1)
λ (Å)	0.71069
ρ_{calc} (g/cm ³)	4.081
μ (mm ⁻¹)	16.75
$R(F)^a$	0.1331
$wR_2(F^2)^b$	0.3145
$^a R = \sum F_o - F_c / \sum F_o $	
$^b wR_2 = [\sum w(F_o^2 - F_c^2)^2 / \sum w(F_o^2)^2]^{1/2}$	

In the case of $\text{Rb}_{10}\text{Nb}_6\text{O}_7\text{F}_{26}\cdot\text{H}_2\text{O}$, this decomposition was cause for serious concern, but there was little that could be done to avoid the problem. With the crystal decomposition and difficulty in assigning the space group in mind, the results obtained here should be considered as somewhat tentative. However, the overall features of the structure are most likely correct considering all parameters converged satisfactorily and

the thermal parameters are acceptable. Moreover, the X-ray pattern calculated from the single-crystal data closely matches the X-ray diffraction pattern obtained experimentally. See figure 4.3.

Based on powder X-ray diffraction, $\text{Rb}_{10}\text{Nb}_6\text{O}_7\text{F}_{26}\cdot\text{H}_2\text{O}$ was first identified by pattern-matching as the existing $\text{Rb}_5\text{Nb}_3\text{O}_3\text{F}_{14}\cdot\text{H}_2\text{O}$ ¹⁹ phase. Doubling the molecular formula for the sake of comparison gives $\text{Rb}_{10}\text{Nb}_6\text{O}_6\text{F}_{28}\cdot\text{H}_2\text{O}$. See figure 4.1. The compounds have similar lattice constants, given in table 4.3. $\text{Rb}_5\text{Nb}_3\text{O}_3\text{F}_{14}\cdot\text{H}_2\text{O}$ was identified in 1976 by Kaidalova and co-workers, who were unable to refine the crystal data below $R = .16$. No reasons were given for the poor refinement, but it is assumed that crystal decomposition played a role. We do not agree with the reported stoichiometry for several reasons. First, the authors report very similar fractional coordinates for two separate atoms, F2 and F5, such that they are superimposed on each other at 0.3320, 0.2300, 0.5170, and 0.3390, 0.2340, 0.5210. Second, the Nb-O/F bridging distance, reported as 2.159 Å, is close to the Nb-O bridging distance of 2.156 Å in $\text{Rb}_5\text{Nb}_3\text{OF}_{18}$. We have therefore, assigned this position an oxygen atom whereas the previous authors assigned it a fluorine atom. This difference accounts for the slight discrepancy in stoichiometries between the two compounds.

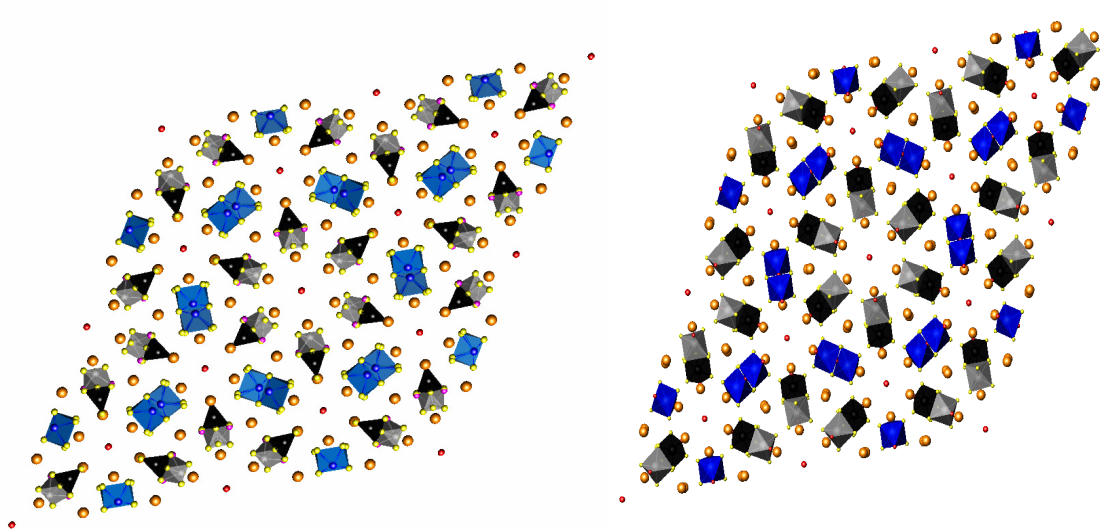


Figure 4.1. Polyhedral representations of the $\text{Rb}_5\text{Nb}_3\text{O}_3\text{F}_{14}\cdot\text{H}_2\text{O}$ (left) and $\text{Rb}_{10}\text{Nb}_6\text{O}_7\text{F}_{26}\cdot\text{H}_2\text{O}$ structures. The hexagonal symmetry is apparent in both structures.

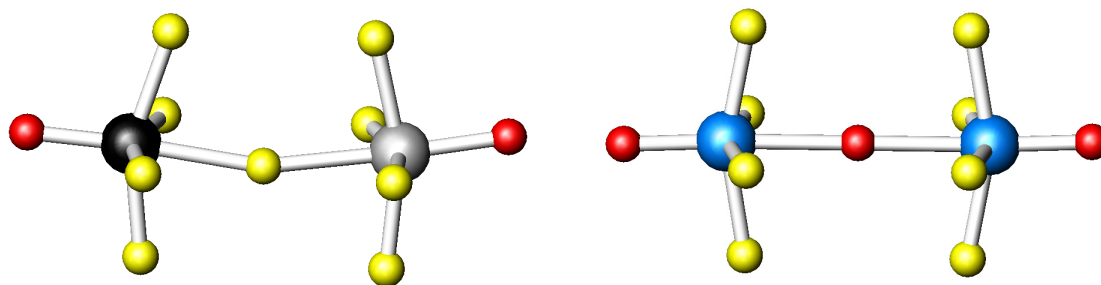


Figure 4.2. The anionic building units which compose the $\text{Rb}_{10}\text{Nb}_6\text{O}_7\text{F}_{26}\cdot\text{H}_2\text{O}$ structure. Red spheres represent oxygen atoms, yellow spheres represent fluorine atoms, and black, gray, and blue spheres represent crystallographically distinct niobium atoms.

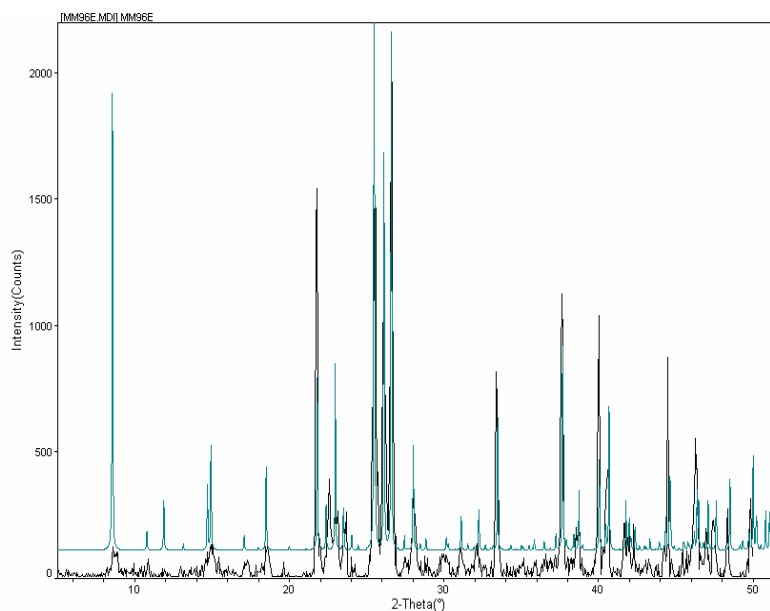


Figure 4.3. The experimental (black) and calculated (blue) powder X-ray diffraction patterns from $\text{Rb}_{10}\text{Nb}_6\text{O}_7\text{F}_{26}\cdot\text{H}_2\text{O}$

Table 4.3. Comparison of the $\text{Rb}_{10}\text{Nb}_6\text{O}_6\text{F}_{28}\cdot\text{H}_2\text{O}$ and $\text{Rb}_{10}\text{Nb}_6\text{O}_7\text{F}_{26}\cdot\text{H}_2\text{O}$ lattice constants.

$\text{Rb}_{10}\text{Nb}_6\text{O}_6\text{F}_{28}\cdot\text{H}_2\text{O}$	$\text{Rb}_{10}\text{Nb}_6\text{O}_7\text{F}_{26}\cdot\text{H}_2\text{O}$
SG: $\text{P6}_3\text{mc}$	SG: P3
$a = 20.48 \text{ \AA}$	$a = 20.35 \text{ \AA}$
$b = 8.14 \text{ \AA}$	$b = 8.10 \text{ \AA}$

The compound reported here is formed of Rb^+ cations and water molecules bound to discrete $[\text{Nb}_2\text{O}_2\text{F}_9]^{3-}$ and $[\text{Nb}_2\text{O}_3\text{F}_8]^{4-}$ anions. Selected bond lengths are given in table 4.4 along with their bond valences. The $[\text{Nb}_2\text{O}_2\text{F}_9]^{3-}$ anion consists of two NbOF_4 units bridged by a fluorine atom which is trans to two terminal, short Nb-O

bonds. The trans-effect has been observed before in crystals containing the $[\text{NbOF}_5]^{2-}$ anion, where a short Nb-O bond is trans to a long Nb-F bond. Strong metal $d\pi$ – oxygen $p\pi$ orbital interactions account for the short Nb-O distance. The Nb distorts toward the oxide and as a result, the *trans* fluoride bond is lengthened. The $[\text{Nb}_2\text{O}_3\text{F}_8]^{4-}$ anion consists of two NbO_2F_4 octahedra linked through a shared oxygen atom. The bridging oxygen atom resides on a mirror plane and thus the two NbO_2F_4 octahedra that form the dimer are equivalent. Unexpectedly, oxide ions are located in the terminal positions *trans* to the bridging oxide. Typically, anions of this sort are characterized by long trans Nb-F bonds opposite the Nb-O bonds. However, based on the reported structure of the related $\text{Rb}_5\text{Nb}_3\text{OF}_{18}$ phase, this assignment seems correct.

Table 4.4. Bond lengths and bond valence values for $\text{Rb}_{10}\text{Nb}_6\text{O}_7\text{F}_{26}\cdot\text{H}_2\text{O}$

Bond	Length (Å)	S_i	V_i-S_i
Nb1-O1	1.800	1.350	0.650
Nb1-F1	1.962	0.685	0.315
Nb1-F2	1.966	0.678	0.322
Nb1-F3	2.237	0.326	0.674
Nb1-F4	1.965	0.679	0.321
Nb1-F5	1.965	0.679	0.321
Nb2-O2	1.681	1.862	0.138
Nb2-O3	2.159	0.512	1.488
Nb2-F6	1.949	0.709	0.291
Nb2-F7	1.940	0.727	0.273
Nb2-F8	1.944	0.719	0.281
Nb2-F9	1.952	0.704	0.296
Nb3-O4	1.697	1.783	0.217
Nb3-F10	2.184	0.376	0.624
Nb3-F11	1.971	0.669	0.331
Nb3-F12	1.983	0.647	0.353
Nb3-F13	1.918	0.771	0.229
Nb3-F14	1.910	0.788	0.212

R_{ij} = bond length of the bond "ij"; $S_{ij} = \exp[(R_0 - R_{ij})/B]$ experimental bond valence of bond "ij", where R_0 = constant dependent on i and j bonded elements, and $B = 0.37$; $R_0(\text{Nb-O}) = 1.911$, $R_0(\text{Nb-F}) = 1.87$

An anion of the same stoichiometry with a different geometry has been reported by Lightfoot et. al.²⁰ In this anion, two distinct Nb positions are present. Moreover,

fluoride ions are located *trans* to the bridging oxide. The current $[\text{Nb}_2\text{O}_3\text{F}_8]^{4-}$ anion, to the best of our knowledge, is the first example of an oxide-bridged anion with oxide ions located *trans* to the bridging oxygen.

4.4 Conclusions

The valence-matching principle, previously applied to oxide crystal chemistry, is also useful in examining cation-anion interactions in solid state oxide fluorides. For example, owing to its high Lewis acidity, the small Na^+ cation forms a stable structure with the $[\text{NbOF}_5]^{2-}$ anion. The less Lewis acidic K^+ , Rb^+ , and Cs^+ cations precipitate from hydrofluoric acid solutions of Nb(V) with less Lewis basic, oligomeric niobium oxide fluoride anions such as $[\text{Nb}_3\text{OF}_{18}]^{5-}$ and $[\text{Nb}_6\text{O}_7\text{F}_{26}]^{10-}$. The Na^+ cation can mitigate the valence differences between the K^+ and Cs^+ cations and the $[\text{NbOF}_5]^{2-}$ anion, as evidenced by the formation of the heterocationic salts KNaNbOF_5 and CsNaNbOF_5 . Similarly, water acts as a bond valence mediator, narrowing the valence difference between Rb^+ and $[\text{NbOF}_5]^{2-}$ in $\text{Rb}_3\text{Na}(\text{NbOF}_5)_2 \cdot \text{H}_2\text{O}$.

CHAPTER FIVE**The Crystal Structures of Rb_2NbOF_5 and Cs_2NbOF_5**

5.1 Introduction

Crystallographic disorder is a challenge often encountered in the search for new oxide fluoride materials. Owing to their similar sizes, oxide and fluoride ions often share available sites, as in FeOF^1 , NbO_2F^2 , and KCrO_3F^3 . In compounds where oxide fluoride order is observed, such as $\text{Ba}_2\text{InO}_3\text{F}^4$ and $\text{Ba}_3\text{In}_2\text{O}_5\text{F}_2^5$, the ordering is attributed to the different cation-anion affinities, i.e. the divalent oxide ion interacts much more strongly with the cations than the monovalent fluoride ion. This phenomenon explains the propensity for oxide and fluoride ions to segregate in layered superconducting cuprates such as $\text{Sr}_2\text{CuO}_2\text{F}_{2+\delta}^6$. It does not, however, fully rationalize the observed oxide fluoride ordering in heterocationic compounds containing the early d^0 transition metal oxide fluoride ions $[\text{MO}_x\text{F}_{6-x}]^{n-}$ with $x = 1$ for $M = \text{Nb}^{5+}$ ($n = 2$) and $x = 2$ for $M = \text{Mo}^{6+}$, W^{6+} ($n = 2$). Certainly, cation-anion affinity contributes, but it is only one of many factors that must be deconvoluted in order to understand how oxide and fluoride ions interact with their cationic bond networks. Such an understanding will further the search for new noncentrosymmetric materials built from these anionic subunits.

Previous chapters in this thesis have enumerated the factors that govern cation-anion interactions in solid state oxide fluorides. Those factors include electronic potentials, chemical hardness, and atomic size. Electronic potentials are accessible through bond valence and Pauling's second crystal rule (PSCR) calculations when oxide fluoride anions are ordered. Their results indicate through which sites oxide

fluoride anions connect to their surrounding bond networks. In general, the oxide and *trans*-fluoride ions of the $[\text{NbOF}_5]^{2-}$ anion are the most reactive and preferentially coordinate to the extended bond network. Consequently, the $[\text{NbOF}_5]^{2-}$ anion is a *trans*-director. In contrast, $[\text{MoO}_2\text{F}_4]^{2-}$ forms primary contacts through the two fluoride ions *trans* to the two oxide ions and is a *cis*-director (Figure 5.1). The $[\text{WO}_2\text{F}_4]^{2-}$ anion can act as both a *trans*-director and a *cis*-director.⁷

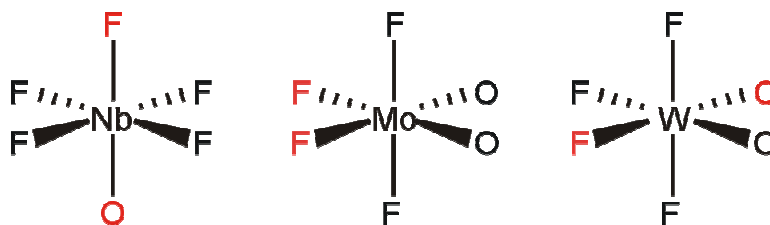


Figure 5.1. $[\text{NbOF}_5]^{2-}$, $[\text{MoO}_2\text{F}_4]^{2-}$, and $[\text{WO}_2\text{F}_4]^{2-}$ anions. The most nucleophilic O^{2-}/F^- ions are drawn in red. Coordination with the extended bond network takes place through these sites.

Chemical hardness is another factor which can be measured with bond valence calculations. For example, in the recently reported mixed cation niobium oxide fluorides, KNaNbOF_5 and CsNaNbOF_5 , the high fluoride:oxide ratios lead to crystal frameworks in which the Na^+ cations are drawn into shorter, stronger electrostatic interactions than their larger counterparts (K^+ , Cs^+).⁸ Bond valence sums showed that

the Na⁺ cations are significantly overbonded (1.20 vu), while the K⁺ and Cs⁺ cations are ideally bound (1.0 vu).

Atomic size is unique in that it does not require bond valence calculations to gauge its effects on the intraoctahedral distortions of the early d⁰ transition metal oxide fluoride anions. Atomic size effects can be evaluated in a more qualitative manner. For example, it was recently shown that increasing the number of cationic contacts to an oxide or fluoride ion bound to an octahedrally coordinated transition metal center weakens the M-O/F bond, which is lengthened as a result. For example, a short Nb–O bond and two-coordinate oxygen is observed in noncentrosymmetric KNaNbOF₅ versus a longer Nb–O bond with oxygen three-coordinate in CsNaNbOF₅. Thus, the noncentrosymmetric structure (KNaNbOF₅) maintains the larger primary electronic distortion of the [NbOF₅]²⁻ anion along with a low coordination number of the electropositive K-ion. In contrast, the Cs-ions of the centrosymmetric structure (CsNaNbOF₅) can exhibit significantly higher coordination numbers and the [NbOF₅]²⁻ anion a greatly reduced primary distortion. Similarly, in Na₂WO₂F₄⁹, each oxide or fluoride ion is coordinated by only two sodium cations and the anion retains W–O/F ordering, and in Cs₂WO₂F₄¹⁰, each oxide or fluoride ion is surrounded by four equidistant cesium cations so that each ligand is in an identical coordination environment and the anion is disordered.

Up to this point, the factors which govern cation-anion interactions in solid state oxide fluorides have been examined with only compounds displaying oxide fluoride

order in mind. Perhaps just as useful is an examination of compounds which do not display oxide fluoride order. The crystal structures of Rb_2NbOF_5 and Cs_2NbOF_5 , in which orientational disorder of the $[\text{NbOF}_5]^{2-}$ anion is observed, are reported. The observed cation-anion interactions in these structures provide insight to the problem of oxide fluoride disorder.

5.2 Synthesis and Characterization

5.2.1 Materials

Caution. Hydrofluoric acid is toxic and corrosive, and must be handled with extreme caution and the appropriate protective gear! If contact with the liquid or vapor occurs, proper treatment procedures should be followed immediately.¹¹⁻¹³

Materials. Nb_2O_5 (99.9%, Aldrich), NaF (99.9%, Aldrich), KF (99.9%, Aldrich), RbF (99.9%, Aldrich), CsF (99.9%, Aldrich), and aqueous hydrofluoric acid (HF) (48% HF by weight, Aldrich) were used as received. Owing to their hygroscopic nature, the alkali fluorides were manipulated under nitrogen in a dry box.

5.2.2 Synthesis

All reactants were sealed in Teflon [fluoro(ethylenepropylene)] "pouches".¹⁴ The pouches were placed in a 125 mL Teflon (PTFE) lined Parr pressure vessel filled 33% with deionized H_2O as backfill. The pressure vessel was heated for 24 hours at

150°C and cooled to room temperature over an additional 24 hours. The pouches were opened in air, and the products were recovered by vacuum filtration.

Rb₂NbOF₅. Rb₂NbOF₅ was synthesized by reacting 0.6686 g of RbF, 1.000 g of Na₂NbOF₅ (see synthesis below), and 1.0 g of H₂O. Clear, colorless plates were recovered in high yield.

Cs₂NbOF₅. Cs₂NbOF₅ was synthesized by reacting 0.9722 g of CsF, 0.1000 g of Na₂NbOF₅ (see synthesis below), and 1.0 g of H₂O. Clear, colorless plates were recovered in high yield.

Na₂NbOF₅. Na₂NbOF₅ was synthesized by reacting 0.1344 g (0.0032 mol) of NaF, 0.4253 g (0.0016 mol) of Nb₂O₅, and 1.200 g (0.0600 mol) of 48% aqueous HF for approximately 24 hours. A white polycrystalline powder was recovered in 88% yield based on Nb.

5.2.3 Crystallographic Determination

Single-crystal X-ray diffraction data were collected with Mo K α radiation ($\lambda = 0.71073 \text{ \AA}$) on a Bruker SMART-1000 CCD diffractometer and integrated with the SAINT-Plus program¹⁵. The structures were solved by direct methods and refined against F^2 by full-matrix least-squares techniques¹⁶. A face-indexed absorption correction was performed numerically using the program XPREP. All structures were checked for missing symmetry elements with PLATON¹⁷. The final refinement includes

anisotropic displacement parameters. Crystallographic data for Rb_2NbOF_5 and Cs_2NbOF_5 are given in Table 5.1.

Table 5.1. Crystallographic data for Rb_2NbOF_5 and Cs_2NbOF_5

Formula	Rb_2NbOF_5	Cs_2NbOF_5
fw	374.85	469.73
space group	P-3m1	P3m1
a (Å)	12.061	6.305
b (Å)	12.061	6.305
c (Å)	9.618	4.990
V (Å ³)	1211.63	171.76
Z	8	4
T (°C)	-120(1)	-120(1)
λ (Å)	0.71069	0.71069
ρ_{calc} (g/cm ³)	4.11	4.941
μ (mm ⁻¹)	17.97	12.21
$R(F)^a$	0.0209	0.0321
$wR_2(F^2)^b$	0.0894	0.1015
^a $R = \frac{\sum F_o - F_c }{\sum F_o }$		
^b $wR_2 = [\sum w(F_o^2 - F_c^2)^2 / \sum w(F_o^2)^2]^{1/2}$		

5.3 Results and Discussion

The hydrothermal syntheses of Rb_2NbOF_5 and Cs_2NbOF_5 directly from suitable starting reagents (AF , Nb_2O_5 , $\text{HF}_{(\text{aq})}$) was not accomplished. Attempts to synthesize these compounds in this way led to the formation of $\text{A}_5\text{Nb}_3\text{OF}_{18}$ ¹⁸ and $\text{A}_{10}\text{Nb}_6\text{O}_7\text{F}_{26} \cdot \text{H}_2\text{O}$. Instead, Rb_2NbOF_5 and Cs_2NbOF_5 were formed by dissolving

Na_2NbOF_5 in a hydrothermal solution along with a large excess of either RbF or CsF . The solutions were slow-cooled to room temperature to promote single-crystal growth.

The Rb_2NbOF_5 and Cs_2NbOF_5 structures are built up of 12-coordinate Rb^+ and Cs^+ cations, respectively, and orientationally disordered $[\text{NbOF}_5]^{2-}$ anions (Figure 5.2). As a result, accurate Nb-O/F bond lengths were not obtained. Based on stoichiometric considerations, the oxide ion must be disordered 1/6 on each of the anion sites bound to the Nb atoms. Although the $[\text{NbOF}_5]^{2-}$ anions are disordered and bond valence calculations cannot be performed, valuable information concerning bond network-anion interactions can still be gleaned from these structures.

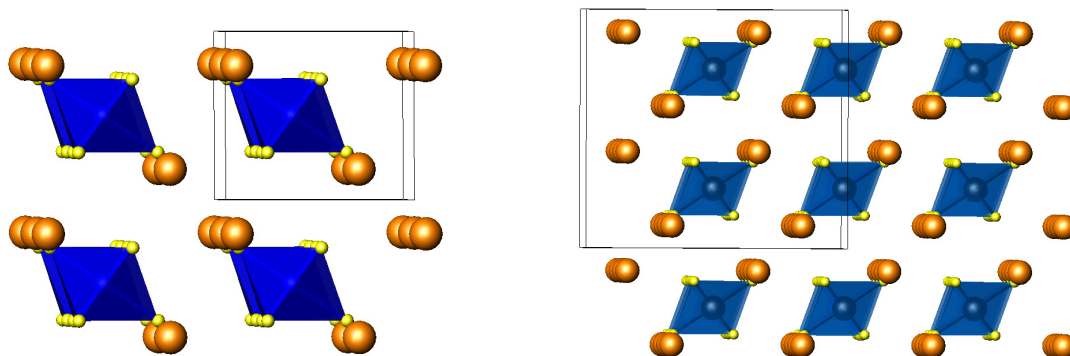


Figure 5.2. The Rb_2NbOF_5 (left) and Cs_2NbOF_5 (right) structures.

Atomic size plays a role in determining how oxide and fluoride ions interact with their cationic extended structures. Recently, it was shown that increasing the

number of cationic contacts to an oxide or fluoride ion bound to an octahedrally coordinated transition metal center weakens the M-O/F bond, which is lengthened as a result. For example, a short Nb–O bond and two-coordinate oxygen is observed in noncentrosymmetric KNaNbOF_5 versus a longer Nb–O bond with oxygen three-coordinate in centrosymmetric CsNaNbOF_5 . Thus, the noncentrosymmetric structure (KNaNbOF_5) maintains the larger primary electronic distortion of the $[\text{NbOF}_5]^{2-}$ anion along with a low coordination number of the electropositive K-ion. In contrast, the Cs-ions of the centrosymmetric structure (CsNaNbOF_5) can exhibit significantly higher coordination numbers and the $[\text{NbOF}_5]^{2-}$ anion a greatly reduced primary distortion. See figure 5.3. Additionally, in $\text{Na}_2\text{WO}_2\text{F}_4$, each oxide or fluoride ion is coordinated by only two sodium cations and the anion retains W–O/F ordering, while in $\text{Cs}_2\text{WO}_2\text{F}_4$, each oxide or fluoride ion is surrounded by four equidistant cesium cations so that each ligand is in an identical coordination environment and the anion is disordered. See figure 5.4.

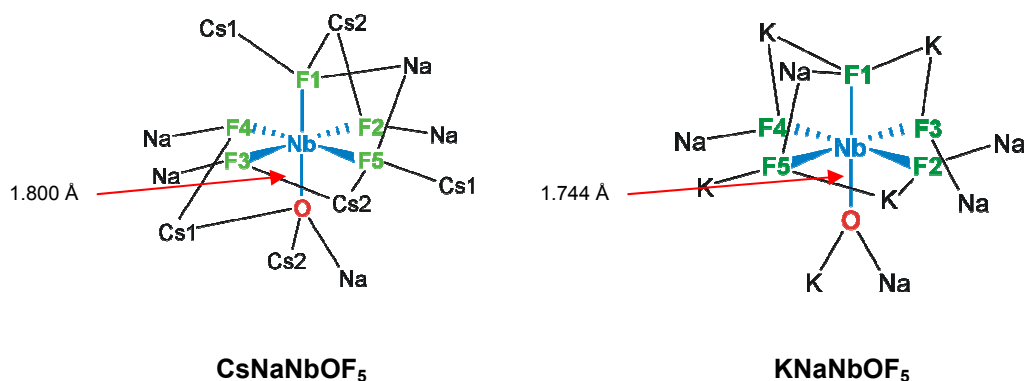


Figure 5.3. The coordination environments surrounding the $[\text{NbOF}_5]^{2-}$ anions in CsNaNbOF_5 and KNaNbOF_5 . Increased coordination to the oxide ion in CsNaNbOF_5 causes a weakening of the primary Nb–O distortion which lengthens as a result.

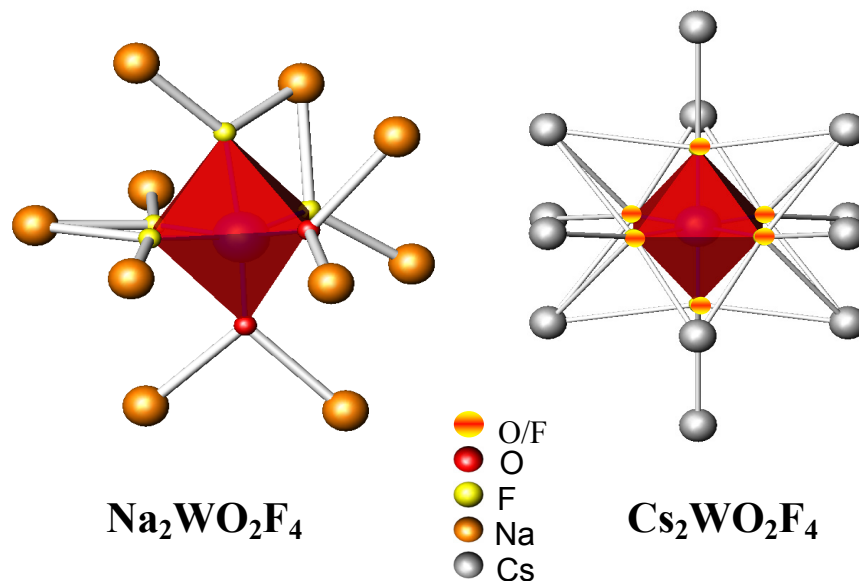


Figure 5.4. The coordination environments surrounding the $[\text{WO}_2\text{F}_4]^{2-}$ anions in $\text{Na}_2\text{WO}_2\text{F}_4$ and $\text{Cs}_2\text{WO}_2\text{F}_4$. Again, increased cationic contact to the anion causes a weakening of the primary distortion, and a disordered anion is observed.

The coordination environments of the oxide/fluoride ions in Rb_2NbOF_5 and Cs_2NbOF_5 are similar to those observed in $\text{Cs}_2\text{WO}_2\text{F}_4$, as each oxide/fluoride ion is surrounded by four equidistant cations (Figure 5.5). As a result, six similar Nb-X bond lengths that represent a combination of Nb-F and Nb-O character are observed (Table 5.2). The increased cationic contact to the $[\text{NbOF}_5]^{2-}$ anion, coupled with the symmetrical coordination environments, preclude crystallographic order of the anion.

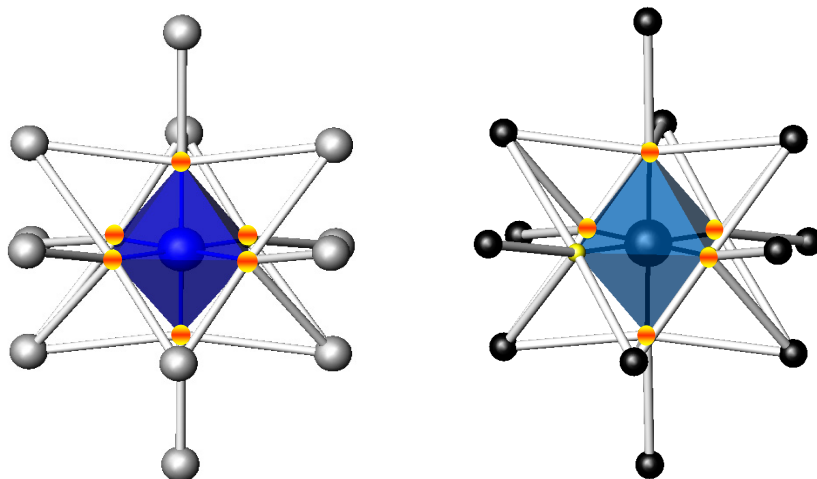


Figure 5.5. The symmetrical nature of the coordination environments surrounding the $[\text{NbOF}_5]^{2-}$ anions in Rb_2NbOF_5 (left) and Cs_2NbOF_5 (right), in addition to the large number of cationic contacts to each O^{2-}/F^- ion leads to orientational disorder of the $[\text{NbOF}_5]^{2-}$ anion.

Table 5.2. Nb-X (X = O/F) bond lengths for Rb_2NbOF_5 and Cs_2NbOF_5 .

Bond	Length (Å)
Rb_2NbOF_5	
Nb-X1 x 3	1.923
Nb-X2 x 3	1.956
Cs_2NbOF_5	
Nb-X1 x 2	1.926
Nb-X2 x 2	1.919
Nb-X3	1.938
Nb-X4	1.932

An examination of all compounds containing octahedral transition metal oxide fluoride anions and alkali cations reveals that all of the compounds containing Na^+ cations have crystallographically ordered anions (Table 5.3). The small Na^+ cation can satisfy its atomic valence by making limited contacts to the anions, and as a result, they retain strong M-O primary distortions owing to undisturbed metal $d\pi$ – oxygen $p\pi$ orbital overlap.

Table 5.3. Compounds composed of the alkali metals and early d^0 transition metal oxide fluoride anions

Disordered	Ordered
Li_2NbOF_5 ¹⁹	Na_2NbOF_5 ²⁰
K_2NbOF_5 ²¹	$\text{Na}_2\text{WO}_2\text{F}_4$ ²²
Rb_2NbOF_5	$\text{Na}_3\text{MoO}_3\text{F}_3$ ²³
Cs_2NbOF_5	
	KNaNbOF_5 ⁸
$\text{K}_2\text{MoO}_2\text{F}_4$ ²⁴	CsNaNbOF_5 ⁸
$\text{Rb}_2\text{MoO}_2\text{F}_4$ ²⁵	$\text{Rb}_3\text{Na}(\text{NbOF}_5)_2 \cdot \text{H}_2\text{O}$
$\text{Cs}_2\text{MoO}_2\text{F}_4$ ²⁵	$\text{Rb}_3\text{Na}(\text{MoO}_2\text{F}_4)_2 \cdot \text{H}_2\text{O}$
	$\text{K}_3\text{Na}(\text{WO}_2\text{F}_4)_2 \cdot \text{H}_2\text{O}$
$\text{K}_2\text{WO}_2\text{F}_4$ ²⁶	$\text{Rb}_3\text{Na}(\text{WO}_2\text{F}_4)_2 \cdot \text{H}_2\text{O}$
$\text{Cs}_2\text{WO}_2\text{F}_4$ ²⁷	

Comparison of four compounds containing the $[\text{NbOF}_5]^{2-}$ anion with bond network compositions having different Na:Rb ratios illustrates the unique bond network effects of the Na^+ cation. In Na_2NbOF_5 , each oxide and fluoride ion contacts two Na^+ cations and a short, Nb-O bond (1.765 Å) is observed. The RbNaNbOF_5 ⁸ bond network increases the number of contacts to the oxide ion to satisfy the coordination sphere of Rb and a longer, weaker Nb-O bond (1.800 Å) is observed. The addition of more Rb^+ cations to the bond network in $\text{Rb}_3\text{Na}(\text{NbOF}_5)_2 \cdot \text{H}_2\text{O}$ results in cocrystallization of disordered and ordered $[\text{NbOF}_5]^{2-}$ anions with Nb-O and Nb-X bond lengths of 1.726 Å and 1.830 Å, respectively. Finally, each anion site bound to the Nb atom in Rb_2NbOF_5 contacts four equidistant Rb^+ cations and the $[\text{NbOF}_5]^{2-}$ anion is disordered and Nb-X bond lengths range from 1.920 to 1.940 Å. See figure 5.6.

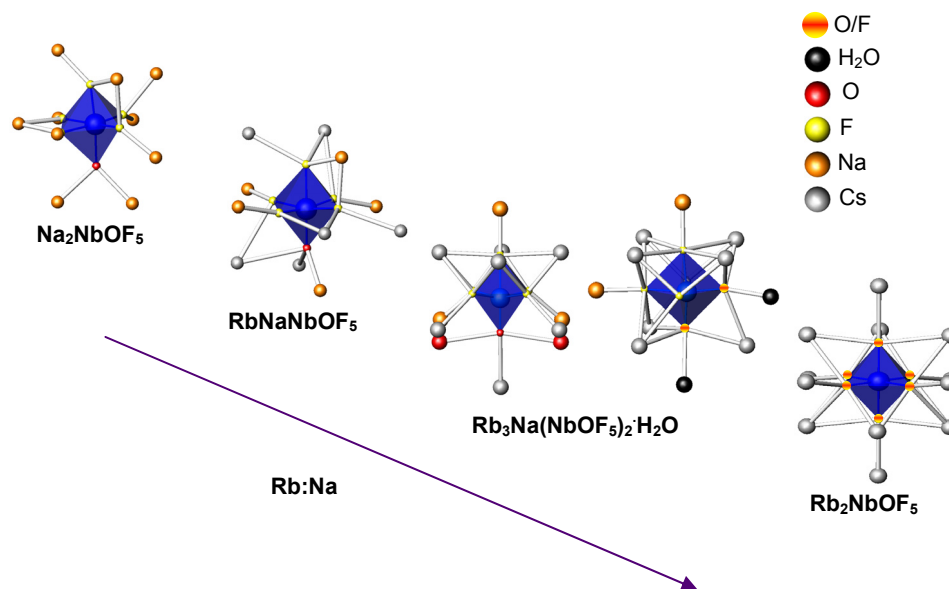


Figure 5.6. The effects of increased cation size on the primary Nb-O distortion of the $[\text{NbOF}_5]^{2-}$ anion. As the bond network composition surrounding the $[\text{NbOF}_5]^{2-}$ anion becomes more Rb^+ -rich, the Nb-O bond weakens until orientational disorder occurs.

5.4 Conclusions

When multiple cationic contacts are made to early d^0 transition metal oxide fluoride anions such as $[\text{NbOF}_5]^{2-}$, the cations typically surround the anions in a symmetric manner. As a result, the M-O primary electronic distortions are weakened and orientational disorder occurs. For these reasons, the $[\text{MO}_x\text{F}_{6-x}]^{n-}$ anions with $x = 1$ for $M = \text{Nb}^{5+}$ ($n = 2$) and $x = 2$ for $M = \text{Mo}^{6+}$, W^{6+} ($n = 2$) are commonly ordered when Na^+ cations are used as counter ions.

CHAPTER SIX
The Elusive KNaNbOF_5

6.1 Introduction

KNaNbOF_5 ¹ is a noncentrosymmetric and polar compound that has an SHG response 0.6 x KDP and is phase-matchable. See figures 6.1 and 6.2. A strong piezoelectric response has also been observed upon grinding single crystals of this material and a ferroelectric response is expected. In order to exploit the technological potential of this material, a facile hydrothermal synthesis capable of yielding high quality single crystals is desired. However, attempts at devising such a synthesis have met with limited success. The majority of synthetic attempts led to the formation of the cubic elpasolite $\text{K}_2\text{NaNbO}_2\text{F}_4$ ².

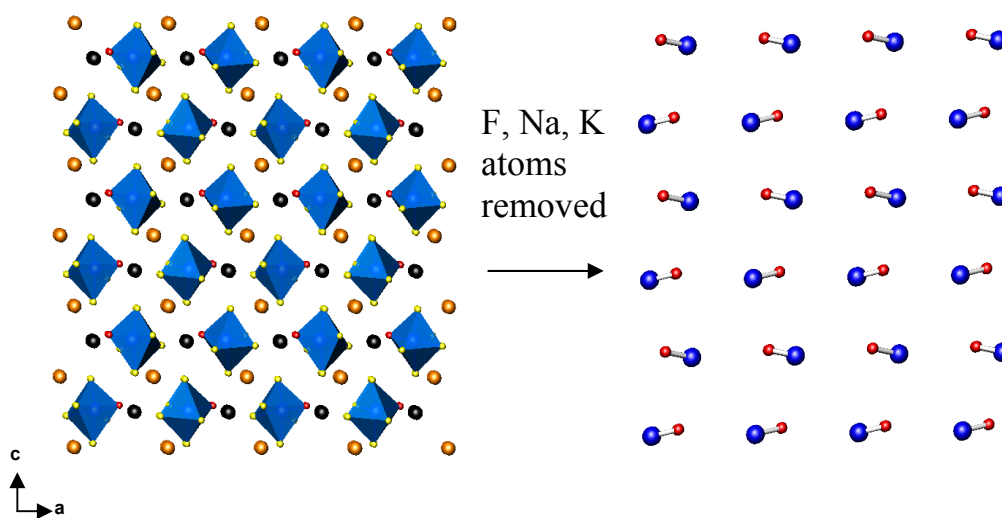


Figure 6.1. View of the primary Nb-O distortions in KNbOF_5 , including all atoms (left) and only Nb and O atoms (right). The partial addition of the individual bond dipoles is enough to observe a significant SHG response (0.6 x KDP).

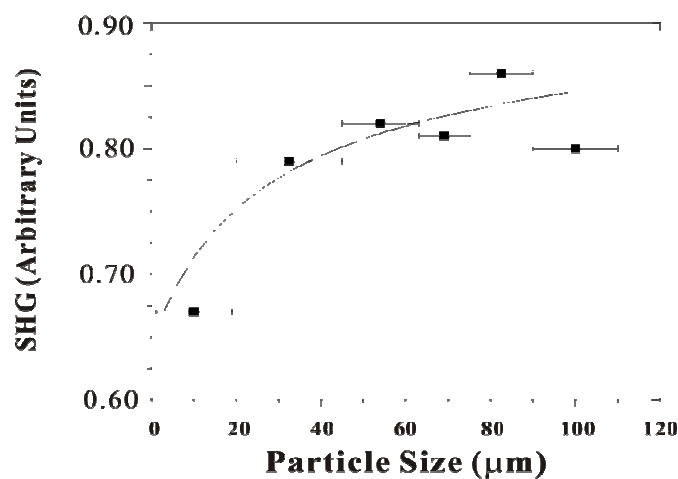


Figure 6.2. Graph of particle sizes vs. SHG responses for KNaNbOF₅. The compound is phase-matchable with an SHG response 0.6 x KDP.

Chapter four detailed the synthesis conditions necessary to target various niobium oxide fluoride anions as well as the chemical factors underpinning those synthesis conditions. It is clear that the small alkali metal cations (Na⁺) preferentially crystallize from solution with the desired [NbOF₅]²⁻ anion while the larger alkali metal cations (K⁺, Rb⁺, Cs⁺) bring forward oligomeric anions. In contrast to these observations, the large Cs⁺ cation can precipitate with the [NbOF₅]²⁻ anion when combined with Na⁺ to give CsNaNbOF₅. Based on this result, it seems reasonable to

expect KNaNbOF_5 to be the stable precipitate from an aqueous solution of Na^+ , K^+ , and $[\text{NbOF}_5]^{2-}$.

This chapter describes the many synthetic approaches to the elusive KNaNbOF_5 phase, as well as possible reasons for their limited successes and more pervasive failures. The various reaction conditions are examined retrospectively and bond valence arguments are used to aid the analysis. Finally, recommendations regarding future synthetic directions are made.

6.2 Synthesis and Characterization

6.2.1 Materials

Caution. Hydrofluoric acid is toxic and corrosive, and must be handled with extreme caution and the appropriate protective gear! If contact with the liquid or vapor occurs, proper treatment procedures should be followed immediately^{3,4}.

Materials. Nb_2O_5 (99.9%, Aldrich), NaF (99.9%, Aldrich), KF (99.9%, Aldrich), and aqueous hydrofluoric acid (HF) (48% HF by weight, Aldrich) were used as received. Owing to their hygroscopic nature, the alkali fluorides were manipulated under nitrogen in a dry box.

6.2.2 Synthesis

In most cases, all reactants were sealed in Teflon [fluoro(ethylenepropylene)] "pouches."⁵ The pouches were placed in a Parr pressure vessel filled 33% with deionized H₂O as backfill. The pressure vessel was heated for 2 to 24 h at 100°C or 150°C and cooled to room temperature at a rate of 0.1°C/min. The pouches were opened in air, and the products were recovered by vacuum filtration. Other reactions were carried out in water baths heated to \approx 100°C. See Table 6.1 for further preparative details.

6.2.3 Product Identification

Synthetic products were identified with powder X-ray diffraction using a Rigaku XDS 2000 diffractometer. Scans were taken from $5^\circ < 2\theta < 60^\circ$ with 0.05° steps and 1 second collection times at each step. Patterns were analyzed using the Jade software suite.

6.3 Results and Discussion

The structure of KNaNbOF₅ is shown in figures 6.3 and 6.4. It is built up of 12-coordinate K⁺ cations, six-coordinate Na⁺ cations, and [NbOF₅]²⁻ anions held together by electrostatic interactions. The framework is formed of (001) [NaNbOF₇]_∞ layers stacked along c. Table 6.1 lists all of the synthetic attempts at forming KNaNbOF₅ with starting reactants, reaction conditions, and observed products. Clearly, K₂NaNbO₂F₄

predominates. $\text{K}_2\text{NaNbO}_2\text{F}_4$ is a cubic, elpasolite-type phase which bears a close resemblance to the perovskite family. See figure 6.5. The crystal structure indicates that the oxide and fluoride ions bound to the Nb center are disordered. The K^+ cations are each twelve-coordinate, the Na^+ cation is six-coordinate and the oxide/fluoride ions are five-coordinate with respect to the alkali metals. These structural features are important because they provide the information necessary to perform a rudimentary bond valence analysis. Although the $[\text{NbO}_2\text{F}_4]^{3-}$ anion is disordered, coordination information is sufficient to determine the Lewis acidities and basicity of the cations and anion, respectively, in the structure.

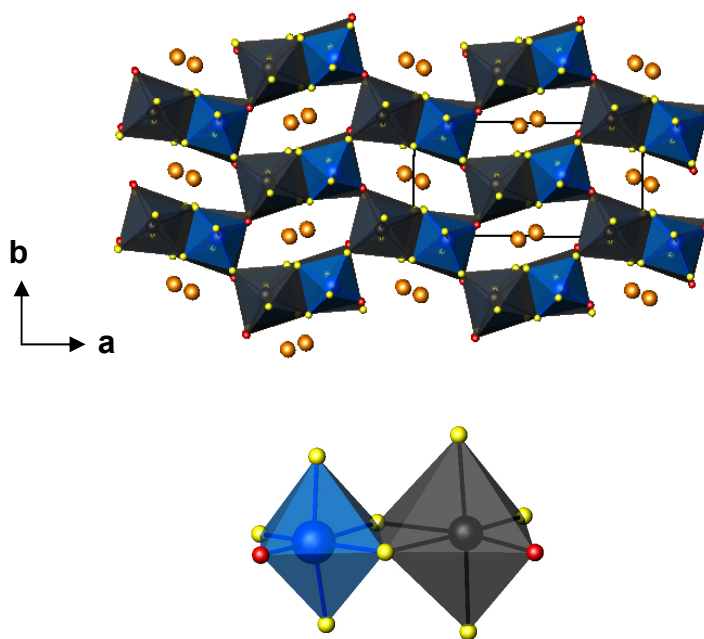


Figure 6.3. A View of the three-dimensional framework in KNaNbOF_5 , formed of (001) $[\text{NaNbOF}_7]_\infty$ layers stacked along c. Inset is a view of the framework structural building unit.

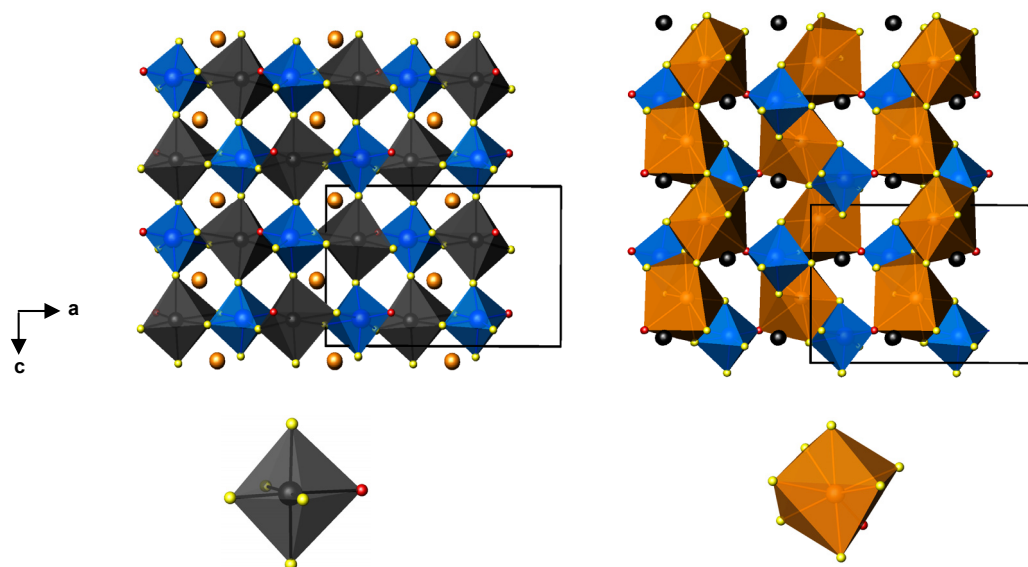


Figure 6.4. Coordination polyhedra in KNaNbOF_5 . Blue octahedra are $[\text{NbOF}_5]^{2-}$ anions, black octahedra are Na-centered, and eight-coordinate orange polyhedra are K-centered. In this schematic, all drawings are shown in the (010) plane with different polyhedra highlighted in each.

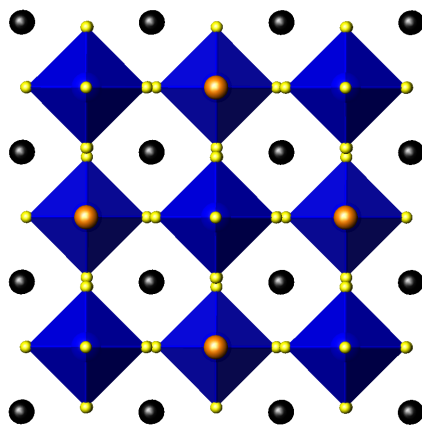


Figure 6.5. The structure of $\text{K}_2\text{NaNbO}_2\text{F}_4$. Blue octahedra are $[\text{NbOF}_5]^{2-}$ anions, orange spheres are Na^+ cations, and black spheres are K^+ cations.

Table 6.1. Reaction labels, reactants, reaction conditions, and observed products for synthetic attempts at KNaNbOF_5 . Those reactions for which the isolated phase could not be identified by X-ray powder diffraction are labeled 'UID' while those for which insufficient product was obtained are labeled 'N/A'.

Reaction Label	Reactants	Temp (°C)	Time (h)	Products
125A	$\text{KF}, \text{Na}_2\text{NbOF}_5, \text{H}_2\text{O}$	150	24	KNaNbOF_5
125B	$5\text{KF}, \text{Na}_2\text{NbOF}_5, \text{H}_2\text{O}$	150	24	$\text{K}_2\text{NaNbO}_2\text{F}_4$
140A	$\text{KF}, \text{Na}_2\text{NbOF}_5, \text{H}_2\text{O}$	150	24	$\text{K}_2\text{NaNbO}_2\text{F}_4$
140B	$\text{KF}, \text{Na}_2\text{NbOF}_5, \text{H}_2\text{O}$	150	24	$\text{K}_2\text{NaNbO}_2\text{F}_4$
140C	$\text{KF}, \text{Na}_2\text{NbOF}_5, \text{H}_2\text{O}$	150	24	$\text{K}_2\text{NaNbO}_2\text{F}_4$
140D	$\text{KF}, \text{Na}_2\text{NbOF}_5, \text{H}_2\text{O}$	150	24	$\text{K}_2\text{NaNbO}_2\text{F}_4$
146D	$\text{KF}, 2\text{Na}_2\text{NbOF}_5, \text{H}_2\text{O}$	150	24	N/A
151A	$\text{KF}, \text{Na}_2\text{NbOF}_5, \text{HF}_{(\text{aq})}$	150	24	UID
151B	$\text{KF}, 2\text{Na}_2\text{NbOF}_5, \text{HF}_{(\text{aq})}$	150	24	UID
151C	$\text{KF}, 4\text{Na}_2\text{NbOF}_5, \text{H}_2\text{O}$	150	24	N/A
151D	$4\text{KF}, \text{Na}_2\text{NbOF}_5, \text{H}_2\text{O}$	150	24	KNaNbOF_5
154A	$4\text{KF}, \text{Na}_2\text{NbOF}_5, \text{H}_2\text{O}$	150	24	$\text{K}_2\text{NaNbO}_2\text{F}_4$
154B	$4\text{KF}, \text{Na}_2\text{NbOF}_5, \text{H}_2\text{O}$	150	24	$\text{K}_2\text{NaNbO}_2\text{F}_4$
154C	$4\text{KF}, \text{Na}_2\text{NbOF}_5, \text{H}_2\text{O}$	150	24	$\text{K}_2\text{NaNbO}_2\text{F}_4$
159A	$3\text{KF}, \text{Na}_2\text{NbOF}_5, \text{H}_2\text{O}$	150	24	$\text{K}_2\text{NaNbO}_2\text{F}_4$
159B	$4\text{KF}, \text{Na}_2\text{NbOF}_5, \text{H}_2\text{O}$	150	24	$\text{K}_2\text{NaNbO}_2\text{F}_4$
159C	$5\text{KF}, \text{Na}_2\text{NbOF}_5, \text{H}_2\text{O}$	150	24	$\text{K}_2\text{NaNbO}_2\text{F}_4$
159D	$6\text{KF}, \text{Na}_2\text{NbOF}_5, \text{H}_2\text{O}$	150	24	$\text{K}_2\text{NaNbO}_2\text{F}_4$
179A	$4\text{KF}, \text{Na}_2\text{NbOF}_5, \text{minimal H}_2\text{O}$	150	24	$\text{K}_2\text{NaNbO}_2\text{F}_4$
198A	$\text{KF}, \text{Na}_2\text{NbOF}_5, \text{H}_2\text{O}$	150	4	$\text{K}_2\text{NaNbO}_2\text{F}_4$
198B	$5\text{KF}, \text{Na}_2\text{NbOF}_5, \text{H}_2\text{O}$	150	3	$\text{K}_2\text{NaNbO}_2\text{F}_4$
201A	$8\text{KF}, \text{Na}_2\text{NbOF}_5, \text{CH}_3\text{OH}$	150	24	Na_2NbOF_5
02A	$\text{KF}, \text{NaF}, \text{Nb}_2\text{O}_5, \text{NH}_4\text{HF}_2, \text{H}_2\text{O}$	150	24	$\text{K}_2\text{NaNbO}_2\text{F}_4$
02B	$\text{KF}, 8\text{NaF}, \text{Nb}_2\text{O}_5, \text{NH}_4\text{HF}_2, \text{H}_2\text{O}$	150	24	UID
03A	$\text{KF}, \text{NaF}, \text{Nb}_2\text{O}_5, \text{NH}_4\text{HF}_2, \text{H}_2\text{O}$	100	24	N/A
03B	$\text{KF}, 8\text{NaF}, \text{Nb}_2\text{O}_5, \text{NH}_4\text{HF}_2, \text{H}_2\text{O}$	100	24	$\text{K}_2\text{NaNbO}_2\text{F}_4$
08A	$\text{KF}, 8\text{NaF}, \text{Nb}_2\text{O}_5, \text{HF}$	150	24	$\text{KNaNbOF}_5?$
08B	$\text{KF}, \text{NaF}, \text{Nb}_2\text{O}_5, \text{HF}$	150	24	$\text{K}_2\text{NaNbO}_2\text{F}_4$
08C	$\text{KF}, 4\text{NaF}, \text{Nb}_2\text{O}_5, \text{HF}$	150	24	Na_2NbOF_5
09A	$\text{KF}, \text{NaNbOF}_4, \text{H}_2\text{O}$	150	24	UID

The Lewis acidities for the alkali metal cations are given in Table 6.2. The Lewis basicity for the $[\text{NbO}_2\text{F}_4]^{3-}$ was determined from all available structures to be 0.10 vu. Chapter four explained that a stable compound is formed when the Lewis acidity of the cation closely matches the Lewis basicity of the anion. Since the Lewis acidity of the K^+ cation, determined from examining all available relevant oxide fluoride compounds, is 0.104 vu, it is not surprising that it commonly brings forward the $[\text{NbO}_2\text{F}_4]^{3-}$ anion from aqueous solutions of Na^+ , K^+ , and Nb^{5+} . In contrast, the higher Lewis acidity of the Cs^+ cation (0.125 vu) favors formation of the more basic $[\text{NbOF}_5]^{2-}$ anion, whose Lewis basicity is 0.167 vu, when combined with Na^+ in solution.

Table 6.2. Alkali cation Lewis Acidities, determined from all available alkali metal oxide fluoride salts .

Cation	Lewis Acidity (v.u.)
Li^+	n/a
Na^+	0.167
K^+	0.104
Rb^+	0.083
Cs^+	0.125

In addition to valence matching considerations⁶, more tangible effects must also be examined. For example, hydrolysis reactions have previously been shown to effect the outcome of reactions aimed at forming oxide fluoride salts of the alkali metals. The $[\text{Nb}_6\text{O}_7\text{F}_{26}]^{10-}$ anion evolves from the $[\text{Nb}_3\text{OF}_{18}]^{5-7}$ anion through a series of hydrolysis reactions. Similarly, it is feasible that the $[\text{NbOF}_5]^{2-}$ anion may be converted through a reaction with one molecule of H_2O to one molecule of HF and one $[\text{NbO}_2\text{F}_4]^{3-}$ anion.

In order to circumvent the problem of hydrolysis, the nonaqueous solvent CH_3OH was employed. The high vapor pressure of this solvent led to the bursting of many teflon pouches and ultimately, this approach was unsuccessful. Thus far, no other nonaqueous solvents have been used. However, this path may prove fruitful if a viable solvent is identified.

Although valence matching and hydrolysis considerations indicate the successful synthesis of KNaNbOF_5 from solution is unlikely, it has been accomplished on two separate occasions. See Table 6.1. Both reactions are quite simple and involve a three component system comprised of KF , Na_2NbOF_5 , and H_2O . It is unclear as to why these reactions were successful and the remaining 28 were not. In both cases, the individual reaction pouches were placed inside a 125 mL autoclave along with 3-4 other pouches. Pouch 125A was placed in the autoclave along with pouch 125B and three other pouches each filled with Ag_2O , Nb_2O_5 , and $\text{HF}_{(\text{aq})}$. Pouch 151D was placed in the autoclave with pouches 151A-151C. In both of these instances the pouches accompanying the KNaNbOF_5 pouch were partially filled with $\text{HF}_{(\text{aq})}$. This observation

has significant implications since $\text{HF}_{(\text{aq})}$ acts as a strong attractor of backfill water. Perhaps deprivation of this backfill water prevents hydrolysis of the $[\text{NbOF}_5]^{2-}$ anion to the $[\text{NbO}_2\text{F}_4]^{3-}$ anion.

Based on the information gained from the many syntheses performed, one potential synthetic route entails the use of nonaqueous solvents to prevent the hydrolysis of $[\text{NbOF}_5]^{2-}$ to $[\text{NbO}_2\text{F}_4]^{3-}$. Another involves using limited water and preventing water migration into the pouch. Lower temperature reactions should also be explored as this may effect water migration. Polycrystalline KNaNbOF_5 is attainable through the solid state reaction of KF with NaNbOF_4 at 385°C under flowing Ar. See figure 6.6. It may be possible to recrystallize this powder from solution.



Figure 6.6. Powder X-ray diffraction patterns of KNaNbOF_5 ground single crystals (red) and polycrystalline powder (black).

6.4 Conclusions

Though the hydrothermal synthesis of high quality crystals of KNaNbOF_5 is a challenge, it is possible. In all, thirty hydrothermal synthetic attempts were made and two were successful. The two successful reaction pouches, containing KF , Na_2NbOF_5 , and H_2O , were both placed in a 125 mL autoclave along with three or four other pouches containing $\text{HF}_{(\text{aq})}$. These observations indicate that water plays a key role in the synthesis of KNaNbOF_5 . In order to target KNaNbOF_5 , the true role of water must be discerned. Additionally, polycrystalline KNaNbOF_5 , readily available through solid state reaction of KF with NaNbOF_4 , may be recrystallized from solution.

CHAPTER SEVEN

Conclusions and Future Directions

7.1 Conclusions

7.1.1 Cation-Anion Interactions and Polar Structures in the Solid State

The crystal structure analyses of KNaNbOF_5 and CsNaNbOF_5 show that small changes to the cationic bond network surrounding the $[\text{NbOF}_5]^{2-}$ anion lead to different crystal symmetries. The $[\text{NbOF}_5]^{2-}$ anion and therefore all individual Nb-O and Nb-F bonds are ordered in noncentrosymmetric KNaNbOF_5 and centrosymmetric CsNaNbOF_5 . Bond valence and Pauling's Second Crystal Rule (PSCR) calculations reveal the essential role of the small K^+ cations in the acentric packing of the $[\text{NbOF}_5]^{2-}$ anion. The low-coordinate K^+ cation makes fewer contacts to the oxide ion than the high-coordinate Cs^+ cation. As a result, KNaNbOF_5 retains the stronger primary, electronic distortion and is noncentrosymmetric and polar.

7.1.2 Chemical Hardness and the Structure-Directing Role of the cis-oxo $[\text{WO}_2\text{F}_4]^{2-}$ Anion

The $[\text{NbOF}_5]^{2-}$, $[\text{MoO}_2\text{F}_4]^{2-}$, and $[\text{WO}_2\text{F}_4]^{2-}$ were crystallized with heterocationic bond networks composed of large alkali metal cations (K^+ , Rb^+) and small alkali metal cations (Na^+) in 3:1 ratios. Bond valence calculations reveal a cation-anion affinity based on chemical hardness in which the small, non-polarizable fluoride ions interact strongly with the Na^+ cations and the more polarizable oxide ions interact with the K^+

and Rb^+ cations and act as hydrogen bond acceptors. The implications of this phenomenon are significant, since the bond networks effect the anion distortion directions by selectively attracting oxide or fluoride ions. Moreover, coordination to the most charged sites on the *cis*-oxo $[\text{WO}_2\text{F}_4]^{2-}$ anion in $\text{K}_3\text{Na}(\text{WO}_2\text{F}_4)_2 \cdot \text{H}_2\text{O}$ and $\text{Rb}_3\text{Na}(\text{WO}_2\text{F}_4)_2 \cdot \text{H}_2\text{O}$ shows unambiguously that the network of bonds surrounding the $[\text{WO}_2\text{F}_4]^{2-}$ anion arranges so that its strongest/shortest contacts are made to the two F sites that are opposite the *cis*-O atoms. The $[\text{WO}_2\text{F}_4]^{2-}$ anion may therefore be labeled a *cis*-director unreservedly for the first time.

7.1.3 The Valence-Matching Principle and Cation-Anion Interactions in Solid State Oxide Fluorides

The valence-matching principle offers a simple, *a priori* method of evaluating the possibility of cation-anion interactions in solid state oxide fluorides. When the Lewis acid strength, i.e. the characteristic valence/mean coordination number, of a cation approaches the Lewis base strength of an anion, the two constituents form a stable structure. Previously applied to silicates and borates, this principle is brought to bear on the crystal chemistry of compounds containing the noncentrosymmetric $[\text{MO}_x\text{F}_{6-x}]^{n-}$ anions ($x = 1$ for $M = \text{Nb}^{5+}$ ($n = 2$) and $x = 2$ for $M = \text{Mo}^{6+}$, W^{6+} ($n = 2$)) and reveals why the small Na^+ cation consistently crystallizes in stable structures with the $[\text{MO}_x\text{F}_{6-x}]^{n-}$ anions and the larger alkali metal cations (K^+ , Rb^+ , Cs^+) form stable structures with oligomeric oxide fluoride anions such as $[\text{Nb}_6\text{O}_7\text{F}_{26}]^{10-}$.

7.1.4 The Crystal Structures of Rb_2NbOF_5 and Cs_2NbOF_5

Although the $[\text{NbOF}_5]^{2-}$ anion is orientationally disordered in the crystal structures of Rb_2NbOF_5 and Cs_2NbOF_5 , valuable information concerning cation-anion interactions can be gleaned from these structures. In both structures, the alkali metal cations are 12-coordinate and each individual oxide and fluoride ion is four-coordinate with respect to the alkali metal cations. The increased coordination to the O^{2-}/F^- sites leads to a decrease in the strength of the primary, Nb-O distortion and a disordered anion.

7.1.5 The Elusive KNaNbOF_5

Numerous attempts were made to hydrothermally synthesize high quality single crystals of KNaNbOF_5 to take advantage of its optical and piezoelectric properties. In all, thirty reactions were run and only two were successful. The valence matching principle and hydrolysis reactions seemingly preclude this phase from forming out of solution. Instead, the solid state reaction of KF and NaNbOF_4 must be employed.

7.2 Future Directions

7.2.1 Cation-Anion Interactions and Polar Structures in the Solid State

The hydrothermal syntheses of KNaNbOF_5 and CsNaNbOF_5 are encouraging results, as they indicate phases with similar compositions such as KNaWO_2F_4 and $\text{CsNaWO}_2\text{F}_4$ should also form from solution. Similarly, $\text{KNaMoO}_2\text{F}_4$ and $\text{CsNaMoO}_2\text{F}_4$ may also be accessible from solution. Since Na_2NbOF_5 and $\text{Na}_2\text{WO}_2\text{F}_4$ and Cs_2NbOF_5 and $\text{Cs}_2\text{WO}_2\text{F}_4$ are isostructural, it is reasonable to assume that these heterocationic phases will be stable and isostructural. Indeed, the recent isolation and structure solution of $\text{CsNaWO}_2\text{F}_4$ indicates that it is isostructural with CsNaNbOF_5 . The K/Na phases are of particular interest since this cation combination has been shown to promote partial alignment of Nb-O bond dipoles in KNaNbOF_5 . In addition to hydrothermal methods, classical solid state reactions are being explored as a means to form KNaWO_2F_4 and $\text{KNaMoO}_2\text{F}_4$. It is anticipated that these phases will be noncentrosymmetric and polar with SHG responses similar to that of KNaNbOF_5 , which has been prepared by a convenient solid state reaction route.

7.2.2 Chemical Hardness and the Structure-Directing Role of the cis-oxo $[\text{WO}_2\text{F}_4]^{2-}$ Anion

Future work in this area should focus on the synthesis of Cs/Na type compounds of similar composition to those reported. Thus far, no such compounds have been

isolated. The isolation of such compounds would, hopefully, confirm the theory that chemical hardness greatly contributes to the segregation of oxide and fluoride ions in structures with heterocationic bond networks. These effects may be more pronounced in compounds where the alkali cation size difference is large, i.e. Na^+ vs. Cs^+ . Additionally, attempts should be made to synthesize compounds containing two large alkali metal cations (K^+ , Rb^+ , Cs^+). Thus far, such attempts have been unsuccessful owing to valence and charge density considerations.

7.2.3 The Valence-Matching Principle and Cation-Anion Interactions in Solid State Oxide Fluorides

Current results indicate that the synthesis of niobium oxide fluoride anions is largely dependent on alkali cation size. This template effect reveals itself consistently, as the small alkali metal cations (Na^+) bring forward small, discrete anions (NbOF_5^{2-}) and the larger alkali metal cations (K^+ , Rb^+ , Cs^+) crystallize with less charge dense, chain-like anions, i.e. $[\text{Nb}_3\text{OF}_{18}]^{5-}$ and $[\text{Nb}_6\text{O}_7\text{F}_{26}]^{10-}$. Ultimately, through clever synthetic approaches, the isolation of A_2NbOF_5 ($\text{A} = \text{K}^+$, Rb^+ , Cs^+) and $\text{A}_5\text{Nb}_3\text{OF}_{18}$ and $\text{A}_{10}\text{Nb}_6\text{O}_7\text{F}_{26}$ ($\text{A} = \text{Na}^+$) compounds from solution is desired. Careful adjustment of the current synthetic parameter windows is a practical first step toward this goal.

7.2.4 The Crystal Structures of Rb_2NbOF_5 and Cs_2NbOF_5

Surprisingly, the crystal structures of these compounds had not been reported until now. Most likely, this is a direct result of their difficulty to obtain from solution, as the large Rb^+ and Cs^+ cations bring forward chain-like anions. Dissolution of Na_2NbOF_5 precursor combined with a large excess of the desired cation in solution and subsequent precipitation was used to circumvent this problem. This method could easily be applied to the synthesis of similar compounds such as $\text{K}_2\text{WO}_2\text{F}_4$, $\text{Rb}_2\text{WO}_2\text{F}_4$, $\text{Rb}_2\text{MoO}_2\text{F}_4$, and $\text{Cs}_2\text{MoO}_2\text{F}_4$, as the crystal structures of these compounds are not known. Moreover, suitable precursors, $\text{Na}_2\text{WO}_2\text{F}_4$ and $\text{Na}_2\text{MoO}_2\text{F}_4$, are easily prepared from hydrofluoric acid solutions of Na_2WO_4 and Na_2MoO_4 , respectively. The potential information that could be gleaned from these crystal structures would only further the search for new and useful noncentrosymmetric oxide fluorides.

7.2.5 The Elusive KNaNbOF_5

Possible approaches to the isolation of this compound have previously been put forward in the body of this thesis. Perseverance may be the true route to high quality single crystals of this elusive compound. Solution methods have not proven very successful. The most realistic approach to the reproduction of this compound may be by making large quantities of the powder by solid state methods and then experimenting with various recrystallization methods.

Chapter References

Chapter 1

1. Ye, N.; Chen, Q.; Wu, B.; Chen, C., *J. Appl. Phys.* **1998**, 84, (1), 555-558.
2. Heier, K. R.; Norquist, A. J.; Wilson, C. G.; Stern, C. L.; Poeppelmeier, K. R., *Inorg. Chem.* **1998**, 37, (1), 76-80.
3. Brown, I. D.; Altermatt, D., *Acta Crystallogr., Sect. B* **1985**, 41, (AUG), 244-247.
4. Heier, K. R.; Norquist, A. J.; Halasyamani, P. S.; Duarte, A.; Stern, C. L.; Poeppelmeier, K. R., *Inorg. Chem.* **1999**, 38, (4), 762-767.
5. Norquist, A. J.; Heier, K. R.; Stern, C. L.; Poeppelmeier, K. R., *Inorg. Chem.* **1998**, 37, (25), 6495-6501.
6. Izumi, H. K.; Kirsch, J. E.; Stern, C. L.; Poeppelmeier, K. R., *Inorg. Chem.* **2005**, 44, (3), 884-895.
7. Marvel, M. R.; Lesage, J.; Baek, J.; Halasyamani, P. S.; Stern, C. L.; Poeppelmeier, K. R., *J. Am. Chem. Soc.* **2007**, 129, (45), 13963-13969.
8. Harrison, W. T. A.; Nenoff, T. M.; Gier, T. E.; Stucky, G. D., *Inorg. Chem.* **1993**, 32, (11), 2437-2441.
9. Sheldrick, G. M. *SHELXTL DOS/Windows/NT*, version 5.10; Bruker Analytical X-Ray Instruments, Inc.: Madison, WI, 1997.

Chapter 2

1. Ye, N.; Chen, Q.; Wu, B.; Chen, C., *J. Appl. Phys.* **1998**, 84, (1), 555-558.
2. Wu, B.; Tang, D.; Ye, N.; Chen, C., *Opt. Mater. (Amsterdam)* **1996**, 5, (1/2), 105-109.
3. Chen, C.; Wang, Y.; Wu, B.; Wu, K.; Zeng, W.; Yu, L., *Nature (London)* **1995**, 374, (6519), 290.
4. Becker, P., *Adv. Mater. (Weinheim, Ger.)* **1998**, 10, (13), 979-992.
5. Kunz, M.; Brown, I. D., *J. Solid State Chem.* **1995**, 115, (2), 395-406.
6. Welk, M. E.; Norquist, A. J.; Arnold, F. P.; Stern, C. L.; Poeppelmeier, K. R., *Inorg. Chem.* **2002**, 41, (20), 5119-5125.
7. Heier, K. R.; Norquist, A. J.; Wilson, C. G.; Stern, C. L.; Poeppelmeier, K. R., *Inorg. Chem.* **1998**, 37, (1), 76-80.
8. Norquist, A. J.; Heier, K. R.; Stern, C. L.; Poeppelmeier, K. R., *Inorg. Chem.* **1998**, 37, (25), 6495-6501.
9. Heier, K. R.; Norquist, A. J.; Halasyamani, P. S.; Duarte, A.; Stern, C. L.; Poeppelmeier, K. R., *Inorg. Chem.* **1999**, 38, (4), 762-767.
10. Needs, R. L.; Weller, M. T., *J. Chem. Soc., Chem. Comm.* **1995**, (3), 353-4.
11. Needs, R. L.; Weller, M. T., *J. Chem. Soc., Dalt. Trans.: Inorg. Chem.* **1995**, (18), 3015-17.
12. Pauling, L., *J. Amer. Chem. Soc.* **1929**, 51, 1010-26.

13. Brown, I. D.; Altermatt, D., *Acta Crystallogr., Sect. B* **1985**, 41, (AUG), 244-247.
14. Welk, M. E.; Norquist, A. J.; Stern, C. L.; Poeppelmeier, K. R., *Inorg. Chem.* **2001**, 40, (22), 5479-5480.
15. Antokhina, T. F.; Ignat'eva, L. N.; Savchenko, N. N.; Tkachenko, I. A.; Kaidalova, T. A., *Zh. Neorg. Khim.* **2003**, 48, (4), 551-558.
16. Bertolini, J. C., *J. Emerg. Med.* **1992**, 10, (2), 163-168.
17. Peters, D.; Miethchen, R., *J. Fluorine Chem.* **1996**, 79, (2), 161-165.
18. Segal, E. B., *Chem. Health Saf.* **2000**, 7, (1), 18-23.
19. Harrison, W. T. A.; Nenoff, T. M.; Gier, T. E.; Stucky, G. D., *Inorg. Chem.* **1993**, 32, (11), 2437-2441.
20. Pausewang, G.; Ruedorff, W., *Z. Anorg. Allg. Chem.* **1969**, 364, (1-2), 69-87.
21. Stomberg, R., *Acta Chem Scand A* **1984**, 38, (8), 603-607.
22. *SAINT-Plus*, version 6.02A; Bruker Analytical X-ray Instruments, Inc.: Madison, WI, 2000.
23. Sheldrick, G. M. *SHELXTL DOS/Windows/NT*, version 5.10; Bruker Analytical X-Ray Instruments, Inc.: Madison, WI, 1997.
24. Flack, H. D., *Acta Crystallogr., Sect. A* **1983**, A39, (6), 876-81.
25. Spek, A. L. *PLATON*, Utrecht University: Utrecht, The Netherlands, 2001.
26. Kurtz, S. K.; Perry, T. T., *J. Appl. Phys.* **1968**, 39, (8), 3798-813.

27. Dougherty, J. P.; Kurtz, S. K., *J. Appl. Crystallogr.* **1976**, 9, Pt. 2, 145-58.
28. Brown, I. D., *The Chemical Bond in Inorganic Chemistry: The Bond Valence Model*. 1st ed.; Oxford University Press: Oxford, 2002; 'Vol.' 1, p 278.
29. Brown, I. D., *Phys. Chem. Miner.* **1987**, 15, (1), 30-4.
30. Tobias, G.; Beltran-Porter, D.; Lebedev, O. I.; Van Tendeloo, G.; Rodriguez-Carvajal, J.; Fuertes, A., *Inorg. Chem.* **2004**, 43, (25), 8010-8017.
31. Brese, N. E.; O'Keeffe, M., *Acta Crystallogr., Sect. B* **1991**, 47, 192-197.
32. Maggard, P. A.; Nault, T. S.; Stern, C. L.; Poeppelmeier, K. R., *J. Solid State Chem.* **2003**, 175, (1), 27-33.
33. Eaton, D. F., *Science (Washington, DC, United States)* **1991**, 253, (5017), 281-7.
34. Pan, S.; Smit, J. P.; Watkins, B.; Marvel, M. R.; Stern, C. L.; Poeppelmeier, K. R., *J. Amer. Chem. Soc.* **2006**, 128, (35), 11631-11634.
35. Li, R.; Chen, C., *Wuli Xuebao* **1985**, 34, (6), 823-7.
36. Izumi, H. K.; Kirsch, J. E.; Stern, C. L.; Poeppelmeier, K. R., *Inorg. Chem.* **2005**, 44, (3), 884-895.
37. Srivastava, A. M.; Ackerman, J. F., *J. Solid State Chem.* **1992**, 98, (1), 144-50.
38. Vlasse, M.; Moutou, J. M.; Cervera-Marzal, M.; Chaminade, J. P.; Hagenmuller, P., *Revue de Chimie Minerale* **1982**, 19, (1), 58-64.
39. Izumi, H. K.; Kirsch, J. E.; Stern, C. L.; Poeppelmeier, K. R., *Inorg. Chem.* **2005**, 44, (4), 884-895.

40. Salinas-Sanchez, A.; Garcia-Munoz, J. L.; Rodriguez-Carvajal, J.; Saez-Puche, R.; Martinez, J. L., *J. Solid State Chem.* **1992**, 100, (2), 201-11.
41. Preiser, C.; Losel, J.; Brown, I. D.; Kunz, M.; Skowron, A., *Acta Crystallogr., Sect. B: Struct. Sci.* **1999**, B55, (5), 698-711.

Chapter 3

1. Ye, N.; Chen, Q.; Wu, B.; Chen, C., *J. Appl. Phys.* **1998**, *84*, 555-558.
2. Wu, B.; Tang, D.; Ye, N.; Chen, C., *Opt. Mater. (Amsterdam)* **1996**, *5*, 105-109.
3. Chen, Q.; Chen, J., *Wuli* **1997**, *26*, 67-73.
4. Becker, P., *Adv. Mater. (Weinheim, Germany)* **1998**, *10*, 979-992.
5. Kunz, M.; Brown, I. D., *J. Solid State Chem.* **1995**, *115*, 395-406.
6. Heier, K. R.; Norquist, A. J.; Wilson, C. G.; Stern, C. L.; Poeppelmeier, K. R., *Inorg. Chem.* **1998**, *37*, 76-80.
7. Brown, I. D.; Altermatt, D., *Acta Crystallogr., Sect. B* **1985**, *41*, 244-247.
8. Heier, K. R.; Norquist, A. J.; Halasyamani, P. S.; Duarte, A.; Stern, C. L.; Poeppelmeier, K. R., *Inorg. Chem.* **1999**, *38*, 762-767.
9. Welk, M. E.; Norquist, A. J.; Stern, C. L.; Poeppelmeier, K. R., *Inorg. Chem.* **2001**, *40*, 5479-5480.
10. Vlasse, M.; Moutou, J. M.; Cervera-Marzal, M.; Chaminade, J. P.; Hagenmueller, P., *Rev. Chim. Maner.* **1982**, *19*, 58-64.
11. Bertolini, J. C., *J. Emerg. Med.* **1992**, *10*, 163-168.
12. Peters, D.; Miethchen, R., *J. Fluorine Chem.* **1996**, *79*, 161-165.
13. Segal, E. B., *Chem. Health Saf.* **2000**, *7*, 18-23.
14. Norquist, A. J.; Heier, K. R.; Stern, C. L.; Poeppelmeier, K. R., *Inorg. Chem.* **1998**, *37*, 6495-6501.
15. Kaidalova, T. A.; Pakhomov, V. I.; Panin, E. S., *Koord. Khimiya* **1976**, *2*, 554-6.
16. *SAINT-Plus*, version 6.02A; Bruker Analytical X-ray Instruments, Inc.: Madison, WI, 2000.

17. Sheldrick, G. M. *SHELXTL DOS/Windows/NT*, version 5.10; Bruker Analytical X-Ray Instruments, Inc.: Madison, WI, 1997.
18. Spek, A. L. *PLATON*, Utrecht University: Utrecht, The Netherlands, 2001.
19. Griffith, W. P.; Wickins, T. D., *J. Chem. Soc. A* **1968**, 400-4.
20. Marvel, M. R.; Lesage, J.; Baek, J.; Halasyamani, P. S.; Stern, C. L.; Poeppelmeier, K. R., *J. Amer. Chem. Soc.* **2007**, *129*, 13963-13969.
21. Welk, M. E.; Norquist, A. J.; Arnold, F. P.; Stern, C. L.; Poeppelmeier, K. R., *Inorg. Chem.* **2002**, *41*, 5119-5125.
22. Pausewang, G.; Schmitt, R.; Dehnicke, K., *Z. Anorg. Allg. Chem.* **1974**, *408*, 1-8.
23. Pauling, L., *J. Amer. Chem. Soc.* **1929**, *51*, 1010-26.
24. Heier, K. R.; Norquist, A. J.; Wilson, C. G.; Stern, C. L.; Poeppelmeier, K. R., *Inorg. Chem.* **1998**, *37*, 76-80.
25. Norquist, A. J.; Doran, M. B.; O'Hare, D., *Inorg. Chem.* **2005**, *44*, 3837-3843.
26. Hagemuller, P., *Inorganic Solid Fluorides*. ed.; Academic Press, Inc.: New York, 1985.
27. Pearson, R. G., *Chemical Hardness*. ed.; John Wiley & Sons, Inc.: New York, 1997.
28. Vlasse, M.; Moutou, J. M.; Cervera-Marzal, M.; Chaminade, J. P.; Hagemuller, P., *Revue de Chimie Minerale* **1982**, *19*, 58-64.
29. Brese, N. E.; O'Keeffe, M., *Acta Crystallogr., Section B: Structural Science* **1991**, *B47*, 192-7.
30. Tsikaeva, D. V.; Agulyanskii, A. I.; Balabanov, Y. I.; Kuznetsov, V. Y.; Kalinnikov, V. T., *Zh. Neorg. Khim.* **1989**, *34*, 3046-52.
31. Marvel, M. R., Personal Communication. Northwestern University, Evanston, IL, 2006.

Chapter 4

1. Eaton, D. F., *Science (Washington, DC, U. S.)* **1991**, 253, (5017), 281-7.
2. Marvel, M. R.; Lesage, J.; Baek, J.; Halasyamani, P. S.; Stern, C. L.; Poeppelmeier, K. R., *J. Am. Chem. Soc.* **2007**, 129, (45), 13963-13969.
3. Tsikaeva, D. V.; Agulyanskii, A. I.; Balabanov, Y. I.; Kuznetsov, V. Y.; Kalinnikov, V. T., *Zh. Neorg. Khim.* **1989**, 34, (12), 3046-52.
4. Stomberg, R., *Acta Chem Scand A* **1984**, 38, (8), 603-607.
5. Agulyansky, A. I.; Ravez, J., *J. Fluorine Chem.* **1994**, 67, (3), 225-7.
6. Bertolini, J. C., *J. Emerg. Med.* **1992**, 10, (2), 163-168.
7. Segal, E. B., *Chem. Health Saf.* **2000**, 7, (1), 18-23.
8. Harrison, W. T. A.; Nenoff, T. M.; Gier, T. E.; Stucky, G. D., *Inorg. Chem.* **1993**, 32, (11), 2437-2441.
9. *SAINT-Plus*, version 6.02A; Bruker Analytical X-ray Instruments, Inc.: Madison, WI, 2000.
10. Sheldrick, G. M. *SHELXTL DOS/Windows/NT*, version 5.10; Bruker Analytical X-Ray Instruments, Inc.: Madison, WI, 1997.
11. Spek, A. L. *PLATON*, Utrecht University: Utrecht, The Netherlands, 2001.
12. Dent Glasser, L. S., *Z. Kristallogr.* **1979**, 149, 291-305.
13. Hawthorne, F. C., *Acta Crystallogr., Sect. B: Struct. Sci.* **1994**, B50, (5), 481-510.
14. Becker, P., *Z. Kristallogr.* **2001**, 216, (10), 523-533.
15. Brown, I. D., *The Chemical Bond in Inorganic Chemistry: The Bond Valence Model*. 1st ed.; Oxford University Press: Oxford, 2002; 'Vol.' 1, p 278.
16. Echigo, T.; Kimata, M., *Z. Kristallogr.* **2006**, 221, (12), 762-769.

17. Hoskins, B. F.; Linden, A.; O'Donnell, T. A., *Inorg. Chem.* **1987**, 26, (14), 2223-8.
18. Mattes, R.; Mennemann, K.; Jaeckel, N.; Rieskamp, H.; Brockmeyer, H. J., *J. Less-Common Met.* **1980**, 76, 199-212.
19. Kaidalova, T. A.; Pakhomov, V. I.; Panin, E. S., *Koord. Khim.* **1976**, 2, (4), 554-6.
20. Stephens, N. F.; Lightfoot, P., *Acta Crystallog., Sect. C* **2005**, C61, (7), m344-m345.

Chapter 5

1. Vlasse, M.; Massies, J. C.; Demazeau, G., *J. Solid State Chem.* **1973**, 8, (2), 109-13.
2. Brink, F. J.; Withers, R. L.; Noren, L., *J. Solid State Chem.* **2002**, 166, (1), 73-80.
3. Diemann, E., *Zeitschrift fuer Naturforschung, Teil B: Anorganische Chemie, Organische Chemie* **1976**, 31B, (11), 1468-71.
4. Needs, R. L.; Weller, M. T., *J. Chem. Soc., Chem. Comm.* **1995**, (3), 353-4.
5. Needs, R. L.; Weller, M. T., *J. Chem. Soc., Dalt. Trans.: Inorg. Chem.* **1995**, (18), 3015-17.
6. Al-Mamouri, M.; Edwards, P. P.; Greaves, C.; Slaski, M., *Nature (London, United Kingdom)* **1994**, 369, (6479), 382-4.
7. Heier, K. R.; Norquist, A. J.; Halasyamani, P. S.; Duarte, A.; Stern, C. L.; Poeppelmeier, K. R., *Inorg. Chem.* **1999**, 38, (4), 762-767.
8. Marvel, M. R.; Lesage, J.; Baek, J.; Halasyamani, P. S.; Stern, C. L.; Poeppelmeier, K. R., *J. Amer. Chem. Soc.* **2007**, 129, (45), 13963-13969.
9. Vlasse, M.; Moutou, J. M.; Cervera-Marzal, M.; Chaminade, J. P.; Hagenmuller, P., *Revue de Chimie Minerale* **1982**, 19, (1), 58-64.
10. Srivastava, A. M.; Ackerman, J. F., *J. Solid State Chem.* **1992**, 98, (1), 144-50.
11. Bertolini, J. C., *J. Emerg. Med.* **1992**, 10, (2), 163-168.
12. Peters, D.; Miethchen, R., *J. Fluorine Chem.* **1996**, 79, (2), 161-165.

13. Segal, E. B., *Chem. Health Saf.* **2000**, 7, (1), 18-23.
14. Harrison, W. T. A.; Nenoff, T. M.; Gier, T. E.; Stucky, G. D., *Inorg. Chem.* **1993**, 32, (11), 2437-2441.
15. *SAINT-Plus*, version 6.02A; Bruker Analytical X-ray Instruments, Inc.: Madison, WI, 2000.
16. Sheldrick, G. M. *SHELXTL DOS/Windows/NT*, version 5.10; Bruker Analytical X-Ray Instruments, Inc.: Madison, WI, 1997.
17. Spek, A. L. *PLATON*, Utrecht University: Utrecht, The Netherlands, 2001.
18. Tsikaeva, D. V.; Agulyanskii, A. I.; Balabanov, Y. I.; Kuznetsov, V. Y.; Kalinnikov, V. T., *Zh. Neorg. Khim.* **1989**, 34, (12), 3046-3052.
19. Galy, J.; Andersson, S.; Portier, J., *Acta Chemica Scandinavica (1947-1973)* **1969**, 23, (9), 2949-54.
20. Stomberg, R., *Acta Chem Scand A* **1984**, 38, (8), 603-607.
21. Pinsker, Z. G., *Kristallografiya* **1966**, 11, (5), 741-8.
22. Vlasse, M.; Moutou, J. M.; Cervera-Marzal, M.; Chaminade, J. P.; Hagenmueller, P., *Rev. Chim. Maner.* **1982**, 19, (1), 58-64.
23. Brink, F. J.; Norén, L.; Goossens, D. J.; Withers, R. L.; Liu, Y.; Xu, C.-N., *J. Solid State Chem.* **2003**, 174, 450-458.
24. Pinsker, G. Z.; Kuznetsov, V. G., *Kristallografiya* **1968**, 13, (1), 74-9.
25. Pausewang, G., *Zeitschrift fuer Naturforschung, Teil B: Anorganische Chemie, Organische Chemie, Biochemie, Biophysik, Biologie* **1971**, 26, (12), 1218-20.

26. Jie, Z. H.; Garcia, A.; Guillen, F.; Chaminade, J. P.; Fouassier, C., *Eur. J. Solid State Inorg. Chem.* **1993**, 30, (7-8), 773-87.
27. Srivastava, A. M.; Ackerman, J. F., *J. Solid State Chem.* **1992**, 98, (1), 144-150.

Chapter 6

1. Marvel, M. R.; Lesage, J.; Baek, J.; Halasyamani, P. S.; Stern, C. L.; Poeppelmeier, K. R., *J. Amer. Chem. Soc.* **2007**, 129, (45), 13963-13969.
2. Pausewang, G.; Ruedorff, W., *Z. Anorg. Allg. Chem.* **1969**, 364, (1-2), 69-87.
3. Segal, E. B., *Chem. Health Saf.* **2000**, 7, (1), 18-23.
4. Bertolini, J. C., *J. Emerg. Med.* **1992**, 10, (2), 163-168.
5. Harrison, W. T. A.; Nenoff, T. M.; Gier, T. E.; Stucky, G. D., *Inorg. Chem.* **1993**, 32, (11), 2437-2441.
6. Brown, I. D., *The Chemical Bond in Inorganic Chemistry: The Bond Valence Model*. 1st ed.; Oxford University Press: Oxford, 2002; 'Vol.' 1, p 278.
7. Sidorov, N.; Mitrofanov, V.; Kuznetsov, V.; Gutsol, A.; Kalinnikov, V.; Stefanovich, S., *Ferroelectrics* **1993**, 144, (1-4), 223-30.

APPENDIX

Table 2.2. Selected Bond Lengths, Experimental Bond Valences, Theoretical Bond Valences, Bond Valence Sums, BSI and GII indices for KNaNbOF₅.

KNaNbOF ₅	K	Na	Nb	$V_i = \sum_j S_{ij}$ $z_i = \sum_j s_{ij}$
R_{ij} (Å)	2.834(5)	2.343(6)	1.745(5)	
S_{ij} (vu) O	0.15	0.23	1.57	1.95
s_{ij} (vu)	0.43	0.45	1.12	2.00
R_{ij} (Å)	2.638(4)	2.726(4)	2.250(4)	2.114(4)
S_{ij} (vu) F1	0.17	0.14	0.21	0.45
s_{ij} (vu)	0.07	0.07	0.10	0.76
R_{ij} (Å)	2.732(2)		2.257(6)	1.946(4)
S_{ij} (vu) F2	0.14		0.21	0.72
s_{ij} (vu)	0.10		0.12	0.79
R_{ij} (Å)	2.700(4)	2.826(4)	2.446(5)	1.968(4)
S_{ij} (vu) F3	0.15	0.10	0.12	0.67
s_{ij} (vu)	0.07	0.07	0.10	0.76
R_{ij} (Å)	2.822(5)		2.297(8)	1.940(5)
S_{ij} (vu) F4	0.11		0.19	0.73
s_{ij} (vu)	0.10		0.12	0.79
R_{ij} (Å)	2.853(4)		2.205(5)	1.941(4)
S_{ij} (vu) F5	0.10		0.24	0.72
s_{ij} (vu)	0.10		0.12	0.79
$V_j = \sum_i S_{ij}$	1.05	1.21	4.86	BSI = 0.09
$z_j = \sum_i s_{ij}$	1.00	1.00	5.00	GII = 0.16

R_{ij} = bond length of the bond "ij".

$S_{ij} = \exp[(R_0 - R_{ij})/B]$ experimental bond valence of bond "ij", where R_0 = constant dependent on i and j bonded elements, and $B = 0.37$.

$R_0(\text{Nb-O}) = 1.911$, $R_0(\text{Nb-F}) = 1.822$; $R_0(\text{Na-O}) = 1.803$, $R_0(\text{Na-F}) = 1.677$;

$R_0(\text{Cs-O}) = 2.417$, $R_0(\text{Cs-F}) = 2.33$; $R_0(\text{K-O}) = 2.132$, $R_0(\text{K-F}) = 1.992$.

s_{ij} = theoretical bond valence of bond "ij", calculated by solving the network equations based

on the methods described by Brown.^{28, 29}

V_i, V_j = experimental valences of anions "i" and cations "j".

z_i, z_j = charge or formal valence of anions "i" and cations "j".

$\text{BSI} = [\langle (S_{ij} - s_{ij})^2 \rangle]^{1/2}$ Bond Strain Index.

$\text{GII} = [\langle (V_{ij} - z_{ij})^2 \rangle]^{1/2}$ Global Instability Index.

Table 2.3. Selected Bond Lengths, Experimental Bond Valences, Theoretical Bond Valences, Bond Valence Sums, BSI and GII indices for CsNaNbOF₅.

CsNaNbOF ₅ ^a	Cs1	Cs2	Na	Nb	$V_i = \sum_j S_{ij}$ $z_i = \sum_j s_{ij}$
R _{ij} (Å)	2 × 3.247(3)	2 × 3.231(3)	2.300(3)	1.800(3)	
S_{ij} (vu)	2 × 0.11	2 × 0.11	0.26	1.35	1.83
<i>s_{ij} (vu)</i>	2 × 0.31	2 × 0.31	0.36	1.03	2.00
R _{ij} (Å)	2 × 3.037(2)	2 × 2.964(2)	2.259(3)	2.056(2)	
S_{ij} (vu)	2 × 0.15	2 × 0.18	0.21	0.53	1.07
<i>s_{ij} (vu)</i>	2 × 0.06	2 × 0.06	0.11	0.78	1.00
R _{ij} (Å)	2 × 3.202(2)		2.293(2)	1.941(2)	
S_{ij} (vu)	2 × 0.10		0.19	0.72	1.01
<i>s_{ij} (vu)</i>	2 × 0.08		0.13	0.79	1.00
R _{ij} (Å)	2 × 3.110(2)	2 × 3.045(2)	2.401(3)	1.955(2)	
S_{ij} (vu)	2 × 0.12	2 × 0.14	0.14	0.70	1.10
<i>s_{ij} (vu)</i>	2 × 0.06	2 × 0.06	0.11	0.78	1.00
R _{ij} (Å)			2.318(2)	1.946(2)	
S_{ij} (vu)			0.18	0.72	0.90
<i>s_{ij} (vu)</i>			0.17	0.83	1.00
R _{ij} (Å)		2 × 3.335(2)	2.238(3)	1.930(2)	
S_{ij} (vu)		2 × 0.07	0.22	0.75	1.04
<i>s_{ij} (vu)</i>		2 × 0.08	0.13	0.79	1.00
$V_j = \sum_i S_{ij}$	0.94	1.00	1.20	4.77	BSI = 0.12
$z_j = \sum_i s_{ij}$	1.00	1.00	1.00	5.00	GII = 0.13

Table 2.4. Estimations of the negative potentials of the ions of the $(\text{NbOF}_5)^{2-}$ anions and the surrounding positive potentials in CsNaNbOF_5 and KNaNbOF_5 , through bond strength and bond valence calculations.

CsNaNbOF₅			
Bond	Anionic BV (vu) ^a	Cationic PSCR sum (vu) ^b	Cationic BV sum (vu) ^c
Nb–O	0.65	0.42	0.48
Nb–F1	0.47	0.42	0.54
Nb–F2	0.28	0.29	0.28
Nb–F3	0.30	0.42	0.40
Nb–F4	0.28	0.17	0.18
Nb–F5	0.25	0.29	0.29

KNaNbOF₅			
Bond	Anionic BV (vu) ^a	Cationic PSCR sum (vu) ^b	Cationic BV sum (vu) ^c
Nb–O	0.43	0.29	0.38
Nb–F1	0.55	0.42	0.52
Nb–F2	0.28	0.29	0.33
Nb–F3	0.33	0.42	0.38
Nb–F4	0.27	0.29	0.30
Nb–F5	0.28	0.29	0.34

^a Anionic BV (Bond Valence) = $z_i - S_{\text{Nb-O/F}}$, where z_i is the electric charge of each ligand and $S_{\text{Nb-O/F}}$ is taken from the Table 2 or 3 for each Nb–O/F bond.

^b Cationic PSCR sum = $\sum_j S'_{j,\text{cat}} = \sum_j \frac{z_{j,\text{cat}}}{v_{j,\text{cat}}}$, where $z_{j,\text{cat}}$ is the electric

charge of each A_i alkali cation bonded to a given ligand and $v_{j,\text{cat}}$ is its coordination number.

^c Cationic BV (bond valence) sum = $\sum_i S_{i,\text{cat}}$, where $S_{i,\text{cat}}$ is taken from

Table 2 or 3 for each A_i –O/F bond.

ELECTRONIC APPENDIX

Key to SHELX files

number	Charlotte's project number
CIF	Crystallographic information file
FCF	SHELX file - structure factors
HKL	hkl file
INS/RES	SHELX file - ins = res files, atomic coordinates, occupancy
LST	SHELX file - bond distances, Fourier peaks
P4P	SHELX file - set up file
PCF	SHELX file - space group determination
PRP	SHELX file - includes absorption correction
RAW	SHELX file - raw data

Chapter 2

KNaNbOF₅

number	s72q
CIF	KNaNbOF ₅
FCF	s72q1m
HKL	s72q1m
INS/RES	s72q1m.res
LST	s72q1m
P4P	s72q1m
PCF	s72q1m
PRP	s72q1m
RAW	s72q1m

CsNaNbOF₅

number	s45q
CIF	CsNaNbOF ₅
FCF	s45q1m
HKL	s45q1m
INS/RES	s45q1m.res
LST	s45q1m
P4P	s45q1m
PCF	s45q1m
PRP	s45q1m
RAW	s45q1m

Chapter 3Rb₃Na(NbOF₅)₂•H₂O

number	s52q
CIF	s52q1m
FCF	s52q1m
HKL	s52q1m
INS/RES	s52q1m.ins
LST	s52q1m
P4P	s52q1m
PCF	s52q1m
PRP	s52q1m
RAW	s52q1m

Rb₃Na(MoO₂F₄)₂•H₂O

number	s01u
CIF	s01u1m
FCF	s01u1m
HKL	s01u1m
INS/RES	s01u1m.ins
LST	s01u1m
P4P	s01u1m
PCF	s01u1m
PRP	s01u1m
RAW	s01u1m

Rb₃Na(WO₂F₄)₂•H₂O

number	s75w
CIF	s75w1m
FCF	s75w1m
HKL	s75w1m
INS/RES	s75w1m.ins
LST	s75w1m
P4P	s75w1m
PCF	s75w1m
PRP	s75w1m
RAW	s75w1m

K₃Na(WO₂F₄)₂•H₂O

number	s82t
CIF	s82t1m
FCF	s82t1m
HKL	s82t1m
INS/RES	s82t1m.ins
LST	s82t1m
P4P	s82t1m
PCF	s82t1m
PRP	s82t1m
RAW	s82t1m

Chapter 4Rb₁₀Nb₆O₇F₂₆•H₂O

number	s18q
CIF	s18q1m
FCF	s18q1m
HKL	s18q1m
INS/RES	s18q1m.res
LST	s18q1m
P4P	s18q1m
PCF	s18q1m
PRP	s18q1m
RAW	s18q1m

Chapter 5Rb₂NbOF₅

number	s65s
CIF	s65s1m
FCF	s65s1m
HKL	s65s1m
INS/RES	s65s1m.res
LST	s65s1m
P4P	s65s1m
PCF	s65s1m
PRP	s65s1m
RAW	s65s1m

<u>Cs₂NbOF₅</u>	
number	s40v
CIF	s40v1m
FCF	s40v1m
HKL	s40v1m
INS/RES	s40v1m.res
LST	s40v1m
P4P	s40v1m
PCF	s40v1m
PRP	s40v1m
RAW	s40v1m

Michael R. Marvel

Work Address:
2145 Sheridan Road
Evanston, IL 60208-3113

Home Address:
3647 N. Hamilton Ave.
Chicago, IL 60618

Phone: (413) 335-5212
E-mail: mikemarv481@gmail.com

Education**Ph.D. Inorganic Chemistry**

Northwestern University, Evanston, Illinois, March 2008
Advisor: Prof. Kenneth R. Poeppelmeier

B.A. Chemistry

Connecticut College, New London, Connecticut, May 2003

Publications

"Chemical Hardness and the Structure-Directing Roles of the d^0 Transition Metal Oxide Fluoride Anions," **Marvel, M. R.**, Pinlac, Rachele Ann, Poeppelmeier, K. R., In Preparation.

"Cation-Anion Interactions and Polar Structures in the Solid State," **Marvel, M. R.**, Lesage, J., Baek, J., Halasyamani, P. Shiv., Stern, C. L., Poeppelmeier, K. R., *J. Am. Chem. Soc.*, 2007, 129(45), 13963-13969.

"Optical Floating Zone Growth of β -BaB₂O₄ from a LiBa₂B₅O₁₀-Based Solvent," Pan, S., Smit, J. P., Lanier, C. H., **Marvel, M. R.**, Marks, L. D., Poeppelmeier, K. R., *Cryst. Growth and Des.*, 2007, 7(8), 1561-1564.

"Structure and Magnetic Properties of Pb₂Cu₃B₄O₁₁: A New Copper Borate Featuring [Cu₃O₈]¹⁰⁻ Units," Pan, S., Watkins, B., Smit, J. P., **Marvel, M. R.**, Saratovsky, I., Poeppelmeier, K. R., *Inorg. Chem.*, 2007, 46(10), 3851-3855.

"Synthesis, Crystal Structure and Nonlinear Optical Properties of Li₆CuB₄O₁₀: a Congruently Melting Compound with Isolated [CuB₄O₁₀]⁶⁻ Units," Pan, S., Smit, J. P., Watkins, B., **Marvel, M. R.**, Stern, C. L., Poeppelmeier, K. R., *J. Am. Chem. Soc.*, 2006, 128(35), 11631-11634.

"Synthesis, Structure, and Properties of $\text{Pb}_2\text{CuB}_2\text{O}_6$," Pan, S., Smit, J. P., **Marvel, M. R.**, Stern, C. L., Watkins, B., Poeppelmeier, K. R., *Mater. Res. Bull.*, 2006, 41(5) 916-924.

"Synthesis of a New Hollandite-Type Manganese Oxide with Framework and Interstitial Cr(III)," Ching, S., Driscoll, P. F., KIELTYKA, K. S., **Marvel, M. R.**, Suib, S. L., *Chem. Comm.*, 2001, (23), 2486-2487.